Distribution Agreement

In presenting this thesis or dissertation as a partial fulfillment of the requirements for an advanced degree from Emory University, I hereby grant to Emory University and its agents the non-exclusive license to archive, make accessible, and display my thesis or dissertation in whole or in part in all forms of media, now or hereafter known, including display on the world wide web. I understand that I may select some access restrictions as part of the online submission of this thesis or dissertation. I retain all ownership rights to the copyright of the thesis or dissertation. I also retain the right to use in future works (such as articles or books) all or part of this thesis or dissertation.

Signature:

Cheyenne Hurst	Date

Integrated Proteomics to Understand the Role of Neuritin (NRN1) as a mediator of Cognitive Resilience to Alzheimer's Disease

By

Cheyenne Danielle Hurst
Doctor of Philosophy

Graduate Division of Biological and Biomedical Sciences
Neuroscience

_____

Nicholas Seyfried, Ph.D.
Advisor

_____

Jeremy Herskowitz, Ph.D.
Committee Member

_____

Shannon Gourley, Ph.D.
Committee Member

_____

Gary Bassell, Ph.D.
Committee Member

_____

Matt Rowan, Ph.D.
Committee Member

Accepted:

_____

Kimberly J. Arriola, Ph.D.
Dean of the James T. Laney School of Graduate Studies

_____

Date

Integrated Proteomics to Understand the Role of Neuritin (NRN1) as a mediator of Cognitive Resilience to Alzheimer's Disease

By

Cheyenne Danielle Hurst
B.S., University of Florida

Advisor: Nicholas T. Seyfried, Ph.D.

An abstract of
a dissertation submitted to the Faculty of
the James T. Laney School of Graduate Studies of Emory University
in partial fulfillment of the requirements for the degree of
Doctor of Philosophy in Neuroscience
2023

Integrated Proteomics to Understand the Role of Neuritin (NRN1) as a mediator of Cognitive Resilience to Alzheimer's Disease

By Cheyenne Danielle Hurst

The molecular mechanisms and pathways enabling certain individuals to remain cognitively normal despite high levels of Alzheimer's disease (AD) pathology remain incompletely understood. These cognitively normal people with AD pathology are described as preclinical or asymptomatic AD (AsymAD) and appear to exhibit cognitive resilience to the clinical manifestations of AD dementia. The body of work presented here provides a novel and comprehensive network-based approach from cases clinically and pathologically defined as AsymAD to map resilience-associated pathways and contributes to mechanistic validation of resilience-associated targets. Multiplex tandem mass tag mass spectrometry (TMT-MS) proteomic data was generated on brain tissue from Brodmann area 6 and Brodmann area 37 (n=109 cases, n=218 total samples) and evaluated by consensus weighted gene correlation network analysis. Notably, Neuritin (NRN1), a neurotrophic factor previously linked to cognitive resilience, was identified as a hub protein in a module associated with synaptic biology. To validate the function of NRN1 with regard to the neurobiology of AD, we conducted microscopy and physiology experiments in a cellular model of AD. NRN1 provided dendritic spine resilience against amyloid-β (Aβ) and blocked Aβ-induced neuronal hyperexcitability in cultured neurons. To better understand the molecular mechanisms of resilience to Aβ provided by NRN1, we assessed how exogenous NRN1 alters the proteome of cultured neurons by TMT-MS and integrated the results with the human AD brain network. This revealed over-lapping synapse-related biology that linked NRN1-induced changes in cultured neurons with human pathways associated with cognitive resilience. Collectively, this work highlights the utility of integrating the proteome from human brain and model systems to advance our understanding of resilience-promoting mechanisms and prioritize therapeutic targets that mediate resilience to AD.

Acknowledgements

These last five years have been some of the most difficult and formative of my entire life. For every person I have encountered along this winding and bumpy road, I thank you for the lessons, the support, the love. For making me who I am today. Thank you.

To my mentor, Nick. Thank you for the countless hours of work we put in together. Thank you for your patience and compassion through the many unexpected challenges life wrought. We have had many laughs and profane littered talks, teased and taunted one another, pep talked and quietly cursed the other. Your brain is a marvel and your inexhaustible enthusiasm for science is the reason I joined your lab. You are a chaotic whirlwind of caffeine and ideas and I am grateful for the place in your lab I have held these last few years.

To the many wonderful and brilliant people that make up the Seyfried lab, Rangaraju lab, many members of the CND and surrounding. Never have I had the pleasure of working alongside so many talented and skilled scientists and thinkers. I certainly did not expect such minds to also possess so much kindness and goodwill. It has been an honor. To Duc Duong, I wouldn't be here without you. You are an invaluable team leader and have helped me so much in both technical guidance and friendly encouragement. Thank you for noticing me and allowing me to learn from you. Lingyan Ping, you are a brilliant goddess of a woman with skills as an experimentalist I aspire to cultivate in myself. Maesho Abreha, you are an endless wealth of knowledge and warmth. Eric Dammer, genius. Seriously. You are a problem solver extraordinaire, creative thinker, absurdly gifted scientist (of multiple disciples) and sweet-souled human. You have helped me and encouraged the growth of my skills countless times. My sincerest of thanks. Erik Johnson, thank you for your seemingly infinite abundance of patience. Your time and energy have made me a far more skilled writer and communicator. Pritha Bagchi, thank you for so many smiles and kind gestures. You are a talented woman in science and a gentle heart. Luming Yin and Kaiming Xu, thank you for your help at various points in my training. You are truly indispensable team members with such skilled and patient hands. To the warrior pack of female grad students of the Seyfried group, keep giving 'em hell. Sydney Sunna, Erica Modeste, Christine Bowen, Juliet Santiago, Sarah Shapley, Christina Ramelow, Madi Bangs, I cannot wait to see the incredible things you will do with your lives as you fearlessly strive to define success and happiness on your own terms. An additional round of thanks to Sydney, my soul sister in science. The duration of our rotation in the Seyfried lab, our names were routinely exchanged and the raucous of our laughter could be heard throughout the fifth floor. We bonded on the beach (and trauma bonded at the bench) and I will forever be in your debt for helping me stay the course, believe in myself, laugh until we cried and celebrate each other along the way. Love you lady. There are many more people I haven't the space to thank from our groups, you are not overlooked. Please know I think of each of you fondly and respectfully.

To the incredible members of my committee, infinite thanks for being generous mentors, sounding boards, supporters and gifted thinkers. You helped shape my thesis over the years, challenge me to be better and listened while I developed my project with a genuine interest that allowed me to

find and strengthen my voice. I will carry aspects of each of your mentoring styles with me into my future. An additional, special thanks to Jeremy Herskowitz and his outstanding team at UAB.

To the McNair and IMSD communities, I am eternally grateful to and humbled by you. Samesha Barnes and Rhonda Vinson, you changed my life. I will hold you dear to my heart the rest of my life. You were the first to call me Doctor and to bring the possibility of my future doctorate into reality. You believed in me, invested in me and built me up. Thank you. To the cohort members I shared my McNair experience with, wherever you end up you are spectacular. I had never felt so accepted and loved by a group of peers before you, thank you. McNair, beware. Forever.

To my family, I think I started this journey for you, but inevitably arrived at its conclusion for myself. Allison Tonner, my mother, you gave me life. I literally would not be here without you. You are a rare soul and a kind heart. My beautiful sisters, Evan Bandy and Latisha Henckel, you have been the source of my survival for years. Such courageous, loving people. I admire you, respect you, adore you, treasure you. Josh Ahmie, self-appointed big brother, I am forever looking forward to the next breakfast we share. To Pauline Hassinger, I miss you every day. You gave me so much unconditional love, I would be a different person without you. To my father, Dale Henckel, you left us too early. You and I never really figured each other out, but I choose to remember you smiling, goofing around and enjoying life like the big kid you were at heart. To the rest of my family, you're mostly a mess but I love you anyways. Yeehaw.

To the beautiful people outside of Emory and science that have filled up my life with so much love and to whom I would be incomplete without. Thank you for making space in your lives for me and loving me even, and perhaps especially, when times were tough. Jeremy Hurst, the good with the bad. I am so happy to still have you in my life. I wish you every happiness. Irasema Hernandes, you are a force of nature and I can't wait to see what you will create for yourself. Katie Harris, Sarah Jeffords, Josh Bradford, you've known me longest. Thank you for sticking by me. To those I have not the space to name individually, but love nonetheless, thank you.

Integrated Proteomics to Understand the Role of Neuritin (NRN1) as a mediator of Cognitive Resilience to Alzheimer's Disease

By

Cheyenne Danielle Hurst
B.S., University of Florida

Advisor: Nicholas T. Seyfried, Ph.D.

A dissertation submitted to the Faculty of the James T. Laney School of Graduate Studies of Emory University in partial fulfillment of the requirements for the degree of
Doctor of Philosophy in Neuroscience
2023

Table of Contents Page

Figure list **Page**

Abbreviations

AD – Alzheimer's disease

AsymAD – Asymptomatic Alzheimer's disease

TMT-MS – tandem mass tag mass spectrometry

LC-MS/MS – liquid chromatography tandem mass spectrometry

NRN1 – Neuritin

Aβ – amyloid-beta

NFTs – neurofibrillary tangles

DLPFC – dorsolateral prefrontal cortex

ROSMAP – Religious Orders Study and Rush Memory and Aging Project

BA6 – Brodmann area 6

BA37 – Brodmann area 37

cWGCNA – consensus weighted gene correlation network analysis

PWAS – proteome wide association study

CERAD – consortium to establish a registry for Alzheimer's disease

APP – amyloid precursor protein

MAPT – microtubule associated protein tau

MMSE – mini mental state exam

GO – gene ontology

MEs – module eigenproteins

BA9 – Brodmann area 9

ThT – thioflavin T

MEA – microelectrode array

DIV – days in vitro

DMSO – dimethyl sulfoxide

FDR – false discovery rate

CPG15 – candidate plasticity gene 15

SPS – synchronous precursor selection

ROTS – reproducibility-optimized test statistic

IRB – institutional review board

SDS-PAGE -- sodium dodecyl sulfate–polyacrylamide gel electrophoresis

1.0 Introduction: Alzheimer's disease and cognitive resilience

1.1 Alzheimer's disease: an overview

1.1.1 Current impacts. Alzheimer's disease (AD) is a progressive, neurodegenerative disease with few treatment options available, posing a mounting public health burden. Currently, approximately 1 in 9 individuals over 65 are living with AD in the United States (1). Globally, AD is the number one cause of dementia, a severely debilitating condition impacting memory, thinking and social abilities that increasingly inhibits even basic functions of daily living. Without new therapeutic strategies to alter, slow or stop the disease process, the prevalence of AD is projected to more than double in the coming decades as the size of the aging population continues to increase.

1.1.2 Defining pathology. The defining pathological hallmarks of AD include the aberrant accumulation of two protein aggregates in a largely stereotyped pattern, this includes extracellular amyloid beta (Aβ) plaques and intracellular microtubule associated protein tau (MAPT) neurofibrillary tangles (NFTs) (2-6). Amyloid plaque deposition initiates and intensifies in the neocortex before eventually spreading to the hippocampus, basal ganglia and cerebellum (2). Tau pathology typically manifests in a reciprocal fashion, initiating in the entorhinal cortex then spreading to temporal cortex and eventually to the neocortex (3). The precise relationship between amyloid and tau pathology is still incompletely understood, however, the progression of these core pathologies is believed to initiate a myriad of downstream molecular and cellular dysfunctions culminating in synaptic dysfunction and stripping, neuronal cell death and brain atrophy (7, 8). A definitive diagnosis of AD is confirmed at autopsy based on extent of amyloid and tau pathology using standardized semi-quantitative, post-mortem evaluation metrics. The Consortium to Establish a Registry for Alzheimer's Disease (CERAD) test determines AD likelihood based on Aβ plaque deposition (9), whereas Braak (staging system named after the neuropathologists Heiko and Eva Braak) scoring is used to estimate the advancement of tau pathology based on regional tau deposition (3).

1.1.3 Genetic contributions. There are two recognized forms of AD, familial AD (FAD) and sporadic AD (1, 10). Autosomal dominant mutations of FAD occur rarely, accounting for only ~2% of all cases, but are highly penetrant and typically result in early onset of clinical symptoms (age 30-60 years). Mutations in amyloid precursor protein (APP) and presenilins 1 and 2 (PSEN1, PSEN2) are considered causal in FAD, each impacting the processing of Aβ and resulting in an accelerated timeline of pathological accumulation and cognitive deterioration. Sporadic AD cases account for the majority of all cases (~98%) and are generally considered to be a subtype of the same disease despite the lack of causal mutations. That said, genetics and family history contribute strongly to susceptibility and person-to-person heterogeneity for both familial and sporadic forms of AD. Twin studies have estimated the heritability of AD to be approximately 60-80% (11). Even among autosomal dominant cases, onset of clinical symptoms can vary significantly across families that carry the same mutation (10). There are also cases categorized as atypical AD, which describes cases with unusual symptom presentation and typically at younger ages without the presence of causal mutations (12, 13). Collectively, these findings afford the inference that AD susceptibility is strongly modified by a concert of genetic variants, many of which exert individually small effects. Genome wide association studies (GWASs) have identified dozens of genetic variants associated with an increased risk for developing AD. Among these, polymorphisms in the apolipoprotein E (APOE) are the strongest known genetic determinants in sporadic AD (14-16). The three APOE alleles include ε2, ε3 and ε4, where one inherited copy of the ε4 allele increases the risk for developing AD by 3-4 fold and two copies of the ε4 allele can increase risk by 9-15 fold (17). Conversely, inheritance of the ε2 allele is protective. Notably, recognition of the lack of diverse population representation in genetic evaluations of AD risk limit interpretation across populations and thus there may yet be many undiscovered variants impacting disease susceptibility or resilience.

1.1.4 Neuroinflammation. In addition to amyloid and tau burden, neuroinflammatory mechanisms are now regarded to contribute as much, if not more, than the primary defining pathologies in the pathogenesis of AD (18). Several genetic mutations and variants of glial receptors support a central role of neuroinflammation in AD (19, 20). For example, variants of triggering receptor expressed on myloid cells 2 (TREM2), encoding a microglial transmembrane receptor, can cause 2-4 fold increase in AD risk (21, 22). Microglia and astrocytes are considered primary drivers in pathologic neuroimmune transitions in AD (18). Microglia are the central phagocytes of the brain, involved in targeting and removal of pathogens and cellular debris to support optimal brain function (23). Microglia also release trophic factors and influence the pruning or protection of synapses under physiological settings (24). Astrocytes also contribute to overall neuronal and tissue maintenance, synaptic connectivity and play important roles in repair and regeneration after injury (25-28). In disease states, a shift from homeostatic to proinflammatory profiles have been observed for both microglia and astrocytes, in which each release a myriad of proinflammatory molecules including cytokines and interleukins (18). Alterations in cell function through both gain-of-function and loss-of-function mechanisms have also been reported. Microglia present with reduced or impaired phagocytic functions, including the clearance of Aβ (29). Reactive astrocytes are commonly observed surrounding senile plaques in AD post-mortem tissue (30). Loss of astrocyte-mediated proteolytic degradation pathways for Aβ clearance have also been implicated in pathological progression (31, 32). The extent to which glial cells contribute to or facilitate AD pathophysiology has been extensively reviewed elsewhere (18, 33, 34).

1.1.5 Disease origins and progression. The classic framework for understanding AD progression, known as the amyloid cascade hypothesis, was based on the assumption that Aβ serves as a causative, neurotoxic trigger in AD and the formation of NFTs, cell death, vascular changes and eventual dementia were a direct result of Aβ deposition (35). Support for the amyloid

cascade hypothesis is primarily based on genetic evidence. The only causal genetic mutations for AD result in pathological processing of Aβ while mutations in MAPT result in phenotypically and pathologically distinct subset of tauopathies (36). Complimentarily, there is an APP mutation that causes decreased Aβ production and reduces the risk for developing AD (37, 38). However, the poor correlation between amyloid and cognitive decline, brain region incongruity between amyloid and tau pathological progression and the high degree of failure in amyloid-directed drug trials has led to alternative and supplemental perspectives on AD progression (39-42). Of the more widely accepted extensions of the amyloid cascade hypothesis, the proposal of a biochemical and cellular phase preceding the clinical phase of disease incorporates more complexity of the underlying biochemical changes including contribution of other cell types and homeostatic dysfunctions that ultimately result in neurodegeneration and clinical manifestation (7).

Antemortem diagnosis of probable AD is assigned with reasonable accuracy based on a combination of estimated neuropathologic severity through cerebrospinal fluid (CSF) or neuroimaging biomarkers and cognitive function. Importantly, studies now suggest pathological brain changes can occur up to two decades before clinical symptom onset, indicating a protracted prodromal phase of the disease (43, 44). That said, there is considerable variability in rates of decline observed in symptomatic AD cases (45, 46). Biofluid and imaging-based biomarkers are actively being investigated to improve understanding of disease progression mechanisms and identify possible early intervention targets.

1.1.6 Additional risk factors and modifiers. Age remains the top risk factor for developing AD, exemplified in both prevalence and incidence of AD dementia. As of 2021 the estimated percentage of Americans living with AD dementia was ~5% for ages 65-74, ~14% for ages 75-83 and ~35% for people 85 and older (1, 47). Biological sex is another demographic-based variable influencing AD risk, where there are more women with AD than men (47). The relationship

between sex and increased or decreased risk for AD is woven into intersections of societal (access to education, social connectedness), environmental (exposure to hazardous materials such as heavy metals) and biological factors (gonadal hormones and chromosomal composition) that are still being disentangled (48). There are also a number of acquired risk factors that influence AD susceptibility, including cerebrovascular disease, hypertension, obesity and diabetes (49). Additionally, stress, depression and sleep disturbances, which are commonly comorbid, all contribute to increased risk for developing dementia, including AD dementia (50-54). There are many additional risk factors that have been explored in relationship to AD that have been discussed elsewhere (55, 56). Importantly, many lifestyle risk factors are highly modifiable, in that changes and prevention of these factors may prevent or delay dementia onset in as many as 40% of cases (8, 55, 56). In recognition of the consequential relationship between lifestyle and health and disease, including AD risk, it cannot be overstated the undeniable burden of socioeconomic deprivation. Individuals that experience area-level or individual-level socioeconomic deprivation (such as low wages, unemployment, neighborhood disadvantages, unstable or unsafe housing conditions) exhibit higher risks for developing dementia compared to those of higher socioeconomic status with a high degree of genetic risk (57).

1.1.7 Current treatment options. Development of pharmacological treatment options for AD have been largely unsuccessful, with high rates of failure at the clinical trial phase. The majority of approved therapies today are aimed at symptom management, these include cholinesterase inhibitors and anti-NMDA modulators (58). Cholinergic neurons are vulnerable in AD development, loss of these neuronal subtypes results in a general deficiency in cholinergic effects that have been linked to some aspects of early attention and memory dysfunctions (59). Cholinesterase inhibitors act to increase synaptic availability of acetylcholine and prescribed in mild-to-moderate stages of symptomatic AD (58). Anti-NMDA receptor modulator Memantine is approved for moderate-to-severe symptomatic stages of AD as its mechanism of action is

proposed to counteract the effect of excitotoxicity resulting from overt cell death occurring as the disease progresses (58). Unfortunately, both cholinesterase inhibitors and anti-NMDA drugs can only provide modest cognitive improvement and neither alter the long-term outcomes of disease progression. Alternatively, non-pharmacological interventions have been reported with positive impacts on cognition and quality of life. Approaches focused on both physical and cognitive training have reported promising improvements in cognitive functions such as working and verbal memory, reduction of neuropsychiatric symptoms and improved overall quality of life (60, 61). The lack of long-term, follow-up data for these strategies, however, limit the interpretation of how physical and cognitive training influence prognosis and outcomes.

More recently, Aducanumab (or aduhelm) has been approved by the FDA for broad-label use across the full spectrum of AD severity. Aducanumab works as a monoclonal antibody targeting both oligomeric and fibrillar forms of Aβ to interrupt aggregation kinetics and ultimately reduce plaque deposition (62). Clinical trial results that led to the drugs approval reported marked decreases in cortical plaque deposition and decreased rate of cognitive decline. However, much debate surrounding the efficacy of the drug remain in the field and there continues to be an unmet need for AD therapies (62-64). Lecanemab, an amyloid targeting monoclonal antibody drug, has also now passed phase three clinical trials reporting reduced amyloid markers and moderately reduced cognitive decline (65). As of 2022, there were 143 agents actively being developed through the AD drug development pipeline, the majority of which are disease modifying (66). Broadly, there are four categories of agents currently being developed (disease-modifying biologics, disease modifying small molecules, neuropsychiatric symptom treatment and cognitive enhancers) that target a wide array of mechanisms not limited to the primary pathologies of the disease. A conceptual illustration of the overarching themes in AD is depicted in **Fig. 1.1**.

1.2 Cognitive Resilience

1.2.1 Healthy brain aging. Individual differences in age-related cognitive performance have long been observed in brain aging research. The rate, degree and types of cognitive change that occurs within healthy aging varies from person to person. That said, cognitive capabilities especially within the domain of fluid intelligence, such as executive functioning, processing speed, types of memory and psychomotor abilities, are particularly vulnerable to age related declines (67, 68). On the other hand, forms of crystallized intelligence, such as vocabulary and general knowledge, tend to remain stable with age or even improve over time (67). Physiologically, loss of brain volume can be observed even in very healthy adults with age (69). Grey matter volume loss in the prefrontal cortex decreases as early as the second decade of life (70). White matter volumetric atrophy of up to 20% has been reported in older adults over 70 without the presence of pathological lesions (71). While some theories exist regarding gross neuronal loss as an explanation of age-related brain atrophy, evidence supports changes in neuronal size and synaptic density may better explain volumetric changes observed across the lifespan (69, 70).

1.2.2 Cognitive resilience in AD. The majority of AD cases initially present with mild cognitive dysfunctions and amnestic symptoms (4, 5, 72). Historically, the pathological hallmarks of AD (amyloid and tau aggregates) were thought to be the driving factors directly related to cognitive impairment in clinical presentations. However, increasing evidence suggests significant discrepancies between pathological burden and cognitive impairment. Estimates from longitudinal aging studies suggest only ~40% of variance in cognitive decline can be accounted for by multiple pathological indices (AD, cerebrovascular disease and Lewy body disease), where global AD pathology alone only accounted for ~22% (73). This leaves the majority of variance explaining cognitive decline in AD unaccounted for. Many older adults incur amyloid deposition or mixed proteinopathies in their brains without converting to dementia or developing clinical AD (74-76). Strikingly, approximately one-third of elderly individuals show little to no signs of cognitive impairment in their lifetime, but actually meet diagnostic criteria for AD when evaluated at autopsy

(77). This subpopulation of cognitively normal people with AD pathology are described as preclinical or asymptomatic AD (AsymAD) and appear to exhibit cognitive resilience to the clinical manifestations of AD dementia (**Fig. 1.2**). Cognitively resilient individuals appear to maintain near normal levels of both neuronal and synaptic densities compared to AD cases (78, 79). Resilient cases also appear to accumulate lower levels of hyperphosphorylated tau (the core constituent of NFTs), while amyloid burden remained comparable to symptomatic AD (78, 80). In addition, increased levels of anti-inflammatory cytokines and neurotrophins along with decreased pro-inflammatory chemokines have been reported in resilient cases, suggesting possible differences in neuroimmune involvement (81).

1.2.3 Resilience vs Reserve. The concept of cognitive resilience, specifically in the context of AD, seeks to define the phenomenon in which certain individuals live into advanced age with intact cognitive function despite the presence of moderate to severe AD pathology in their brains. These individuals arrive at autopsy having shown no signs of dementia during their life, yet harbor classic, defining AD lesions at levels meeting diagnostic criteria (77). The concept of reserve, which is distinct, suggests the brain can tolerate more pathology before clinical presentation due to larger starting material, such as having more neurons or synapses, larger brain to start with (82). Whereas resilience suggests possible compensatory mechanisms enable preservation of cognitive faculties despite increasing pathological burden.

1.3 Synaptic resilience

1.3.1 Dendritic spines. Postsynaptic sites for the majority of all excitatory synapses in the brain reside at dendritic spines, actin rich protrusions along neuronal dendrites (83). Spines are composed of a neck and head compartment, of which the structural features indicate their molecular composition, functional capacities and stratify them into types for classification (84). There are three primary subclasses of dendritic spines, thin, mushroom and stubby (85). Thin spines have small necks and heads, indicating little to no detectable postsynaptic density (PSD).

In fact, approximately 60% of cortical thin spines are considered “silent” synapses, indicating the absence of AMPA receptors and an immature synaptic site (86, 87). Thin spines are considered highly plastic, dynamic structures commonly associated with new learning that emerge from dendritic segments over shorter periods of time and can either stabilize or retract (83, 88-90). Mushroom spines have large heads and small necks, indicating increased postsynaptic density and functional signaling capacity. Mushroom spines remain stable over long periods of time and subserve long term storage of information and memory (89-91). Stubby spine heads are connected directly to the dendritic shaft by a wide neck. The functional significance of stubby spines is less well known than thin or mushroom, they are believed to be transitional structures or immature structures that disappear during development (83, 92-94). Dendritic spines are highly dynamic biochemical compartments constantly morphometrically modified over varied timescales to accommodate physiological states and cognitive processes. The volume of spine heads is proportional to the size of the PSD, which contains scaffolding proteins and signaling complexes, the patterning of which is also functionally relevant (92, 95, 96). The spine neck is also a critical regulator of synaptic function, achieving compartmentalization of individual synaptic inputs by restricting calcium transients (83, 97).

1.3.2 Spine changes in aging and disease. Alterations in synaptic density and functionality are often observed in the normal aging process (98). Synaptic changes in brain regions such as the hippocampus and the prefrontal cortex are associated with age related cognitive decline (87). In humans and nonhuman primates, loss of volume in the prefrontal cortex (PFC) cannot be explained by neuronal loss (99, 100). Instead, evidence suggests alterations in synaptic biology, such as connectivity, integrity and density, are more likely to explain age-related cognitive changes. In particular, thin spines appear to be more vulnerable than mushroom or stubby spine types, with more than half of age-related spine loss in PFC accounted for by thin spines (101, 102). In contrast, thin spines appear to remain relatively spared in the hippocampus, where loss

of larger, complex synaptic sites better accounts for age-related cognitive losses (87, 103, 104). Collectively, these findings highlight age-related, region-specific synaptic changes that impact different aspects of cognitive processes over time.

In AD, loss of synaptic density is the strongest correlate to cognitive decline (105, 106). Each primary pathology in AD is believed to contribute in unique ways to synaptic failure and removal. Amyloid (especially oligomeric species) has been well documented to cause dendritic spine loss, including through preferential binding of spines and interaction with several synaptic targets (107-112). Aβ oligomers may also induce synaptotoxicity by forming pores in the cell membrane and altering calcium permeability (113). The result of Aβ-induced synaptic dysfunction and loss is functionally related to network level abnormalities of hypersynchronicity and epileptiform electrophysiology (114). The relationship between tau and synaptic loss is less clear. Numerous reports suggest tau's role in synaptic dysfunction or loss is in collaboration with Aβ pathology (115-119). Tau localizes to dendritic compartments under both physiological and pathological contexts, the differentiation between states and how post-synaptic tau may participate or contribute to disease pathogenesis remains a topic of ongoing investigation (120). Alternatively, preserved numbers of neurons and overall spine density have been reported in AsymAD cases (78, 79, 121). In addition, resilient cases appear to have more thin and mushroom spines compared to symptomatic AD cases and the lengths of spines from resilient cases were significantly longer than those from both control and AD brains (79). Together these findings could implicate compensatory synaptic remodeling in resilient cases as a means to sustain cognitive abilities in the context of AD pathology. Furthermore, synaptic resilience, or the ability to maintain functional synaptic connections in the presence of AD pathology, may represent a physiological basis subserving cognitive resilience.

1.4 Resilience candidates and NRN1

1.4.1 Resilience candidates. Understanding the underlying molecular pathways influencing cognitive resilience despite AD pathological brain changes represents a complimentary approach to traditional investigation. Identifying potential targets and pathways that enable maintained synaptic density and function in an increasingly toxic cellular environment represents an avenue for novel therapeutic development that could be harnessed to benefit those at risk for AD. Previously, a proteome wide association study (PWAS) of cognitive trajectory aimed to identify individual proteins related to stable cognition independent of neuropathology, highlighting themes of increased synaptic abundance and reduced neuroinflammation which is consistent with what has been reported in the brains of resilient cases (122). In a separate study, a PWAS of cognitive resilience ranked individual proteins conferring increased or decreased cognitive resilience and identified 8 cortical proteins strongly associated with increased resilience after adjusting for common neuropathological indices, including AD (123). Seven out of the eight significant proteins were associated with increased resilience, with increased abundance of Neuritin (NRN1) as the most significant for conferring increased cognitive resilience. More recently, a large-scale proteomic analysis from our group of more than 500 control, AD and AsymAD cases identified NRN1 as the most significantly differentially abundant proteins in AsymAD cases compared to AD, with NRN1 being significantly increased in AsymAD (124).

1.4.2 Neuritin. Neuritin (NRN1) was first discovered in 1993 by Elly Nedivi and colleagues, subsequently named for its function in promoting neurite outgrowth (125-127). NRN1, encoded by candidate plasticity gene 15 (CPG15), is an activity-regulated neurotrophic factor. In brain tissue, where NRN1 is the most abundant, NRN1 is expressed in the neuronal cell body, dendrites, axons and axon terminals (127, 128). Two forms of NRN1 have been described, a soluble form and a membrane bound form attached by a glycosylphosphatidylinosotol (GPI) anchor. In the adult CNS, NRN1 exists predominantly in the soluble form where it functions in a diffusible, non-cell autonomous manner (129). Functions of NRN1 have been described as

biphasic, contributing to neurodevelopment and later in neural plasticity. In the developing brain NRN1 promotes the survival of progenitor cells, neuritogenesis, axonal and dendritic elaboration and synaptic maturation contributing to the establishment of functional neuronal circuits (127, 129-132). In the developed brain, NRN1 mediates neuronal communication through modified synaptic plasticity and transmission efficiency (133-135).

Importantly, the role of NRN1 has been reported in the context of several disease modifying conditions, including depression, stress and psychiatric disease (133, 136-142). Models of depression and stress indicate a role for neuritin in preventing stress-induced dendritic atrophy, modifying depression-related executive dysfunction and increased levels of NRN1 following both electroconvulsive therapy and antidepressant administration have been reported (133, 136-139). Evidence from genetic and neuroimaging data also link NRN1 to modification of cognitive deficits and onset of symptoms in schizophrenia and bipolar disorders (140-142). Specifically in the context of AD, NRN1 is significantly decreased in human AD brains (124, 143) and experimental evidence suggests NRN1 can rescue AD pathology induced deficits in neuronal communication and behavior. In the Tg2576 mouse model of AD (a widely used amyloid-centric transgenic model that overexpresses human mutant APP resulting amyloid plaque deposition and cognitive decline (144)), NRN1 administration restored dendritic complexity and improved long-term potentiation in hippocampal neurons (145). In the same mouse model, NRN1 infusion resulted in increased presynaptic protein marker expression and improved outcomes in learning paradigms (143). NRN1 represents a potentially valuable protein target in mediating resilience in AD (**Fig. 1.3**).

1.5 Research objectives and contributions.

The dissertation work presented here includes the characterization and unbiased nomination of resilience associated molecular signatures in human post-mortem brain from

cognitively resilient individuals. This was followed by a series of validation experiments that provide insights into neuroprotective roles of NRN1 as a resilience candidate in the context AD relevant insults and provide a framework for future target validation. Quantitative proteomics of matched tissue from two brain regions (Brodmann area 6 and Brodmann area 37) paired with consensus network analysis resulted in several co-expressed protein clusters (modules) positively correlated with stable cognition in the context of significant AD pathology. Integration of external proteomic results prioritizing associations with increased or decreased cognitive resilience nominated four modules significantly enriched for markers of increased resilience. Importantly, NRN1 was identified as a hub protein of a top resilience module and among the most significantly differentially expressed proteins increased in asymptomatic cases. NRN1 has gained increasing recognition as a potential resilience-associated candidate from our work and that of others. To validate our systems level analysis and determine the function of NRN1 in the context of AD neurobiology, microscopy and physiology-based analyses were performed in a rat primary cell model of AD. We report that NRN1 co-treatment with amyloid oligomers was sufficient to rescue gross spine density loss due to Aβ. In addition, NRN1 co-treatment rescued hyperexcitability induced by Aβ exposure. Proteomic analysis of NRN1 treatment in primary neurons revealed strong enrichment of synaptic biology markers following incubation. Integration of results from our cellular model with the consensus human network revealed proteins increased following NRN1 treatment largely overlapped with module members of top resilience modules from human brain. Clear questions remain regarding mechanisms of protection that may result from NRN1 treatment, however, the results presented herein support NRN1 as a promising target for promoting resilience. Novel contributions to the field include: 1) the use of multi-region brain proteomics network analysis to characterize proteins and pathways associated with resilience in human brain, 2) mechanistic validation of NRN1 as protective from Aβ oligomer insult in vitro, and

3) demonstration that NRN1 induced neuronal proteomic changes are biologically relevant to human brain modules strongly associated with cognitive resilience.

1.6 Figures

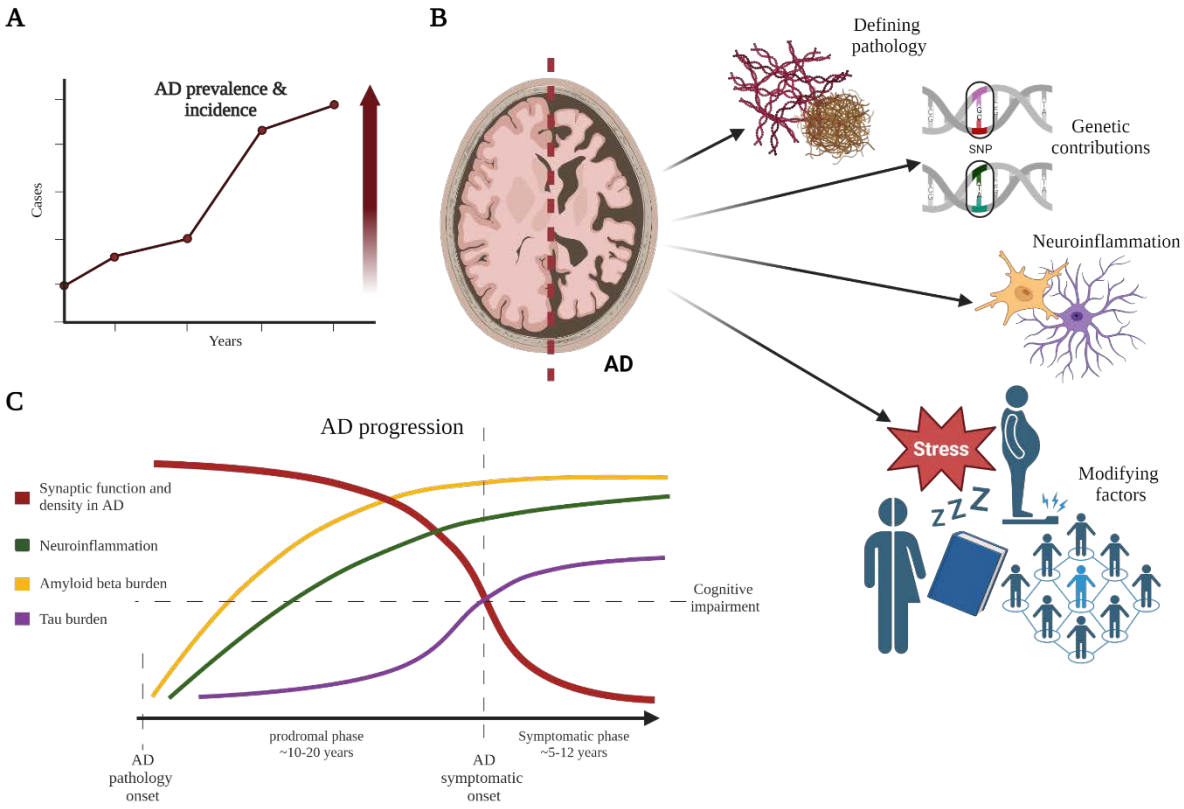

Figure 1.1: Overview of Alzheimer's disease. Conceptual illustration of the overarching themes in AD research. **A**) The prevalence and incidence of AD continues to rise (1), presenting an increasing public health burden. **B**) AD is a multifactorial disease defined by pathological hallmarks (amyloid and tau deposition) and modified by genetics, physiology and various lifestyle and health factors. **C**) Theoretical model (Jack curve style (146)) of disease progression over time in which pathological changes can begin decades prior to clinical manifestation.

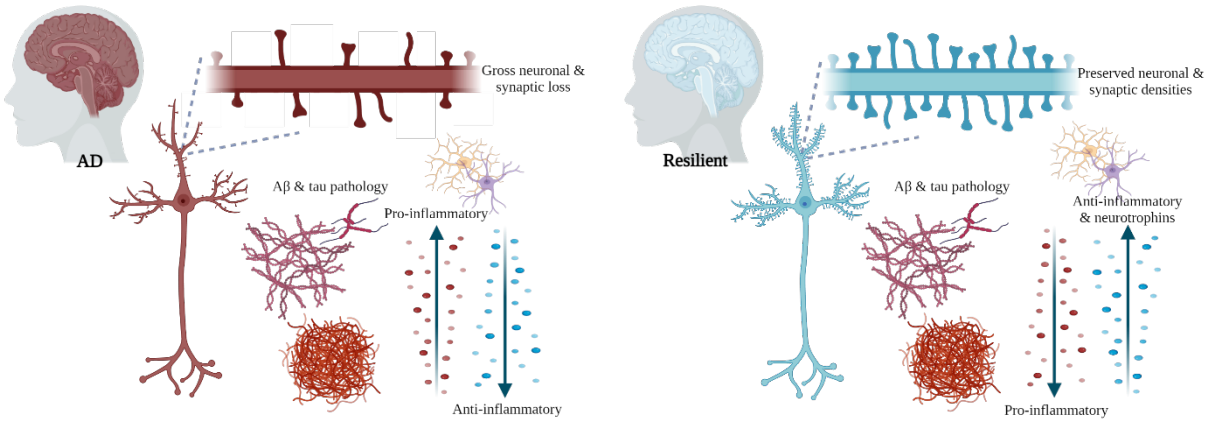

Figure 1.2: Features of cognitively resilient individuals. Illustration of notable features reported for cognitively resilient individuals that contrast with typical symptomatic AD cases, including preserved neuronal and synaptic densities despite accumulation of moderate to severe AD pathology. Observation of decreased pro-inflimmatry molecules and increased anti-inflammatory molecules and neurotrophins in the brain of asymptomatic cases have also been reported.

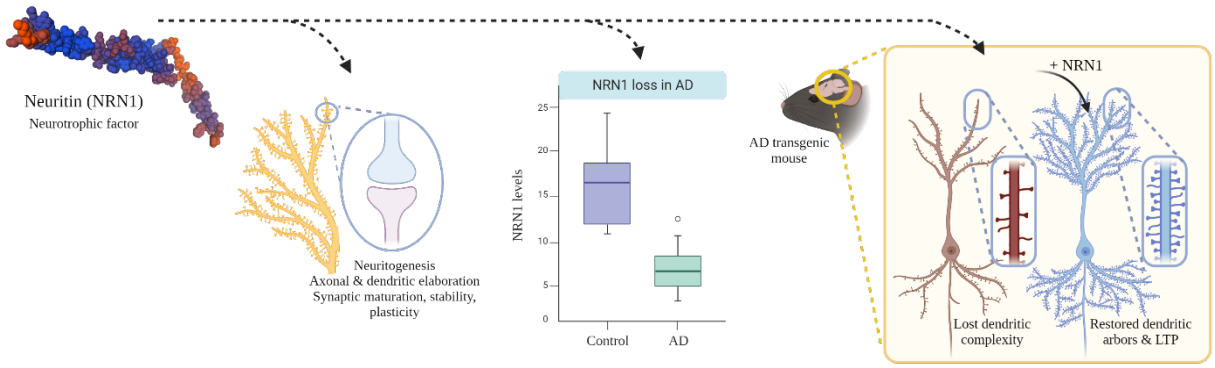

Figure 1.3: Neuritin (NRN1) as a candidate resilience-promoting factor. NRN1 is a small neurotrophic factor with potentially attractive functions that may explain it's reported relationship with cognitive resilience. NRN1 modifies and regulates synaptic biology, is significantly lost in human AD brains and can restore dendritic complexity and long term potnentiation (LTP) in AD transgenic mice.

Chapter 2.0: Discovery proteomics to characterize molecular signatures in cognitively resilient cohorts

* This chapter was adapted from findings published in the *Molecular and Cellular Proteomics* Journal in April 2023. https://doi.org/10.1016/j.mcpro.2023.100542

2.1 Introduction

As the aging population continues to expand, the public health burden of Alzheimer's disease (AD) is projected to reach staggering numbers without the advent of effective disease altering therapies (147). AD is an irreversible neurodegenerative disease defined by its pathological hallmarks, amyloid-beta (Aβ) plaques and tau neurofibrillary tangles (NFTs) (148). Functional imaging and biomarker studies suggest AD pathological brain changes could initiate up to two decades before symptom onset, indicating a protracted prodromal disease phase ideal for early intervention (43). Importantly, many older individuals without dementia or mild cognitive impairment (MCI) meet pathologic criteria for AD. Approximately one-third of individuals harbor high levels of AD and related disease pathology in their brains at autopsy but showed little to no signs of cognitive impairment in their lifetime (77, 149). These cognitively normal people with AD pathology are described as preclinical or asymptomatic AD (AsymAD) and appear to exhibit cognitive resilience to the clinical manifestations of AD dementia. One working hypothesis is that such individuals possess physiological resilience that confers the ability to maintain cognitive function despite the accumulation of AD-related pathologies (150-152). Identifying the specific mechanisms by which older individuals with AD pathology avoid dementia onset is one of the most pivotal, unanswered questions in the field.

Cognitive impairment in AD is the result of lost neuronal connectivity in brain regions critical to memory and other cognitive processes. For cognitive impairment to develop, there must be loss or dysfunction of the neural elements that subserve cognition, e.g., neurons, synapses and dendritic spines. Our work and that of others demonstrate preservation of neuron numbers and synaptic markers as well as enhanced dendritic spine remodeling in resilient cases (78, 79, 153). Together this implies that the ability to maintain cognitive function in an environment of AD pathology is linked to the preservation and maintenance of synapses or spines. These findings raise important questions: 1) what are the molecular pathways that drive preservation of synaptic

connections and maintenance of cognitive abilities in resilient individuals? 2) How can we identify protein targets to exploit these mechanisms for therapies in at risk patients?

Previous efforts to address these gaps in knowledge using proteomics have focused primarily on a single brain region, the dorsolateral prefrontal cortex (DLPFC) (122-124). Individual proteins and protein communities have been reported with associations to cognitive resilience, but it is not clear whether these proteome changes are exclusive to the brain region that was analyzed. AD pathology is present across numerous cortical and subcortical regions in the brain (2, 3), therefore, we hypothesized that proteins contributing to physiological resilience would likely act across more than one brain region. In the present study we implemented a systems-level multi-region network analysis of human postmortem brain tissue derived from the Religious Order and Rush Memory and Aging Project (ROSMAP). ROSMAP is an information-rich longitudinal cohort-based study in which participants enroll without dementia, undergo annual cognitive and clinical assessments and donate their brains at death (154). Matched brain tissue from two brain regions was analyzed via multiplex tandem mass tag mass spectrometry (TMT-MS) based proteomics followed by consensus correlation network analysis (cWGCNA). Brodmann area 6 (BA6) and Brodmann area 37 (BA37) were selected for their pathologically distinct features, where BA6 (frontal cortex) has predominant amyloid pathology and BA37 (temporal cortex) exhibits prominent tau-related pathology. We prioritized modules or communities of proteins that were enriched with markers of cognitive resilience identified from an independent brain proteome wide association study (PWAS) of cognitive trajectory (123). This revealed proteins linked to synaptic biology and cellular energetics. Notably, neuritin (NRN1) was identified as a hub protein that co-expressed with other synaptic proteins that remained increased in AsymAD compared to symptomatic AD cases. Identification of NRN1 and its relationship to resilience corroborates previous results of increased NRN1 abundance in cognitive stability and thus suggests NRN1 as an attractive potential resilience-promoting target (123, 124).

2.2 Results

2.2.1 Proteomic measurements align with neuropathological scores

Matched post-mortem brain tissue samples from Brodmann area 6 (BA6) and Brodmann area 37 (BA37) from 109 Religious Orders Study and Rush Memory and Aging Project (ROSMAP, n=218 samples total) cases were analyzed using multiplex tandem mass tag mass spectrometry (TMT-MS; **Fig. 2.1A**). BA6 is a frontal cortex area containing the premotor and supplementary motor cortices, important for roles in motor, language and memory functions (155). BA37 resides in the temporal cortex and contains the fusiform gyrus which has been linked to disrupted language and memory function in AD (156). Cases were classified as Control, asymptomatic Alzheimer's disease (AsymAD) or Alzheimer's disease (AD) based on semi-quantitative measures of amyloid (CERAD) and tau (Braak) deposition as well as cognitive function near time of death (**Fig. S2.1**) (124, 157). This classification strategy, similar in concept to the A/T/N framework, which stratifies cases based on presence or absence of Amyloid, Tau and Neurodegeneration, allows distinction of cases with increased neuropathological burden but intact cognitive function (158). TMT-MS quantified protein levels were filtered for missing values in less than 50% of samples and adjusted for batch-effects, outlier removal and confounding effects of covariates (age, sex and post-mortem interval or PMI) for a final expression dataset of 7,787 proteins (**Fig. S2.2**).

Protein levels related to the primary AD pathologies, APP (amyloid precursor protein) and MAPT (microtubule associated protein tau), were compared across disease groups and brain regions (**Fig. 2.1B-C**). APP levels served as a surrogate measurement for Aβ and as expected were significantly higher in AsymAD and AD cases compared to Controls in both brain regions (**Fig. 2.1B;** (124, 159)). Consistently, we also assessed individual tryptic peptides mapping to the Aβ sequence in APP. As seen at the protein level with APP, these Aβ peptides were significantly increased in both AsymAD and AD cases compared to control and positively correlated with

CERAD scores in each brain region (**Fig. S2.3**). MAPT levels were significantly higher in AD compared to AsymAD in BA6 and significantly increased in AD compared to both Control and AsymAD in BA37 (**Fig. 2.1C**). APP levels positively correlated with CERAD scores, irrespective of brain region, and exhibited higher baseline levels in BA6 (**Fig. 2.1D**). MAPT levels in BA37, but not BA6, positively correlated with Braak scores (**Fig. 2.1E**). These measurements align with well-established region-specific neuropathological burden observed in AD in which amyloid pathology manifests initially in neocortical regions while NFT pathology originates and intensifies in trans-entorhinal cortex regions before spreading to temporal and frontal cortical areas (2, 3). CERAD and Braak scores are both semi-quantitative measurements that profile global plaque or NFT pathology, respectively. Whereas, APP and MAPT protein abundance discussed here is quantified in a single brain region (BA6 or BA37), offering an explanation for the lack of correlation of MAPT and Braak in BA6. Collectively, these strong positive correlations of APP levels with CERAD scores and MAPT levels with Braak scores highlight the accuracy of the proteomic measurements in quantifying relevant AD neuropathological burden.

Consistent with these targeted pathology-linked proteins (APP and MAPT), differential expression of all quantified proteins was assessed (**Supplemental Tables 1 and 2**). As expected, proportional numbers of significantly different proteins were identified in disease groups across brain regions compared to controls (BA6: Control vs AsymAD = 222, Control vs AD = 1,102; BA37: Control vs AsymAD = 129, Control vs AD = 1,550). This suggests that the differences in the proteome correspond proportionately with differences in neuropathology as previously described (159). In addition, the greater number of differentially expressed proteins in BA37 compared to BA6, underscores the regional difference across the two brain regions. Our analysis provides a comprehensive list of differentially expressed proteins that align with brain region-specific pathology in AD.

2.2.2 Regional brain co-expression network analysis reveals modules associated with AD pathology and cognition

A correlation network was constructed using the consensus weighted gene co-expression network analysis (cWGCNA) algorithm, a systems biology approach to identify biologically meaningful, co-expression patterns (160, 161). The consensus configuration allows the identification of highly preserved modules, or clusters of interconnected proteins, shared across BA6 and BA37 while retaining region-specific relationships (**Fig. S2.2B-C**). A total of 39 co-expression modules (M1-M39) were defined, ranging in size from 36 members (M39) as the smallest and 473 members (M1) as the largest **(Fig. 2.2A**; **Supplemental Tables 3 and 4**). Similar patterns of inter-module relationships were observed in BA6 and BA37 (**Fig. S2.4A**). Gene Ontology (GO) analysis was performed on the protein members of each consensus module and top-ranking GO terms across multiple ontology types were considered in determining representative module biology. To detect modules related to neuropathological burden and cognitive changes, module eigenproteins (the first principle component of the expression matrix; MEs) were correlated with Aβ plaque ("Amyloid") and neurofibrillary tangle (NFT; "Tangles") burden in the brain at autopsy as well as global cognitive scores and cognitive slope for each person prior to death (**Supplemental Tables 5 and 6**). Immunohistochemistry and systematic sampling of 8 brain regions were averaged to determine Amyloid and Tangle load (162). Global cognition is a composite score of 19 cognitive performance tests and cognitive slope is calculated based on changes in cognitive performance over time (154). To understand group-wise differences in MEs, modules were further characterized according to AD vs Control and AsymAD vs AD pairwise differences. Finally, cell-type contribution of each module was assessed by determining cell-type marker enrichment for neuronal, oligodendrocyte, astrocyte, microglia and endothelial cell-types (**Supplemental Tables 7 and 8**) (124).

Module preservation of the current consensus regional network was compared to a recent, large-scale network analysis of human dorsolateral prefrontal cortex (Brodmann area 9, BA9) generated from ROSMAP and Banner cases (124). Preservation of modules from the BA9 network were checked in multiple brain regions, including the data of the current study. However, the current network configuration is a new analysis in which BA6 and BA37 are being considered in a single, shared network. Notably, approximately 95% (37/39) of the consensus modules preserved with the previous TMT-MS network (**Fig. S2.5A**) and all 39 consensus modules from this study had significant protein overlap with at least one module from the BA9 network (**Fig. S2.5B**). Thus, modules generated by cWGCNA are robust and highly preserved across different cohorts and brain regions.

From the present network, we observed interplay of module biology with cognition, disease status and brain region. Specifically, a cluster of five modules were identified as positively correlated with cognition and were increased in AsymAD compared to AD similarly in both brain regions: M22 Synapse, M5 Synapse, M36 Exocytosis, M25 Ribosome, M30 Mitochondria/ER (**Fig. 2.2**). We also observed modules following this pattern in only one brain region: M2 Mitochondrion was only significant in BA37 and M4 Synaptic vesicle was only significant in BA6. In contrast, M15 MAPK signaling and M16 Gluconeogenesis were the most strongly negatively correlated with cognition and decreased in AsymAD compared with AD. These findings are consistent with previous proteomic findings in BA9 where sugar metabolism and MAPK signaling modules were significantly related to cognition (124). Overall, we generated a consensus network, highly consistent with previous brain proteome network modules, that sufficiently outlined key differences and an interrelationship among clinical traits, disease groups and even regional brain differences.

2.2.3 Nomination of resilience-associated modules and NRN1 as top protein candidate

To increase external validity while expanding upon previous findings and unbiasedly nominating consensus modules linked to resilience, we integrated the results from a recent brain proteome-wide association study (PWAS) of cognition that evaluated the association of cortical protein abundances with cognitive resilience from an independent TMT-MS proteomic analysis of ROSMAP tissues adjusted for AD pathologies (123). Samples from the current study and previous PWAS were processed and analyzed separately, with only 30 cases shared across cohorts. Higher abundances of proteins related to slower rates of cognitive decline were considered to confer greater resilience while higher abundance of proteins associated with faster rate of cognitive decline were considered to confer less resilience. Four modules were identified as significantly enriched with proteins conferring greater cognitive resilience: M22 Synapse, M5 Synapse, M36 Exocytosis and M30 Mitochondria/ER (**Fig. 2.3A; Supplemental Table 9**). In addition, four modules were found to be significantly enriched for proteins conferring less cognitive resilience: M11 Proteosome, M15 MAPK signaling, M32 GPCR signaling and M16 Gluconeogenesis (**Supplemental Table 10**). Of the modules associated with greater resilience, the protein constituents of M5 and M22 were strongly representative of synaptic biology and enriched for neuronal markers. To further confirm association of M5 and M22 to cognitive preservation, MEs were correlated to cognitive slope and indicated strong positive correlation in both brain regions (**Fig. 2.3B**). Consistently, differential expression comparing AsymAD with AD of proteins specific to M5 and M22 exhibited a strong bias towards an increase or upregulation of proteins in AsymAD **(Fig. 2.3C**). Two proteins significantly upregulated in AsymAD were also significant in the aforementioned PWAS of cognition (123), Neuritin (NRN1) and Rabphilin-3A (RPH3A). NRN1 was more significantly differentially expressed than RPH3A and NRN1 was the most significant protein associated with increased cognitive resilience in the PWAS. NRN1 abundance in both brain regions was compared across disease groups and indicated comparable levels in AsymAD and controls but NRN1 was significantly downregulated in AD (**Fig. 2.3D**).

NRN1 abundance also strongly, positively correlated with cognitive measures including global cognition and cognitive slope (Global cognition: BA6 pvalue= 2.9e-09, BA37 pvalue= 2.2e-09; Cognitive slope: BA6 pvalue= 1.8e-08, BA37 pvalue= 6.4e-07 **Fig. 2.3E-F**). Furthermore, variance partition analysis of global cognition in BA6 and BA37 identified NRN1 as the top (B6: ~26% variance explained) and second (BA37: ~38% variance explained) protein explaining the highest variance in global cognition (**Fig. S2.6A-B; Supplemental Tables 11 and 12**).

In summary, integration of independent human proteomic datasets prioritized protein modules associated with cognitive resilience across two brain regions. Four modules (M22, M5, M36, and M30) were significantly enriched for proteins linked to greater cognitive resilience in life. Two modules (M22 and M5) captured biology related to synaptic integrity and were found to be vulnerable in AD but preserved in asymptomatic cases. NRN1 was identified as a hub protein in M5 and NRN1 abundance levels were significantly increased in AsymAD cases compared to AD. Notably, the differences between AsymAD and AD across brain regions observed in this study via TMT-MS is highly consistent with other large-scale label free proteomic datasets from several patient cohorts (157). The reproducibility and rigor of this analysis strongly supports our hypothesis that NRN1 is a protein mediator of cognitive resilience.

2.3 Materials and methods

Human postmortem brain tissue and case classification

Paired brain tissue samples from frontal cortex (Brodmann area 6, BA6) and temporal cortex (Brodmann area 37, BA37) were obtained from the Religious Orders Study and Rush Memory and Aging Project (ROS/MAP; n=256 total samples) in accordance with proper Institutional Review Board (IRB) protocols of the home institution. Postmortem neuropathological evaluation of neuritic plaque distribution was performed according to the Consortium to Establish a Registry for Alzheimer's Disease (CERAD) criteria (9) and extent of neurofibrillary tangle pathology was assessed with the Braak staging system (3). All case metadata were provided as deidentified and are available at https://www.synapse.org/#!Synapse:syn22695346. Case classification was determined according to a previously established and peer-reviewed strategy (124, 157). In brief, cases with CERAD scores of 0-1 and Braak scores 0-3 without dementia at last evaluation were defined as control (if Braak equals 3, then CERAD must equal 0; BA6: n=24, BA37: n=24); cases with CERAD scores 1-3 and Braak scores 3-6 without dementia at last evaluation were defined as AsymAD (BA6: n=53, BA37: n=52); cases with CERAD 2-3 and Braak 3-6 with dementia at last evaluation were defined as AD (BA6: n=32, BA37: n=33). Dementia was defined at MMSE (Mini Mental State Examination) scores <24 (163).

Brain tissue homogenization

Sample homogenization was performed as previously descried (124). Approximately 100 mg (wet tissue weight) of brain tissue was homogenized in 8 M urea lysis buffer (8 M urea, 10 mM Tris, 100 mM NaH_2PO_4, pH 8.5) with HALT protease and phosphatase inhibitor cocktail (Thermo Fisher Scientific) using a Bullet Blender (Next Advance). Each RINO sample tube (Next Advance) was supplemented with ~100 µl of stainless-steel beads (0.9–2.0 mm blend, Next Advance) and 500 µl of lysis buffer. Tissues were added immediately after excision and homogenized with Bullet Blender at 4 °C with two full 5-min cycles. The lysates were transferred to new Eppendorf LoBind

tubes and sonicated for three cycles consisting of 5 s of active sonication at 30% amplitude, followed by 15 s on ice. Samples were then centrifuged for 5 min at 15,000*g* and the supernatant transferred to a new tube. Protein concentration was determined by bicinchoninic acid assay (Pierce) and one-dimensional SDS-PAGE gels were run followed by Coomassie blue staining as quality control for protein integrity and equal loading before proceeding to protein digestion.

Brain protein digestion

For protein digestion (as described (124, 159, 164)), 100 µg of each sample was aliquoted, and volumes were normalized with additional lysis buffer. Samples were reduced with 1 mM dithiothreitol at room temperature for 30 min, followed by 5 mM iodoacetamide alkylation in the dark for another 30 min. Lysyl endopeptidase (Wako) at 1:100 (wt/wt) was added, and digestion was allowed to proceed overnight. Samples were then seven-fold diluted with 50 mM ammonium bicarbonate. Trypsin (Promega) was added at 1:50 (wt/wt), and digestion was carried out for another 16 h. The peptide solutions were acidified to a final concentration of 1% (vol/vol) formic acid (FA) and 0.1% (vol/vol) trifluoroacetic acid (TFA) and de-salted with a 30-mg HLB column (Oasis). Each HLB column was first rinsed with 1 ml of methanol, washed with 1 ml of 50% (vol/vol) acetonitrile (ACN) and equilibrated with 2× 1 ml of 0.1% (vol/vol) TFA. The samples were then loaded onto the column and washed with 2× 1 ml of 0.1% (vol/vol) TFA. Elution was performed with 2 volumes of 0.5 ml of 50% (vol/vol) ACN. An equal amount of peptide from each sample was aliquoted and pooled as the pooled global internal standard (GIS), which was split and labeled in each TMT batch as described below. The eluates were then dried to completeness using a SpeedVac.

Tandem Mass Tag (TMT) peptide labeling for the brain proteome

Before TMT labeling, cases were randomized by covariates (age, sex, PMI, diagnosis, etc.), into the 26 total batches. Peptides from each individual case and the GIS pooled standard or bridging sample (at least one per batch) were labeled using the TMT 11-plex kit (ThermoFisher 90406).

Labeling was performed as described (124, 164-166). In each batch, up to two TMT channels were used to label GIS standards, and the remaining TMT channels were reserved for individual samples after randomization. In brief, each sample (containing 100 µg of peptides) was re-suspended in 100 mM TEAB buffer (100 µl). The TMT labeling reagents (5 mg) were equilibrated to room temperature, and anhydrous ACN (256 µl) was added to each reagent channel. Each channel was gently vortexed for 5 min, and then 41 µl from each TMT channel was transferred to the peptide solutions and allowed to incubate for 1 h at room temperature. The reaction was quenched with 5% (vol/vol) hydroxylamine (8 µl) (Pierce). All channels were then combined and dried by SpeedVac (Labconco) to approximately 150 µl and diluted with 1 ml of 0.1% (vol/vol) TFA and then acidified to a final concentration of 1% (vol/vol) FA and 0.1% (vol/vol) TFA. Labeled peptides were de-salted with a 200-mg C18 Sep-Pak column (Waters). Each Sep-Pak column was activated with 3 ml of methanol, washed with 3 ml of 50% (vol/vol) ACN and equilibrated with 2× 3 ml of 0.1% TFA. The samples were then loaded, and each column was washed with 2× 3 ml of 0.1% (vol/vol) TFA, followed by 2 ml of 1% (vol/vol) FA. Elution was performed with 2 volumes of 1.5-ml 50% (vol/vol) ACN. The eluates were then dried to completeness using a SpeedVac.

High-pH offline fractionation for the brain proteome

Fractionation was conducted as described (124, 165, 167). Dried samples were re-suspended in high-pH loading buffer (0.07% v/v NH4OH, 0.045% v/v FA, 2% v/v ACN) and loaded onto an Agilent ZORBAX 300 Extend-C18 column (2.1 mm x 150 mm with 3.5 um beads). An Agilent 1100 HPLC system was used to carry out the fractionation. Solvent A consisted of 0.0175% (vol/vol) NH4OH, 0.01125% (vol/vol) FA, and 2% (vol/vol) ACN; solvent B consisted of 0.0175% (vol/vol) NH4OH, 0.01125% (vol/vol) FA, and 90% (vol/vol) ACN. The sample elution was performed over a 58.6 min gradient with a flow rate of 0.4 mL/min. The gradient consisted of 100% solvent A for 2 min, then 0% to 12% solvent B over 6 min, then 12% to 40 % over 28 min, then 40% to 44% over 4 min, then 44% to 60% over 5 min, and then held constant at 60% solvent B for 13.6 min.

A total of 96 individual equal volume fractions were collected across the gradient and subsequently pooled by concatenation (167) into 24 fractions and dried to completeness using a SpeedVac.

Liquid chromatography- tandem mass spectrometry (LC-MS/MS) for the brain proteome

All fractions were resuspended in an equal volume of loading buffer (0.1% FA, 0.03% TFA, 1% ACN) and analyzed by LC–MS/MS essentially as described (124, 168)Peptide eluents were separated on a self-packed C18 (1.9 µm, Dr. Maisch) fused silica column (25 cm × 75 µM internal diameter, New Objective) by a Dionex UltiMate 3000 RSLCnano liquid chromatography system (Thermo Fisher Scientific) for the ROSMAP samples. Peptides were monitored on an Orbitrap Fusion mass spectrometer (Thermo Fisher Scientific). sample elution was performed over a 120-min gradient with flow rate of 300 nl min^{-1} with buffer B ranging from 1% to 50% (buffer A: 0.1% FA in water; buffer B: 0.1% FA in 80% ACN). The mass spectrometer was set to acquire in data-dependent mode using the top speed workflow with a cycle time of 3 s. Each cycle consisted of one full scan followed by as many MS/MS (MS2) scans that could fit within the time window. Full MS scans were collected at a resolution of 120,000 (400–1,400 *m*/*z* range, 4×10^5 AGC, 50-ms maximum ion injection time). All HCD MS/MS spectra were acquired at a resolution of 60,000 (1.6 *m*/*z* isolation width, 35% collision energy, 5×10^4 AGC target, 50-ms maximum ion time). Dynamic exclusion was set to exclude previously sequenced peaks for 20 s within a 10-ppm isolation window.

Database searching and protein quantification for the brain proteome

All raw MS data files (624 total RAW files generated across 26 batches) were analyzed in the Proteome Discover software suite (version 2.3, ThermoFisher) and MS/MS spectra were searched against the UniProtKB human proteome database (downloaded April 2015 with 90,411 total sequences). The Sequest HT search engine was used with the following parameters: fully tryptic specificity; maximum of two missed cleavages; minimum peptide length of 6; fixed

modifications for TMT tags on lysine residues and peptide N-termini (+229.162932 Da) and carbamidomethylation of cysteine residues (+57.02146 Da); variable modification for oxidation of methionine residues (+15.99492 Da) and deamidation of asparagine and glutamine (+0.984 Da); precursor mass tolerance of 20 ppm; and fragment mass tolerance of 0.05 Da. Peptide spectral matches (PSMs) were filtered to a false discovery rate (FDR) of less than 1% using the Percolator node. Following spectral alignment, peptides were assembled into proteins and further filtered based on the combined probabilities of their constituent peptides to a final FDR of 1%. Multi-consensus was performed to achieve parsimony across individual batches. In cases of redundancy, shared peptides were assigned to the protein sequence in adherence with the principles of parsimony. Reporter ions were quantified from MS2 scans using integration tolerance of 20 ppm with the most confident centroid setting. Only PSMs with less than 50% isolation interference were used for quantification and only unique and razor (i.e., parsimonious) peptides were considered for quantification.

Batch correction and data pre-processing for the brain proteome

A total of 10,426 high confidence, master proteins were identified across all 26 TMT batches, but only proteins quantified in >50% of samples were included in subsequent analyses (n=7,787 proteins). Log2 abundances were normalized as a ratio dividing by the central tendency of pooled standards (Global Internal Standards; GIS). As previously applied, batch correction was performed using a Tunable Approach for Median Polish of Ratio (https://github.com/edammer/TAMPOR; TAMPOR), an iterative median polish algorithm for removing technical variance across batch (124). Multidemensional scaling (MDS) plots were used to visualize batch contributions to variation before and after batch correction (**Fig. S1**). Network connectivity was used to remove outliers, that is samples that were greater than 3 standard deviations away from the mean as described (124). Finally, non-parametric bootstrap regression was performed to remove the potentially confounding covariates of age, sex and post-mortem

interval (PMI). Each trait was subtracted times the median coefficient from 1000 iterations of fitting for each protein, while protecting for diagnosis (Control, AsymAD, AD).

Consensus Weighted Gene Correlation Network Analysis (cWGCNA)

We used the consensus Weighted Gene Correlation Network Analysis (cWGCNA; version 1.69) algorithm to generate a central network of co-expression modules from both brain regions (160, 161). The WGCNA::blockwiseConsensusModules function was run with soft threshold power at 7.0, deepsplit of 4, minimum module size of 30, merge cut height at 0.07, mean topological overlap matrix (TOM) denominator, using bicor correlation, signed network type, pamStage and pamRespectsDendro parameters both set to TRUE and a reassignment threshold of 0.05. This function calculates pair-wise biweight mid-correlations (bicor) between protein pairs. The resulting correlation matrix is then transformed into a signed adjacency matrix which is used to calculate a topological overlap matrix (TOM), representing expression similarity across samples for all proteins in the network. This approach uses hierarchical clustering analysis as 1 minus TOM and dynamic tree cutting lends to module identification. Following construction, module eigenprotein (ME) values were defined – representative abundance values for a module that also explain modular protein covariance. Pearson correlation between proteins and MEs was used as a module membership measure, defined as kME.

Network preservation

We used the WGCNA::modulePreservation() function to assess the network module preservation of our current consensus network with recent large-scale TMT network from Brodmann area 9 (BA9) (124). Zsummary composite preservation scores were obtained using the consensus network as the test network and the previous BA9 TMT network as the reference network., with 500 permutations. Random seed was set to 1 for reproducibility, and the quickCor option was set to 0.

Gene ontology (GO) and cell type marker enrichment analyses for the brain proteome

To characterize differentially expressed proteins and co-expressed proteins based on GO annotation we used GO Elite (version 1.2.5) as previously described (124, 159, 169), with pruned output visualization using an in-house R script. Cell type enrichment was also investigated as previously published (124, 159, 169). An in-house marker list combined previously published cell type marker lists from Sharma et al. (170) and Zhang t al. (171) were used for the cell type marker enrichment analysis for each of the five cell types assessed (neuron, astrocyte, microglia, oligodendrocyte and endothelial; **Supplemental Table 7**). If, after the lists from Sharma et al. and Zhang et al. were merged, gene symbol was assigned to two cell types, we defaulted to the cell type defined by the Zhang et al. list such that each gene symbol was affiliated with only one cell type. The gene symbols in the list were processed through MyGene to ensure updated nomenclature and then converted human symbols using homology lookup. Fisher's exact tests were performed using the human cell type marker lists to determine cell type enrichment and were corrected by the Benjamini-Hochberg procedure (**Supplemental Table 8**).

Proteome Wide Association Study (PWAS) results module enrichment analysis

Proteins (*n* = 8,356) tested in the PWAS study by Yu et al. (172) for correlation to cognitive resilience (or decline, when negatively correlated) were split into lists of unique gene symbols representing protein gene products positively correlated (*n* = 645) and negatively correlated (*n* = 575) to cognitive resilience, and then these lists with corresponding *P* values were separately checked for enrichment in consensus TMT network modules using a permutation-based test (10,000 permutations) implemented in R with exact *P* values for the permutation tests calculated using the permp function of the statmod package. Module-specific mean *P* values for risk enrichment were determined as a *Z* score, specifically as the difference in mean *P* value of gene product proteins hitting a module at the level of gene symbol minus the mean *P* value of genes

hit in the 10,000 random replacement permutations, divided by the standard deviation of *P* value means also determined in the random permutations (**Supplemental Tables 9 and 10**).

Additional statistical analyses

All proteomic statistical analyses were performed in R (version 4.0.3). Box plots represent the median and 25th and 75th percentile extremes; thus the hinges of a box represent the interquartile range of the two middle quartiles of data within a group. Error bars extents are defined by the farthest data points up to 1.5 times the interquartile range away from the box hinges. Correlations were performed using biweight midcorrelation function from the WGCNA package. Group comparisons in human brain samples were performed with one-way ANOVA with Holm post hoc correction of all comparisons.

2.4 Discussion

Work presented here includes the implementation of an integrative pipeline for systems-level nomination of proteins and pathways related to cognitive resilience to Alzheimer's disease in multiple human brain regions. This approach enables both unbiased profiling and bidirectional integration of molecular and clinical data. Following the current framework, TMT-MS based proteomic data from two independent studies and a total of three brain regions were incorporated to characterize communities of proteins from an in-depth proteomic dataset strongly related to cognitive resilience. NRN1, a neurotrophic factor previously reported for its association to resilience and synaptic function, was identified as a hub protein in the human consensus network.

Correlation networks have been applied successfully to many biological and translational questions and have demonstrated validity in identifying candidate biomarkers and therapeutic targets (160, 173). Herein, cWGCNA resolved 39 co-expression modules across two brain regions from Control, AsymAD and AD cases from ROSMAP. Applying the consensus configuration of WGCNA for matched brain tissues from the same cases identified protein communities shared across both BA6 and BA37. Module eigenprotein correlation with pathological and clinical traits further illuminated patterns of preservation in asymptomatic cases related to synaptic biology, cellular energetics and protein translation. Importantly, the majority of modules identified in this study preserve with a recent, large-scale network analysis, generated under different parameters, which included over 1000 cases from multiple institutions, supporting the strength and reproducibility of our findings (124). Results from an independent proteome-wide association study of cognition were then integrated to outline resilience associated modules in our network, which included four modules significantly enriched for proteins conferring increased resilience. Among these, M5 and M22 were the most significantly enriched for synaptic biology and displayed strong positive correlation with cognitive performance in life. NRN1, a hub of M5, has been identified as a top protein candidate of resilience previously by its relationship with

cognitive trajectory (123), which is corroborated in the current study by its preservation in AsymAD cases and correlation with elevated cognitive function in life. NRN1, also known as candidate plasticity gene 15 (*CPG15*), is a neurotrophic factor that was initially discovered in a screen to identify genes involved in activity-dependent synaptic plasticity in the rat dentate gyrus (125). Over the past two decades, the role of NRN1 in regulating neurodevelopment, specifically the formation of axonal arbors and dendritic branching, has been extensively studied (126, 127, 131, 132, 145, 174-176). In adult brain, NRN1 strongly correlates with synaptic maturation, long-term stability and activity-related plasticity (125, 131, 132, 135, 175, 176). Importantly, NRN1 was identified among proteins previously shown in multiple studies to relate to increased cognitive function and resilience to AD, including VGF, NPTX2, and RPH3A (122, 124, 172). The established link between synaptic loss and cognitive impairment in AD and the predominance of synaptic proteins in our top resilience-associated modules, warrants examining the impact of NRN1 on synaptic integrity and maintenance as foundational to determining NRN1's role in resilience.

Despite the advantages of TMT for multiplex analysis, quantification of isobaric tags at the MS2 level has been hampered by co-isolation and co-fragmentation of interfering ions, resulting in inaccurate or suppressed TMT ratios (177, 178). This co-isolation problem can be mitigated by deep off-line fractionation and/or synchronous precursor selection (SPS)-based MS3 (SPS-MS3) quantification, both of which decrease TMT reporter ion suppression effects. Although we chose to use MS2 scans for TMT quantification in this study, these samples were all off-line fractionated using high pH prior to LC-MS/MS analysis, helping to minimize peptide co-isolation. In addition, we only used quantitation from peptide spectral matches with 50% or less isolation interference (**Fig. S10**). Of note, approximately 90% of all spectra had 50% or less interference and nearly 70% had less than 25% interference, further increasing our confidence in quantitative accuracy. Furthermore, applying cWGCNA ensures that the biological relevance we are

interpreting is not due to potential quantitative inconsistencies because the changes observed are based on the cumulated levels of a community of proteins in a module rather than individual protein abundances.

The ROSMAP studies are information-rich longitudinal aging studies that have invaluably contributed to understanding the complexity of aging and disease-related changes over time. However, this cohort is primarily made up of non-Latino white participants and historically lacks equal representation from diverse populations. Recent reports indicate Black and Hispanic populations are disproportionately more likely to have AD compared to older white Americans (1), which highlights a potential limitation of the current study. In addition to population demographics, the use of multiple definitions of resilience and how researchers identify this group adds complexity to generalizable interpretation of findings (151, 152). The current study used the combination of pathological and cognitive metrics to differentiate asymptomatic from symptomatic cases by imposing cutoffs which would identify resilient cases with the greatest confidence. However, there may be more to learn from cases not captured by this strategy.

2.5 Figures

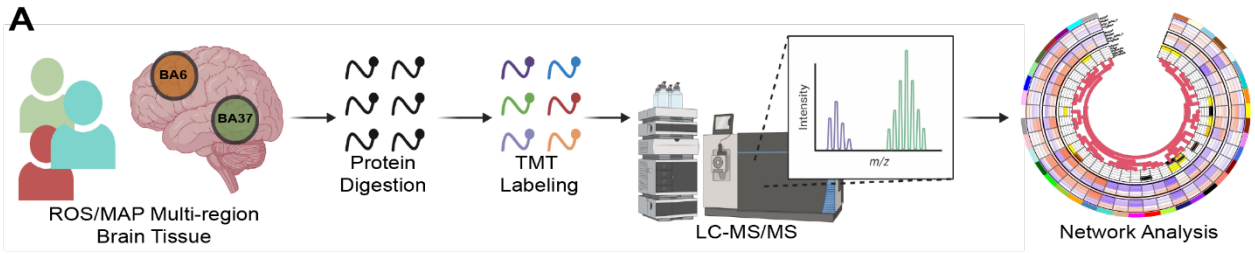
A
BA6
BA37
ROS/MAP Multi-region
Brain Tissue
Protein
Digestion
TMT
Labeling
Intensity
m/z
LC-MS/MS
Network Analysis

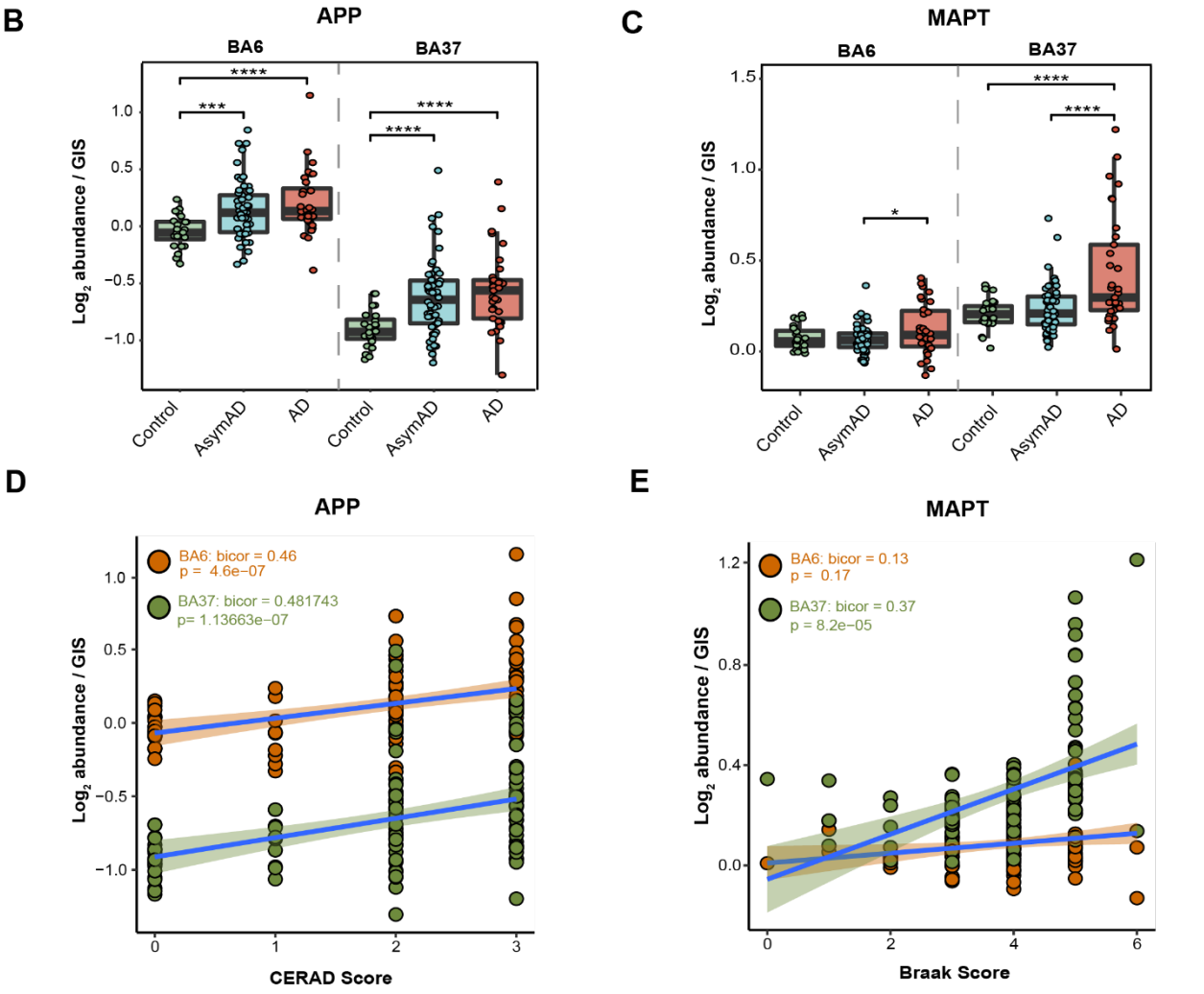
B
APP
BA6
BA37
Log2 abundance / GIS
Control
AsymAD
AD
C
MAPT
D
APP
BA6: bicor = 0.46
p = 4.6e−07
BA37: bicor = 0.481743
p= 1.13663e−07
CERAD Score
E
MAPT
BA6: bicor = 0.13
p = 0.17
BA37: bicor = 0.37
p = 8.2e−05
Braak Score

Figure 2.1: Proteomic measurements of amyloid and tau align with region-specific neuropathological burden. (**A**) Schematic representation of experimental workflow for matched human brain tissue samples across regions BA6 and BA37 from 109 ROSMAP cases that were enzymatically digested with trypsin into peptides and individually labeled with isobaric tandem mass tags (TMT) followed by LC-MS/MS. Log_2 abundances were normalized as a ratio dividing by the central tendency of pooled standards (global internal standards, GIS) and median centered. Protein abundances were analyzed using differential and co-expression methods. (**B**) TMT-MS quantified APP normalized abundance is significantly increased in AsymAD and AD cases compared to Control. One-way ANOVA (BA6: F= 7.987, p=>0.001; BA37: F=9.469, p=>0.001) with Tukey's multiple comparisons test. (**C**) TMT-MS quantified MAPT normalized abundance is significantly increased in AD. One-way ANOVA (BA6: F= 3.522, p=<0.05; BA37: F= 12.69, p=>0.001) with Tukey's multiple comparisons test. (**D**) APP normalized abundance and CERAD scores positively correlate in each brain region. Biweight midcorrelation (Bicor) and pvalue (BA6: bicor=0.46, p=4.6e-07; BA37: bicor=0.482, p=1.1e-07). Best fit line for each region determined by linear model, confidence interval is shaded around line. (**E**) MAPT normalized abundance and Braak scores positively correlate in BA37. Bicor and pvalue (BA6: bicor=0.13, p=0.17; BA37: bicor=0.37, p=8.2e-05). Best fit line for each region determined by linear model, confidence interval is shaded around line. *p<0.05, ***p<0.005, ****p<0.001; F=F value; Bicor= biweight midcorrelation.

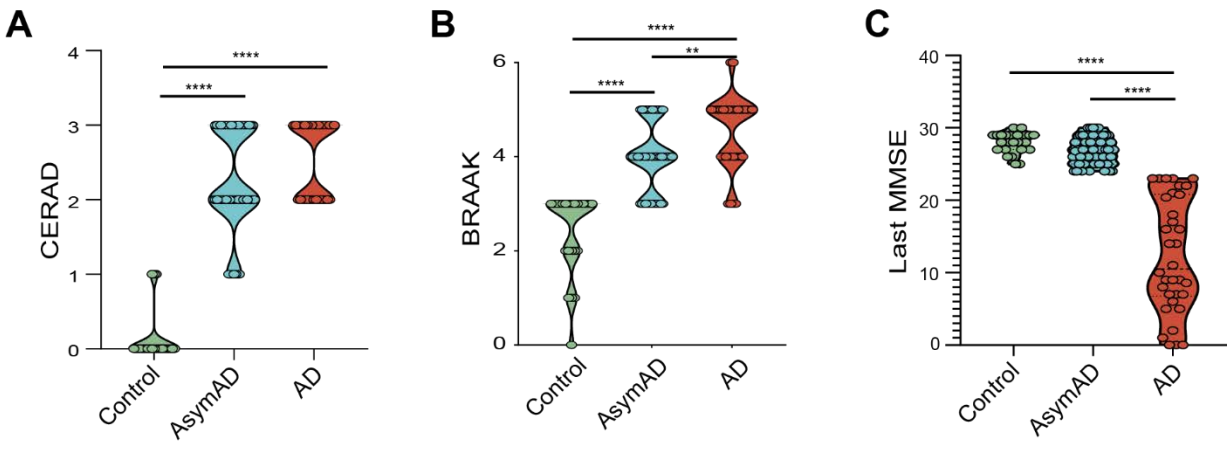
A
CERAD
4
3
2
1
0
****
****
Control
AsymAD
AD
B
BRAAK
6
4
2
0
****
**
****
Control
AsymAD
AD
C
Last MMSE
40
30
20
10
0
****
****
Control
AsymAD
AD

Figure 2.2: Case classification traits distribution. (**A**) CERAD scores are significantly increased in AsymAD and AD cases compared to control. (**B**) Braak scores are significantly different across all three groups. (**C**) Last mini mental state exam (MMSE) scores are significantly reduced in AD compared to control and AsymAD.

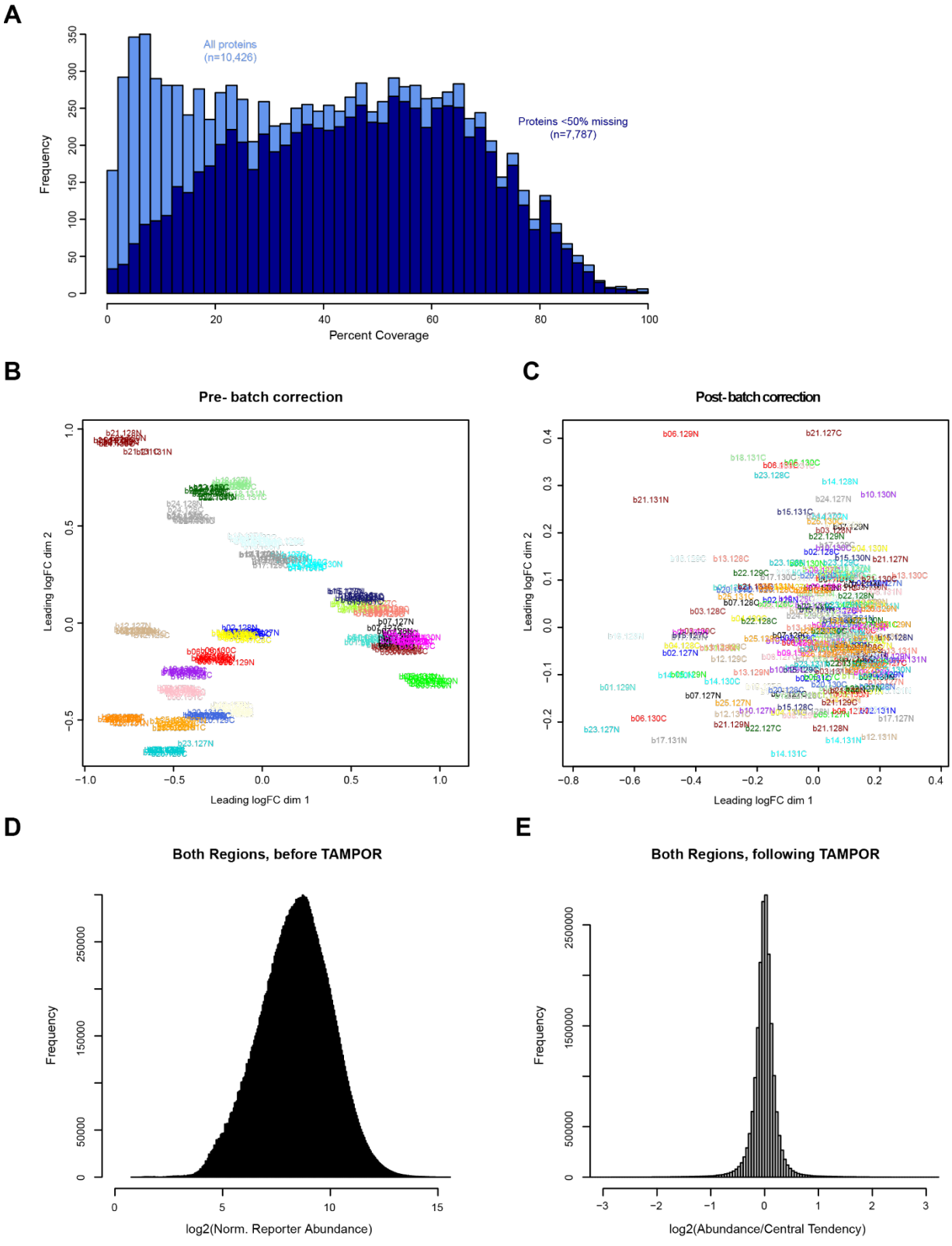
A
All proteins
(n=10,426)
Proteins <50% missing
(n=7,787)
Frequency
Percent Coverage
B
Pre- batch correction
Leading logFC dim 2
Leading logFC dim 1
C
Post-batch correction
Leading logFC dim 2
Leading logFC dim 1
D
Both Regions, before TAMPOR
Frequency
log2(Norm. Reporter Abundance)
E
Both Regions, following TAMPOR
Frequency
log2(Abundance/Central Tendency)

Figure 2.3: Percent coverage and TMT batch correction across BA6 and BA37. (**A**) Percent protein coverage for all quantified high confidence, master proteins (n=10,426) and the those present in at least 50% of all cases in both brain regions (n=7,787) after outlier removal. **(B-C)** A median polish batch correction approach was implemented to remove technical batch variance across the 26 TMT 11-plex batches. (**B**) Multidimensional scaling (MDS) plots visualize original log_2 transformed protein abundances, normalized to the pooled global internal standards (GIS). (**C**) MDS of batch-corrected normalized log_2 abundance after 175 iterations. Samples are color-coded by batch. (**D-E**) Distribution of log2 abundance data before (**D**) and after (**E**) batch correction.

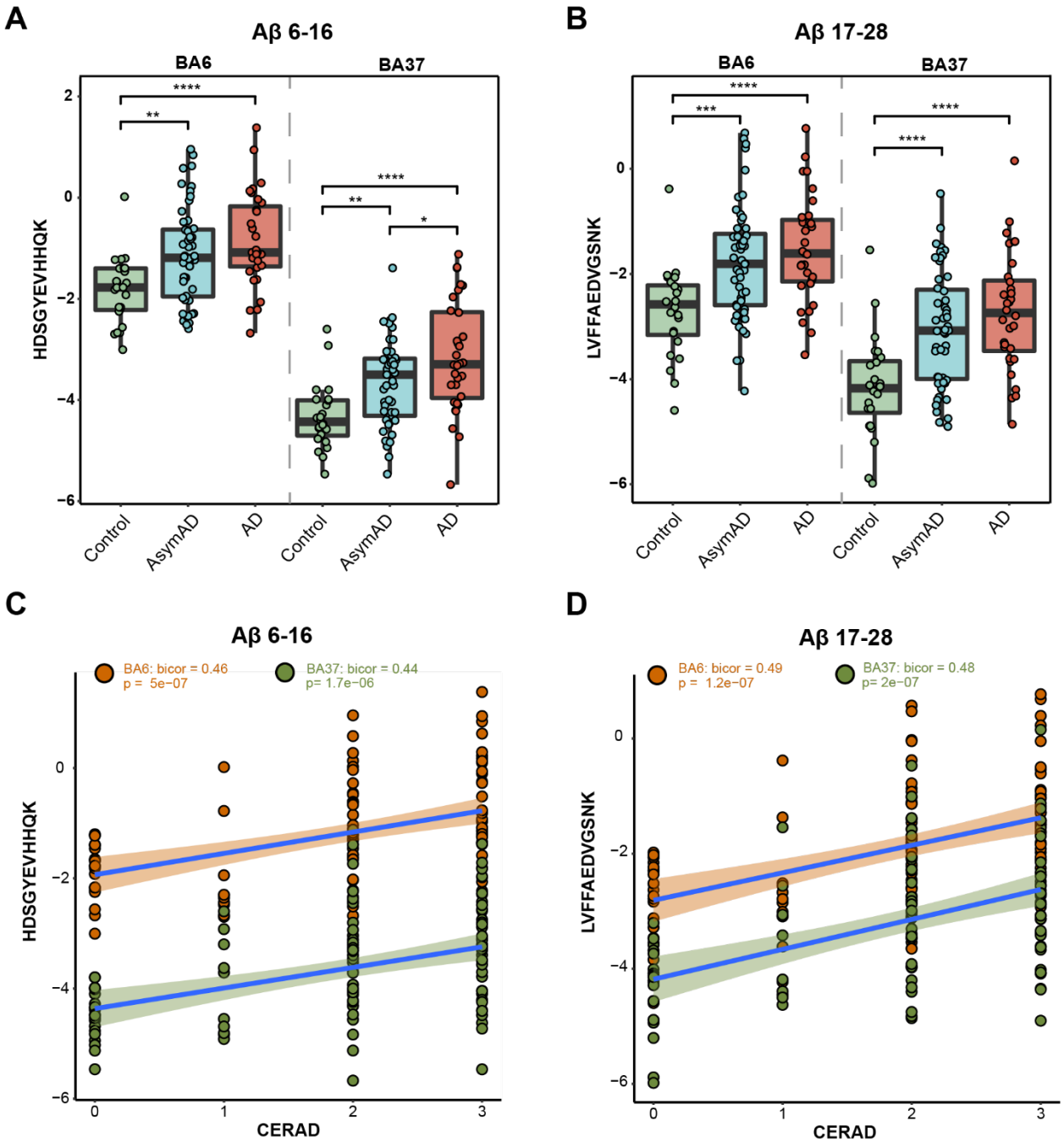
A
Aβ 6-16
BA6
BA37
HDSGYEVHHQK
Control
AsymAD
AD
B
Aβ 17-28
LVFFAEDVGSNK
C
Aβ 6-16
BA6: bicor = 0.46
p = 5e−07
BA37: bicor = 0.44
p= 1.7e−06
CERAD
D
Aβ 17-28
BA6: bicor = 0.49
p = 1.2e−07
BA37: bicor = 0.48
p= 2e−07

Figure 2.4: Amyloid beta peptide measurements. (**A**) Fully tryptic peptide mapping to the Aβ region (residue 6-16) is significantly increased in AsymAD and AD compared to control cases. One-way ANOVA (BA6: F= 8.671, p<0.001; BA37: F= 12.23, p<0.001) with Tukey multiple comparisons test. (**B**) Fully tryptic peptide mapping to the Aβ region (17-28) is significantly increased in AsymAD and AD compared to control and AD is significantly increased compared to AsymAD in BA37. One-way ANOVA (BA6: F= 9.963, p<0.001; BA37: F= 13.03, p<0.001) with Tukey multiple comparisons test. (**C**) Aβ peptide (6-16) positively correlates with CERAD scores in each brain region. Biweight (bircor) and pvalue (BA6: bicor=0.46, p=5e-07; BA37: bicor=0.44, p=1.7e-06). Best fit line for each regional correlation determined by linear mode, confidence interval is shaded around line. (**D**) Aβ peptide (17-28) positively correlates with CERAD scores in each brain region. Bicor and pvalue (BA6: bicor=0.49, p=1.2e-07; BA37: bicor=0.48, p=2e-07). Best fit line for each regional correlation determined by linear mode, confidence interval is shaded around line.

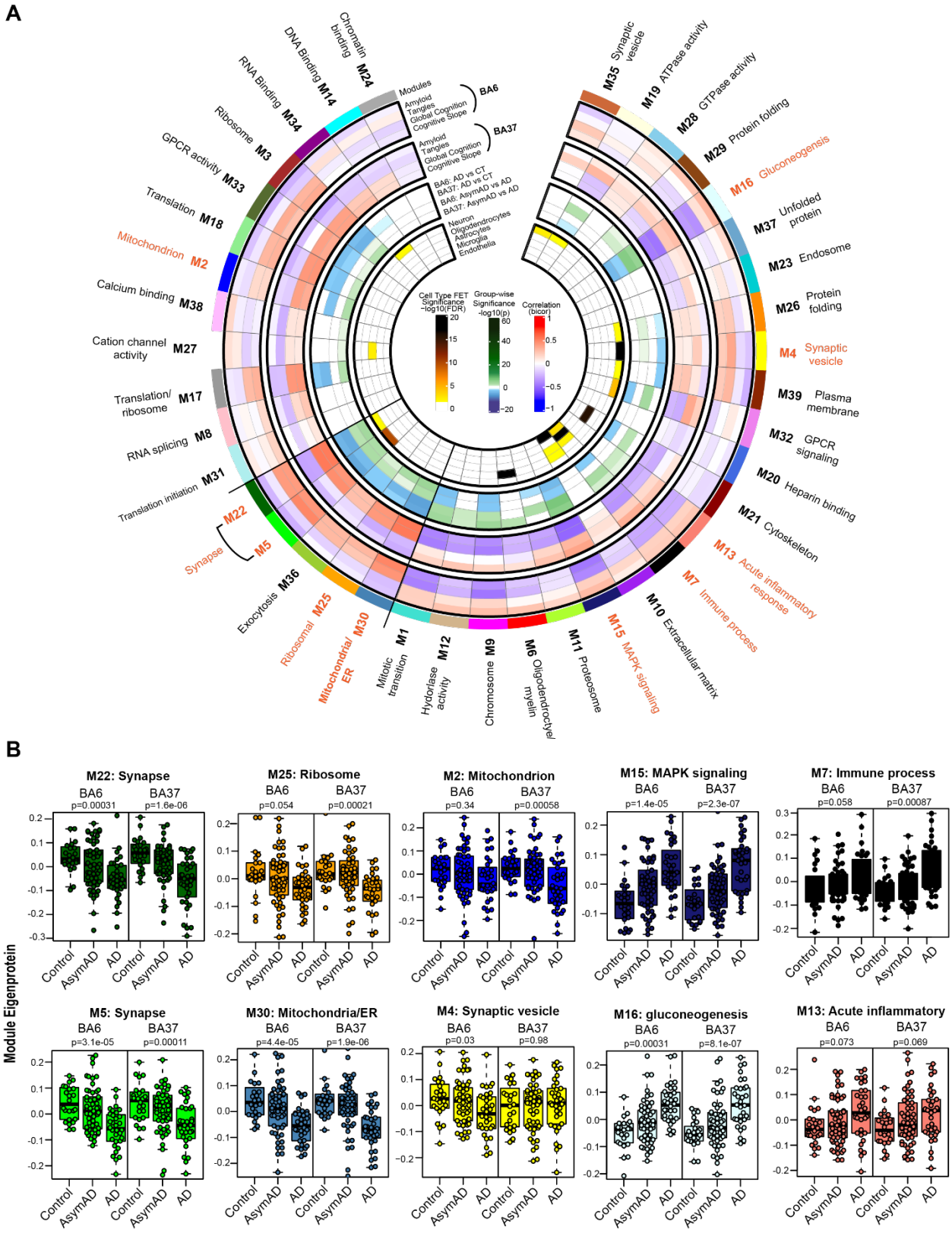
A
Modules
Amyloid
Tangles
Global Cognition
Cognitive Slope
BA6
BA37
BA6: AD vs CT
BA37: AD vs CT
BA6: AsymAD vs AD
BA37: AsymAD vs AD
Neuron
Oligodendrocytes
Astrocytes
Microglia
Endothelia
Cell Type FET Significance -log10(FDR)
Group-wise Significance -log10(p)
Correlation (bicor)
M24 Chromatin binding
M14 DNA Binding
M34 RNA Binding
M3 Ribosome
M33 GPCR activity
M18 Translation
M2 Mitochondrion
M38 Calcium binding
M27 Cation channel activity
M17 Translation/ ribosome
M8 RNA splicing
M31 Translation initiation
M22 Synapse
M5 Synapse
M36 Exocytosis
M25 Ribosomal
M30 Mitochondrial ER
M1 Mitotic transition
M12 Hydrolase activity
M9 Chromosome
M6 Oligodendrocyte/ myelin
M11 Proteosome
M15 MAPK signaling
M10 Extracellular matrix
M7 Immune process
M13 Acute inflammatory response
M21 Cytoskeleton
M20 Heparin binding
M32 GPCR signaling
M39 Plasma membrane
M4 Synaptic vesicle
M26 Protein folding
M23 Endosome
M37 Unfolded protein
M16 Gluconeogenesis
M29 Protein folding
M28 GTPase activity
M19 ATPase activity
M35 Synaptic vesicle
B
Module Eigenprotein
M22: Synapse
BA6 p=0.00031
BA37 p=1.6e-06
M25: Ribosome
BA6 p=0.054
BA37 p=0.00021
M2: Mitochondrion
BA6 p=0.34
BA37 p=0.00058
M15: MAPK signaling
BA6 p=1.4e-05
BA37 p=2.3e-07
M7: Immune process
BA6 p=0.058
BA37 p=0.00087
M5: Synapse
BA6 p=3.1e-05
BA37 p=0.00011
M30: Mitochondria/ER
BA6 p=4.4e-05
BA37 p=1.9e-06
M4: Synaptic vesicle
BA6 p=0.03
BA37 p=0.98
M16: gluconeogenesis
BA6 p=0.00031
BA37 p=8.1e-07
M13: Acute inflammatory
BA6 p=0.073
BA37 p=0.069
Control
AsymAD
AD

Figure 2.5: Consensus correlation network of a multi-region human brain proteome. (**A**) A consensus correlation network (cWGCNA) was constructed with 7,787 proteins across BA6 and BA37 and yielded 39 co-expression protein modules. In the inner-most heatmap, enrichment of cell-type markers (as determined by one-way Fisher's exact test) for each module is visualized for neuronal, oligodendrocyte, astrocyte, microglial and endothelial cell-types. The panel outside of the cell-type results highlights group-wise differences in module eigenproteins for AD vs Control and AsymAD vs AD in each brain region. The two outer-most heatmaps depict the correlation (Bicor) of module eigenproteins with pathological (Amyloid and Tangle burden) and clinical (Global cognitive function and cognitive slope) phenotypes for both brain regions. Modules are identified by color and number, accompanied by top gene ontology (GO) terms representative of modular biology. Scale bars for cell-type enrichment (darker color indicates stronger enrichment), weighted group-wise eigenprotein difference (darker green correspond to stronger positive relationship and deeper blue indicates stronger negative relationship) and bi-directional module—trait relationships (red indicating positive correlation and blue indicating negative correlation) are at the center of the plot. (**B**) Module eigenproteins (MEs) grouped by diagnosis (Control, AsymAD and AD) were plotted as box and whisker plots for modules of interest, chosen based on their preservation in AsymAD compared to AD and relationships to cognitive measures. MEs were compared in each brain region using one-way ANOVA, unadjusted pvalues are shown. Box plots represent median, 25th and 75th percentiles. Box hinges represent the interquartile range of the two middle quartiles with a group. Error bars are based on data points 1.5 times the interquartile range from the box hinge.

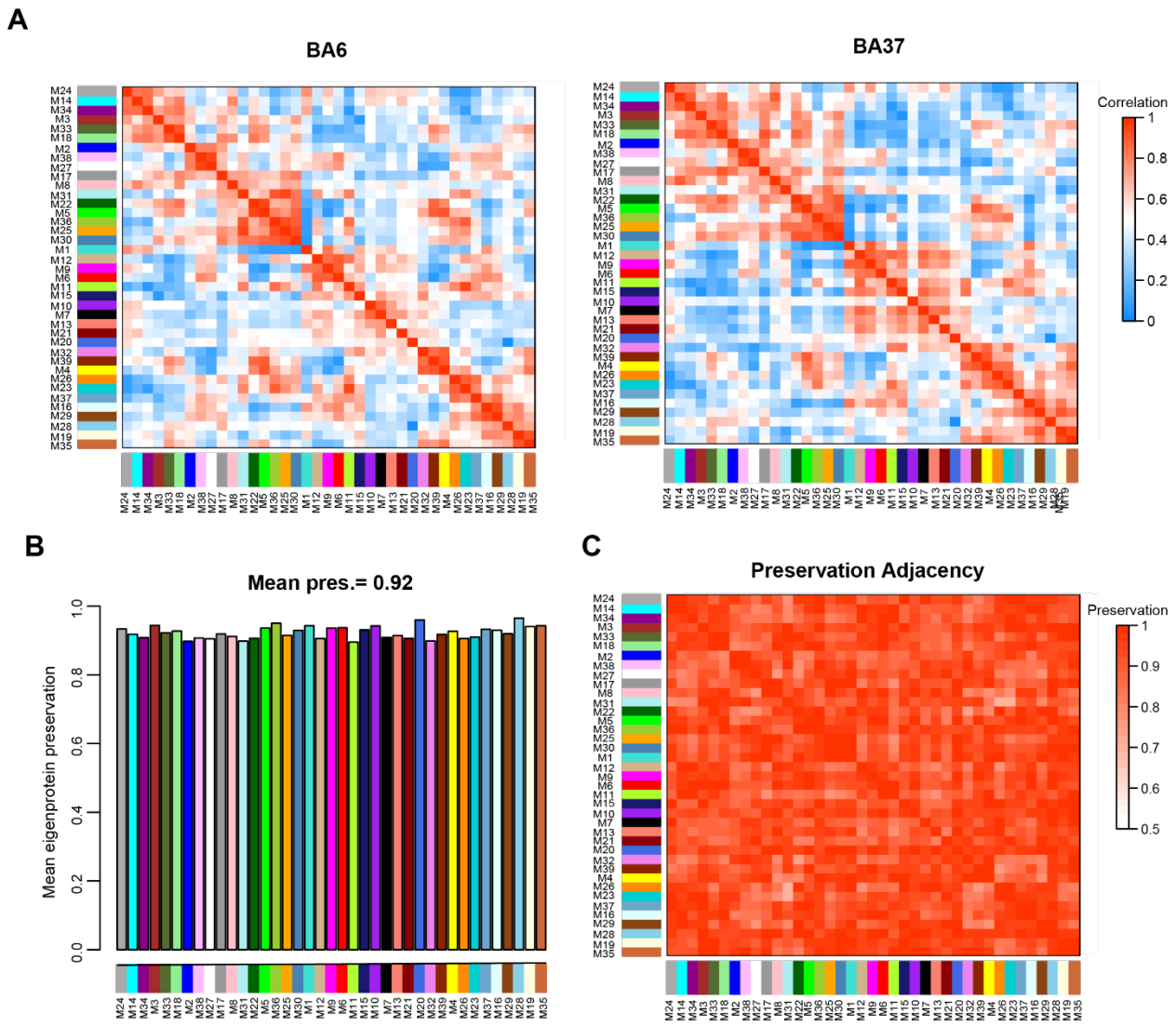
A
BA6
BA37
Correlation
1
0.8
0.6
0.4
0.2
0
B
Mean pres.= 0.92
Mean eigenprotein preservation
0.0
0.2
0.4
0.6
0.8
1.0
C
Preservation Adjacency
Preservation
1
0.9
0.8
0.7
0.6
0.5

Figure 2.6: Consensus modules are highly preserved in BA6 and BA37. (**A**) Modules eigenproteins were correlated to visualize inter-module relationships in BA6 and BA37, respectively. Heat blocks along the diagonal could be observed similarly in both brain regions. (**B**) Mean preservation relationship for each eigenprotein was calculated for the consensus network, with mean preservation of 0.92 indicating very high preservation. (**C**) Preservation adjacency of the consensus network, visualized as a heatmap, further support that most relationships in the network across both brain regions are highly preserved and biologically meaningful.

A

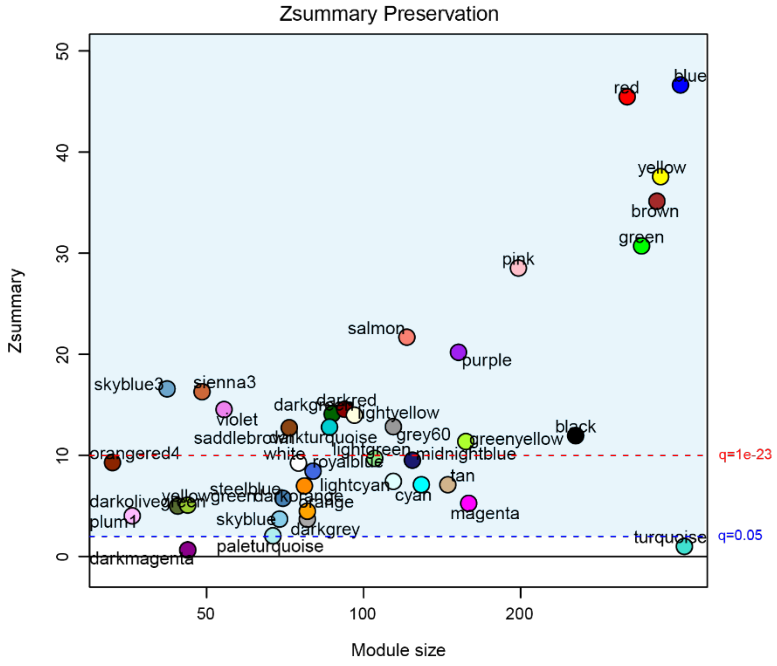
Zsummary Preservation
Zsummary
Module size
q=1e-23
q=0.05
blue
red
yellow
brown
green
pink
salmon
purple
skyblue3
sienna3
violet
darkred
lightyellow
black
saddlebrown
darkturquoise
grey60
greenyellow
orangered4
white
lightgreen
midnightblue
royalblue
tan
lightcyan
cyan
steelblue
yellowgreen
darkorange
orange
darkolivegreen
plum1
skyblue
darkgrey
magenta
turquoise
paleturquoise
darkmagenta

B

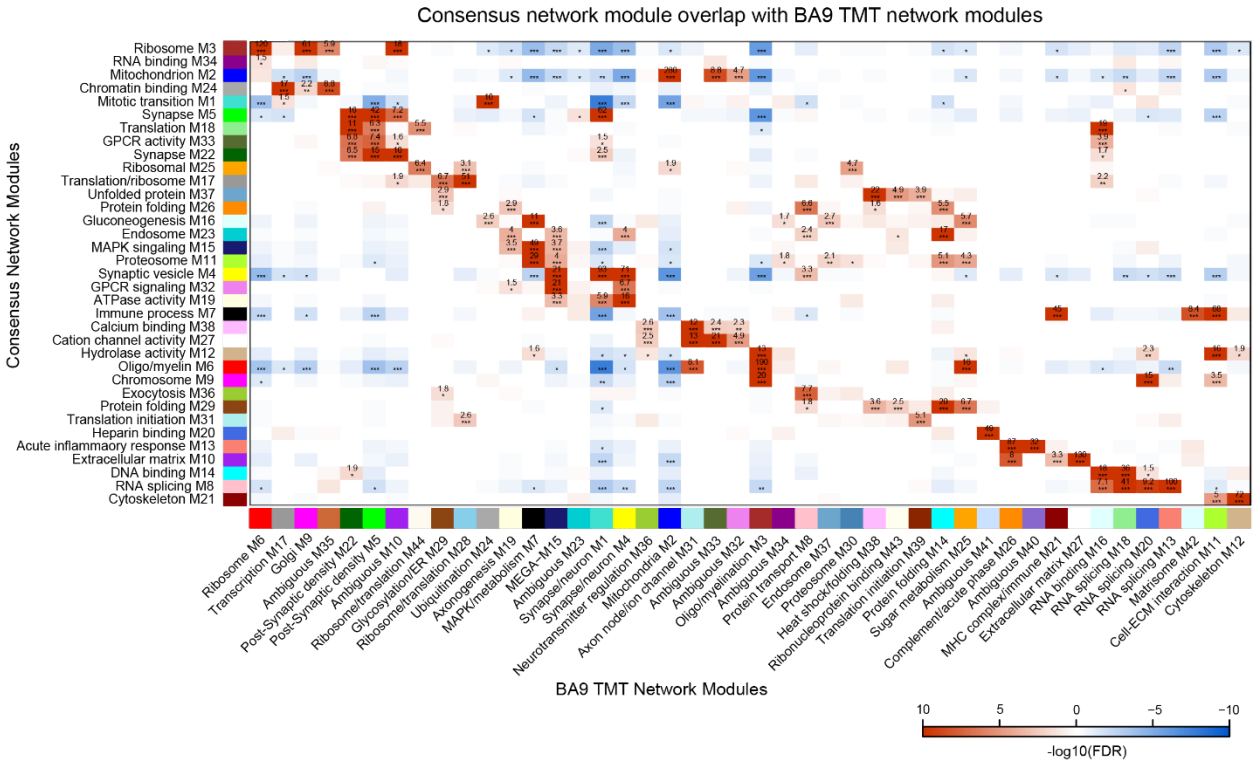
Consensus network module overlap with BA9 TMT network modules
Consensus Network Modules
Ribosome M3
RNA binding M34
Mitochondrion M2
Chromatin binding M24
Mitotic transition M1
Synapse M5
Translation M18
GPCR activity M33
Synapse M22
Ribosomal M25
Translation/ribosome M17
Unfolded protein M37
Protein folding M26
Gluconeogenesis M16
Endosome M23
MAPK singaling M15
Proteosome M11
Synaptic vesicle M4
GPCR signaling M32
ATPase activity M19
Immune process M7
Calcium binding M38
Cation channel activity M27
Hydrolase activity M12
Oligo/myelin M6
Chromosome M9
Exocytosis M36
Protein folding M29
Translation initiation M31
Heparin binding M20
Acute inflammaory response M13
Extracellular matrix M10
DNA binding M14
RNA splicing M8
Cytoskeleton M21
Ribosome M6
Transcription M17
Golgi M9
Ambiguous M35
Post-Synaptic density M22
Post-Synaptic density M5
Ambiguous M10
Ribosome/translation M44
Glycosylation/ER M29
Ribosome/translation M28
Ubiquitination M24
Axonogenesis M19
MAPK/metabolism M7
MECA-M15
Ambiguous M23
Synapse/neuron M1
Synapse/neuron M4
Neurotransmitter regulation M36
Axon node/ion channel M2
Mitochondria M31
Ambiguous M53
Ambiguous M32
Oligo/myelination M3
Ambiguous M34
Protein transport M8
Endosome M37
Proteosome M30
Heat shock/folding M38
Ribonucleoprotein binding M43
Translation initiation M39
Protein folding M14
Sugar metabolism M25
Ambiguous M41
Complement/acute phase M26
Ambiguous M40
MHC complex/immune M21
Extracellular matrix M27
RNA binding M16
RNA splicing M18
RNA splicing M20
RNA splicing M13
Matrisome M42
Cell-ECM interaction M11
Cytoskeleton M12
BA9 TMT Network Modules
10
5
0
−5
−10
-log10(FDR)

Figure 2.7: Consensus network preservation. (**A**) Zsummary indicates nearly all consensus modules preserve with previous BA9 TMT network modules reported in Johnson et al. Module Zsummary greater than or equal to 1.96 (q=0.05, dashed blue line) are considered preserved and modules with Zsummary of 10 or higher (q=1e-23, dashed red line) are considered highly preserved. (**B**) Overrepresentation analysis of consensus modules members with previous BA9 TMT module members. $-\log_{10}$ FDR corrected overlap values are shown. The heatmap threshold is at a 10% FDR (0.1).

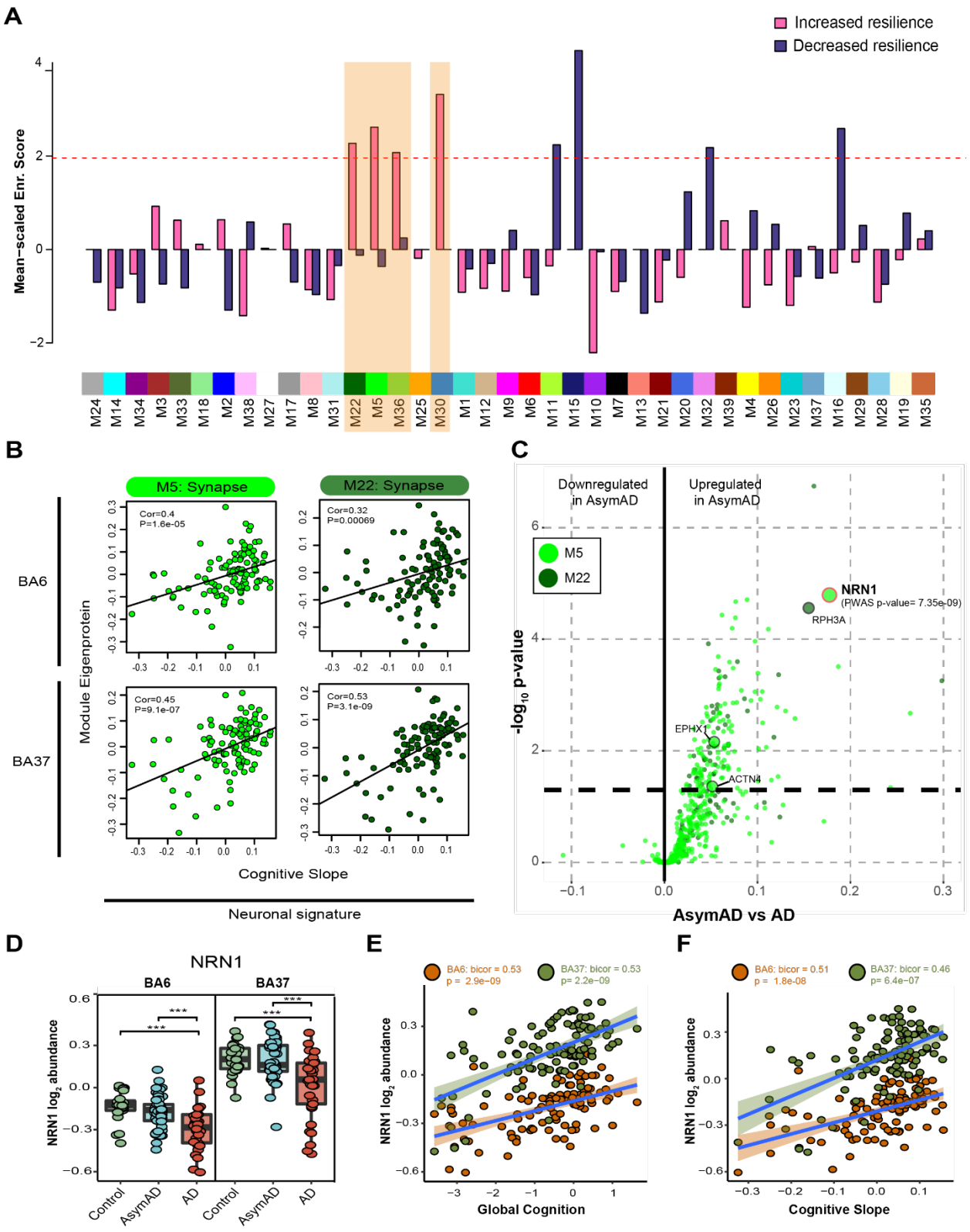
A
Increased resilience
Decreased resilience
Mean−scaled Enr. Score
M24 M14 M34 M3 M33 M18 M2 M38 M27 M17 M8 M31 M22 M5 M36 M25 M30 M1 M12 M9 M6 M11 M15 M10 M7 M13 M21 M20 M32 M39 M4 M26 M23 M37 M16 M29 M28 M19 M35
B
M5: Synapse
M22: Synapse
BA6
BA37
Cor=0.4 P=1.6e-05
Cor=0.32 P=0.00069
Cor=0.45 P=9.1e-07
Cor=0.53 P=3.1e-09
Module Eigenprotein
Cognitive Slope
Neuronal signature
C
Downregulated in AsymAD
Upregulated in AsymAD
M5
M22
NRN1
(PWAS p-value= 7.35e-09)
RPH3A
EPHX1
ACTN4
-log10 p-value
AsymAD vs AD
D
NRN1
BA6
BA37
NRN1 log2 abundance
Control
AsymAD
AD
E
BA6: bicor = 0.53
p = 2.9e−09
BA37: bicor = 0.53
p= 2.2e−09
NRN1 log2 abundance
Global Cognition
F
BA6: bicor = 0.51
p = 1.8e−08
BA37: bicor = 0.46
p= 6.4e−07
NRN1 log2 abundance
Cognitive Slope

Figure 2.8: Integrated proteomics of human brain reveals NRN1 as a top resilience candidate. (**A**) Significant enrichment of modules associated with increased cognitive resilience were identified by PWAS in consensus modules. The dashed red line illustrates the significance cutoff corresponding to a Z score of 1.96 or p=0.05. Significant, increased resilience modules are highlighted in orange. (**B**) PWAS significant, synaptic modules M5 and M22 positively correlate with cognitive slope, irrespective of brain region. Bicor and pvalues (BA6: M22 cor=0.32, M22 p=0.00069, M5 cor=0.4, M5 p=1.6e-05; BA37: M22 cor=0.53, M22 p=3.1e-09, M5 cor=0.45, M5 p=9.1e-07). (**C**) Differential expression comparing AsymAD and AD groups from M5 and M22 module members. Protein fold-change is the x-coordinate and the $-\log_{10}$ pvalue from one-way ANOVA is the y coordinate for each protein. Proteins above the dashed line (p=0.05) are considered significantly differentially expressed. Large circles highlight proteins that were significant by PWAS (α=5e-06). (**D**) NRN1 abundance is significantly reduced in AD. One-way ANOVA (BA6: F=13.25, p=<0.001; BA37: F=13.68, p=<0.001) with Tukey test. (**E**) NRN1 abundance correlates positively with global cognitive performance. Bicor and pvalues (BA6: bicor=0.53, p=2.9e-09; BA37: bicor=0.53, p=2.2e-09). (**F**) NRN1 abundance correlates positively with cognitive slope. Bicor and pvalues (BA6: bicor=0.51, p=1.8e-08; BA37: bicor=0.46, p=6.4e-07).

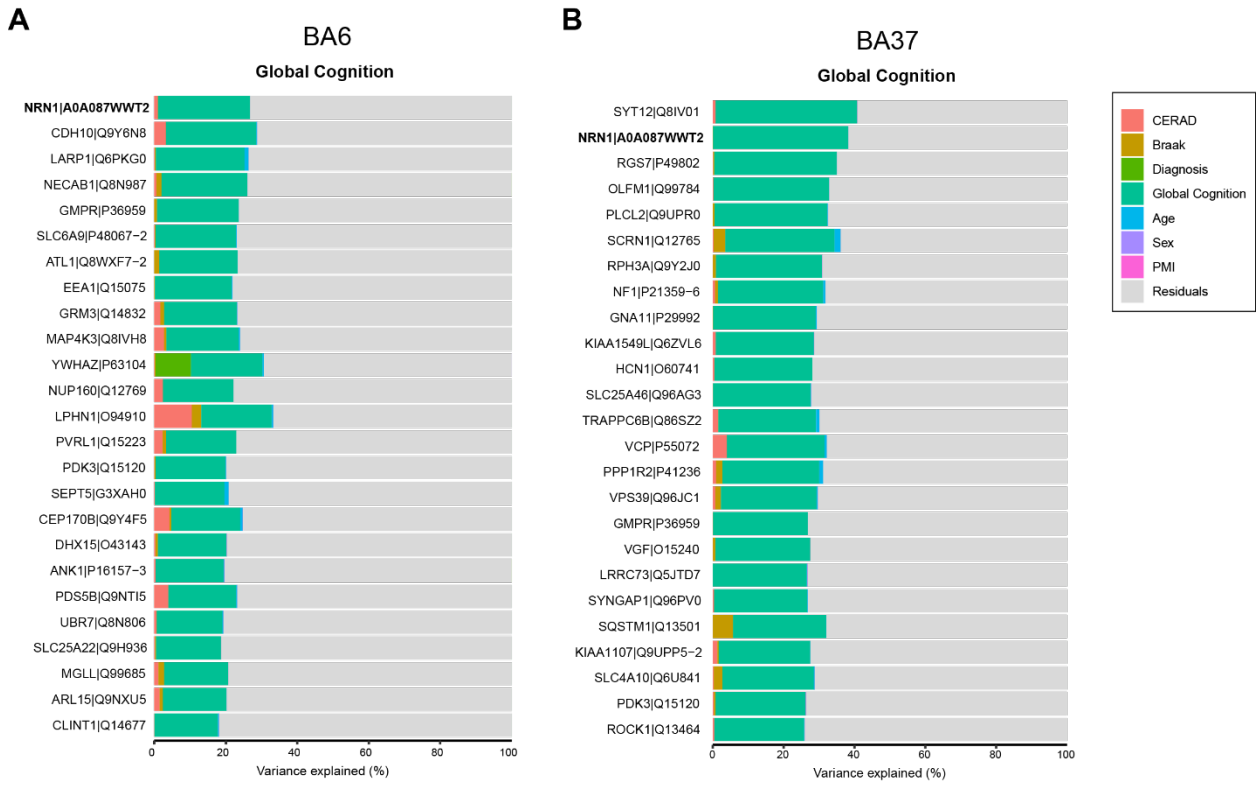
A
BA6
Global Cognition
NRN1|A0A087WWT2
CDH10|Q9Y6N8
LARP1|Q6PKG0
NECAB1|Q8N987
GMPR|P36959
SLC6A9|P48067−2
ATL1|Q8WXF7−2
EEA1|Q15075
GRM3|Q14832
MAP4K3|Q8IVH8
YWHAZ|P63104
NUP160|Q12769
LPHN1|O94910
PVRL1|Q15223
PDK3|Q15120
SEPT5|G3XAH0
CEP170B|Q9Y4F5
DHX15|O43143
ANK1|P16157−3
PDS5B|Q9NTI5
UBR7|Q8N806
SLC25A22|Q9H936
MGLL|Q99685
ARL15|Q9NXU5
CLINT1|Q14677
0
20
40
60
80
100
Variance explained (%)
B
BA37
Global Cognition
SYT12|Q8IV01
NRN1|A0A087WWT2
RGS7|P49802
OLFM1|Q99784
PLCL2|Q9UPR0
SCRN1|Q12765
RPH3A|Q9Y2J0
NF1|P21359−6
GNA11|P29992
KIAA1549L|Q6ZVL6
HCN1|O60741
SLC25A46|Q96AG3
TRAPPC6B|Q86SZ2
VCP|P55072
PPP1R2|P41236
VPS39|Q96JC1
GMPR|P36959
VGF|O15240
LRRC73|Q5JTD7
SYNGAP1|Q96PV0
SQSTM1|Q13501
KIAA1107|Q9UPP5−2
SLC4A10|Q6U841
PDK3|Q15120
ROCK1|Q13464
0
20
40
60
80
100
Variance explained (%)
CERAD
Braak
Diagnosis
Global Cognition
Age
Sex
PMI
Residuals

Figure 2.9: Percent variance in protein expression explained by global cognition. A linear mixed model approach was implemented to estimate the percent variance explained by proteins in relationship to diagnosis, CERAD score, Braak score and global cognition across region, respectively. The rank order in the percent variation in protein expression explained by global cognition (top 20 proteins) were plotted for BA6 (**A**) and BA37 (**B**).

3.0 Neuritin (NRN1): candidate resilience-promoting protein

*This chapter was adapted from findings published in the *Molecular and Cellular Proteomics* Journal in April 2023. https://doi.org/10.1016/j.mcpro.2023.100542

Author contributions

C. H., D. A. P., N. T. S., and J. H. H. investigation; C. H., D. A. P., M. H. A., and D. M. D. investigation; C. H. and D. A. P. formal analysis; N. T. S., J. H. H., and E. B. D. data curation. C. H. and D. A. P. writing–original draft. D. A. B. resources. C. H., D. A. P., M. H. A., D. M. D., E. B. D., D. A. B., J. H. H., and N. T. S. writing–review and editing.

3.1 Introduction

Neuritin (NRN1) is an activity-dependent neurotrophic factor that modifies neuronal communication through positive regulation of synaptic plasticity and stability (179). Recently, the potential significance of NRN1 as a therapeutic agent in disease contexts has gained momentum. Increased abundance of NRN1 has been linked to increased cognitive resilience (123) and AsymAD cases have significantly increased NRN1 compared to AD cases (124, 180). In AD model systems, NRN1 has been linked to rescued synaptic retention and cognitive functions despite pathological insult (143, 145). Understanding the role of NRN1 in neuroprotection from AD insult and mediating cognitive resilience remains a critical unanswered question.

To begin to address these gaps in knowledge, the present work includes experimental evaluation of NRN1's ability to protect dendritic spines from amyloid-induced loss and dysfunction. Aβ oligomers have been extensively characterized as particularly toxic to dendric spine structures where they preferentially bind and result in gross density losses (107-112). Importantly, AsymAD cases accumulate comparable levels of Aβ pathology in their brains yet maintain synaptic connections (78, 79). Therefore, protecting spines from Aβ-induced loss is hypothesized as a potential physiological basis in promoting resilience to AD. In this chapter, the neuroprotective potential of NRN1 against Aβ oligomers was tested in a primary cell model of AD. Dendritic spine morphometric analysis revealed NRN1 co-treatment with Aβ oligomers prevented spine density loss. We also report that Aβ-induced hyperexcitability was rescued by NRN1 co-treatment. To better understand how NRN1 promotes neuroprotection, we also performed proteomic analysis of NRN1 or vehicle treated neurons. Results indicate NRN1 exposure significantly increases proteins relating to synaptic biology, the majority of which map back to modules of cognitive resilience from the human brain proteomic network. This work provides valuable insights into the functions of NRN1 in neuroprotection from AD-relevant insult and establishes biological relevance of NRN1 target engagement in human resilience phenotypes.

3.2 Results

3.2.1 NRN1 prevents $A\beta_{42}$-induced dendritic spine degeneration

The preservation of dendritic spines is hypothesized to maintain memory and information processing in resilient patients who harbor high levels of Aβ pathology but are cognitively normal (79, 181). Numerous studies indicate that Aβ can induce dendritic spine degeneration in cellular and animal models of AD (109-111, 182). Henceforth, protecting spines from Aβ represents a rational therapeutic strategy to promote resilience and delay dementia onset. Past studies provided evidence that NRN1 exists predominantly as a soluble form *in vivo* and exerts neurotrophic effects on synaptic maintenance and neuronal survival (127-129). Based on our network analysis, we hypothesized that NRN1 could protect against Aβ-induced dendritic spine degeneration. To test this, rat hippocampal neurons were isolated at E18 and cultured at high-density on glass coverslips. To visualize dendritic architecture, neurons were transiently transfected with a plasmid encoding Lifeact-GFP at DIV 12. Cultures were treated with NRN1 or co-treated with NRN1 and $A\beta_{42}$ oligomers for 6 hours, then fixed, and processed for widefield microscopy followed by three-dimensional image reconstructions for dendritic spine morphometric analysis (**Fig. 3.1A**). Consistent with previous reports (112), spine density was reduced significantly after exposure to $A\beta_{42}$ in comparison to DMSO controls, however co-treatment with NRN1 prevented $A\beta_{42}$-induced spine degeneration (**Fig. 3.1, B and C**). Examination of dendritic spine morphologic subclasses revealed that $A\beta_{42}$ exposure significantly decreased thin spine density in comparison to DMSO controls, however, these detrimental effects were blocked in the presence of NRN1 (**Fig. 3.1D**). Notably, the proportion of thin spines were increased with NRN1 treatment compared to DMSO, while $A\beta_{42}$ promoted an increase in the proportion of dendritic filopodia (**Fig. 3.1E**). Exposure to $A\beta_{42}$ and/or NRN1 did not significantly alter dendritic spine length or head diameter in comparison to DMSO controls (**Fig. 3.1, F and G**

and **Fig. S3., A and B**). These findings suggest that NRN1 can protect against $A\beta_{42}$-induced dendritic spine loss.

To exclude the possibility that NRN1 directly binds to soluble $A\beta_{42}$ oligomers and in turn neutralizes each protein's independent effects in primary neurons, we performed an *in vitro* amyloid aggregation assay. Human recombinant $A\beta_{42}$ fibrilization was measured by thioflavin T (ThT) fluorescence in the presence or absence of NRN1 for 20 consecutive hours (**Fig. S8A**). There were no distinguishable differences in self-assembly and aggregation between $A\beta_{42}$ alone or $A\beta_{42}$ and NRN1 together. Following the fluorometric assay, soluble and pellet fractions were probed via western blot and silver stain (**Fig. S8B-C**). Nearly all NRN1 immunoreactivity was detected in the soluble fraction whereas $A\beta_{42}$ was primarily concentrated in the pellet fraction. Importantly, the molar concentration of $A\beta_{42}$ was 10-fold greater in the aggregation assay and the molar concentration of NRN1 was >30-fold greater, suggesting that even at very high concentrations NRN1 does not impede $A\beta_{42}$ fibrilization. These studies suggest that it is highly unlikely an artifact of NRN1 and $A\beta_{42}$ directly binding immediately prior to exposure on primary neurons could account for NRN1's preventative role in $A\beta_{42}$-induced dendritic spine loss.

3.2.2 NRN1 protects against $A\beta_{42}$-induced neuronal hyperexcitability

Aβ-induced dendritic degeneration and spine loss cause reductions in the overall area and volume of neurons, rendering them more electrically compact (109, 182). The loss of dendritic spines and overall surface area of the neuron induces hyperexcitability, which consequently drives abnormal circuit synchronization and cognitive impairment in AD mouse models and patients (109, 183, 184). To test whether NRN1 is protective against $A\beta_{42}$-induced neuronal hyperexcitability, we seeded rat primary hippocampal neurons on microelectrode arrays (MEAs) and performed baseline recordings at DIV 14. Action potential frequency, referred to as mean firing rate, was measured to assess neuronal excitability. Immediately after the baseline recording, neurons were exposed to DMSO, $A\beta_{42}$, NRN1, and/or NRN1 plus $A\beta_{42}$ for 6 hours

followed by a second recording (**Fig. 5A**). DMSO did not increase mean firing rates in comparison to baseline (**Fig. 5, B and C**). Consistent with previous findings(182), $A\beta_{42}$ significantly increased mean firing rates in comparison to baseline (**Fig. 5, B and D**). While NRN1 significantly increased mean firing rates in comparison to baseline, simultaneous exposure to $A\beta_{42}$ and NRN1 was comparable to baseline (**Fig. 5, B, E, and F**). The total number of active neurons per experimental group could not account for the effects on mean firing rates (**Fig. S9**). These results reproduce past studies indicating that $A\beta_{42}$-induced dendritic spine loss in cultured neurons causes hyperexcitability (112). Notably, NRN1 exposure did not alter spine density or morphology (**Fig. 4**); therefore, the increase in mean firing rate that was exhibited following NRN1 treatment must be the result of a different mechanism (**Fig. 5E**). Together, these findings indicate that the dendritic spine resilience provided by NRN1 is protective against $A\beta_{42}$-induced hyperexcitability.

3.2.3 NRN1 treatment alters the proteome in cultured neurons

To identify proteins and broader pathways impacted by NRN1 treatment, rat primary neurons were treated with NRN1 recombinant protein at DIV14 for 6 hours at the same concentration as previously tested in dendritic spine and MEA assays (**Fig. 6A**). Following treatment, cells were lysed and prepared for TMT-MS

analysis. A total of 8,238 proteins were quantified and used for differential expression analysis (**Supplemental Table 13**). Comparing NRN1 treated and vehicle treated neurons, 507 proteins were significantly increased, and 489 proteins were significantly decreased following NRN1 treatment (**Fig. 6B**; **Supplemental Table 14).** Of these, 216 were below a 10% FDR following correction (large sports, **Fig. 6B**). NRN1 was identified among proteins significantly increased in the NRN1 treatment group. GO analysis of significantly changed proteins found strong bias of synaptic and cell projection functions upregulated with NRN1 exposure (**Fig. 6C**). In addition, proteins involved in functions related to oxidation and metabolic processes were decreased following NRN1 treatment. These results support previously observed functions of NRN1 in

promoting synaptic function (135). Our findings provide a reference of downstream and putative co-regulated proteins that are altered by exposure to NRN1. Based on this analysis, it is possible to infer protein mediators that could be driving the increase in neuronal firing that was observed in our MEA experiments. Furthermore, the pathways decreased following NRN1 treatment were related to metabolism and cellular energetics, which are systems often dysregulated and increased in AD (124). This supports the hypothesis of NRN1 as a dual-action molecular effector that may increase proteins typically vulnerable in AD, while decreasing proteins that are aberrantly increased in AD.

3.2.4 NRN1 engages protein targets linked to cognitive resilience in human brain

The ability of a nominated resilience protein candidate to engage relevant human biology is critically important to the clinical translation of the target. Therefore, we applied an integrative analysis to resolve how NRN1-driven changes that were observed in the rat neuronal proteome related to the human brain proteome. Significance of protein overlap between the rat neuronal proteome and individual modules within the human brain consensus network was determined by one-tailed Fisher's exact test (**Fig. 7A; Supplemental Table 15**). The rat neuronal proteomic data was subset into three for this analysis and included: I) all proteins quantified, II) only those that were significantly increased following NRN1 treatment and III) only those that were significantly decreased following NRN1 treatment. This analysis revealed 17 of the 39 modules with statistically significant overlap from rat neuronal proteins into the human brain network (**Fig. 7A** - top row, $p<0.05$ FDR corrected). Seven modules overlapped with rat neuronal proteins significantly differentially expressed with NRN1 treatment (middle and bottom rows). M22 Synapse, M5 Synapse, M4 Synaptic vesicle and M19 ATPase activity in the human brain network were enriched for proteins increased following NRN1 treatment. Human modules M8 RNA splicing, M31 Translation initiation and M12 Hydrolase activity were enriched for proteins decreased following NRN1 treatment. The majority of proteins significantly upregulated by NRN1

treatment in the rat neuronal proteome overlapped with human modules M5 and M22 (**Fig. 7B**). Notably, M5 and M22 were enriched with neuronal markers and identified as top resilience-associated modules (**Fig. 3A-B**). Further, nearly all proteins increased by NRN1 in the rat neuronal proteome were significantly increased in the human asymptomatic cases (**Supplemental Table 16**) and significantly correlated with cognitive slope (58 out of 83 or ~70%, pvalue≤0.05; **Supplemental Table 17**). These findings provide evidence to support the hypothesis that NRN1 is capable of engaging relevant human biology.

3.3 Materials and methods

Primary rat hippocampal culture

Primary rat hippocampal cultures were generated from E18 Sprague-Dawley rat embryos as previously described (Swanger, Mattheyses et al. 2015, Henderson, Greathouse et al. 2019). All experimental procedures were performed under a protocol approved by the Institutional Animal Care and Use Committee (IACUC) at the University of Alabama at Birmingham (UAB). Rats were euthanized with procedures that are consistent with the recommendations of the American Veterinary Medical Association (AVMA) Guidelines for the Euthanasia of Animals and approved by the UAB IACUC. Briefly, cell culture plates were coated overnight with 1 mg/mL poly-L-lysine (Sigma-Aldrich, catalog no. P2636-100MG) and rinsed with diH20. Neurons were cultured at a density of 4 x 10^5 cells per 18-mm glass coverslip in 12-well culture plates (Fisher Scientific, catalog no. 353043). Neurons were cultured in Neurobasal medium (Fisher Scientific, catalog no. 21103-049) supplemented with B27 (Fisher Scientific, catalog no. 17504-044), conditioned by separate cultures of primary rat astrocytes and glia, in a humidified CO2 (5%) incubator at 37°C. Neurons were treated at DIV 4 with 5μM cytosine β-D-arabinofuranoside hydrochloride (Sigma-Aldrich, catalog no. C6645) to eliminate the presence of native astrocytes and glia on the glass coverslips. Medium was changed every three to four days with new glia-conditioned Neurobasal medium for proper culture maintenance. At DIV 12, neurons were transfected with plasmid using Lipofectamine 2000 (Invitrogen, catalog no. 11-668-019) according to the manufacturer's instructions. At DIV 14, primary hippocampal neurons were dosed with either DMSO, 500nM $A\beta_{42}$, 150 ng/mL recombinant neuritin (NRN1), or a combination of 500nM $A\beta_{42}$ plus 150 ng/mL NRN1 for 6 hours. 6 hours was chosen based on past studies demonstrating that $A\beta_{42}$-induced spine loss in cultured neurons plateaus at approximately 6 hours post exposure(110, 182).

Static widefield microscopy

On DIV 14, neurons were fixed with room temperature 2% paraformaldehyde (PFA) in 0.1M phosphate-buffered saline (PBS), washed two times with 1X PBS, and coverslips were mounted on microscope slides (Fisher Scientific, catalog no. 12-550-15) using Vectashield mounting media (Vector Labs, catalog no. H1000). A blinded experimenter performed all microscopy. Images were captured on a Nikon (Tokyo, Japan) Eclipse Ni upright microscope, using a Nikon Intensilight and Photometrics Coolsnap HQ2 camera to image Lifeact-GFP. Previous studies demonstrated that Lifeact-expressing neurons display normal, physiological actin dynamics and dendritic spine morphology (185, 186). Images were captured with Nikon Elements 4.20.02 image capture software using 60X oil-immersion objective (Nikon Plan Apo, N.A. 1.40). Z-series images were acquired at 0.10µm increments through the entire visible dendrite. Dendrites were selected for imaging by using the following criteria: 1) minimum of 25µm from the soma; 2) no overlap with other branches; 3) must be a secondary dendritic branch. Prior to analysis, capture images were deconvolved using Huygens Deconvolution System (16.05, Scientific Volume Imaging, the Netherlands) with the following settings: CMLE; maximum iterations: 50; signal to noise ratio: 40; quality: 0.1. Deconvolved images were saved in .tif formation.

Dendritic spine morphometry analysis

Image analysis was performed with Neurolucida 360 (2.70.1, MBD Biosciences, Williston, Vermont) based on previously described methods (182). Dendritic spine reconstruction was performed automatically using a voxel-clustering algorithm and the following parameters: outer range: 10.0µm; minimum height: 0.5µm; detector sensitivity 100%; minimum count: 8 voxels. Next, the experimenter manually verified that the classifier correctly identified all protrusions. When necessary, the experimenter added any protrusions semi-automatically by increasing detector sensitivity. Each dendritic protrusion was automatically classified as a dendritic filopodium, thin spine, stubby spine, or mushroom spine based on previously described morphological measurements(187). Reconstructions were collected in Neurolucida Explorer

(2.70.1, MBF Biosciences, Williston, Vermont) for branched structure analysis, and then exported to Microsoft Excel (Redmond, WA). Spine density was calculated as the number of spines per 10μm of dendrite length.

Multi-electrode array recording and analysis

Single neuron electrophysiological activity was recorded using a Maestro Edge multiwell microelectrode array and Impedance system (Axion Biosystems). 24 hours prior to multielectrode array (MEA) culturing, each well of a 6-well plate (Axion Biosystems, catalog no. M384-tMEA-6W-5) was coated with 1 mg/mL Poly-L-lysine (Sigma, catalog no. P2636-100MG). The next day, wells were washed with diH_2O. E18 rat primary hippocampal neurons were harvested as described above and plated in a 6-well MEA at a density of 4 x 10^5 cells per well. Each MEA well contained 64 extracellular recording electrodes. Neurons were cultured DIV 0 to DIV 4 in Neurocult™ Neuronal Plating Medium (Stemcell Technologies, catalog no. 05713) with SM1 neuronal supplement (Stemcell Technologies, catalog no. 05711). At DIV 4, media was changed to BrainPhys™ Neuronal Medium (Stemcell Technologies, catalog no. 05790) with SM1 neuronal supplement. At DIV 14, a 5-min MEA prerecording was performed followed by application of DMSO, 500nM $A\beta_{42}$, 150 ng/mL NRN1, or 150 ng/mL NRN1 and 500nM $A\beta_{42}$. After 6 hours, a follow-up 5-min MEA recording was performed to determine effects on neuronal firing. All recordings were performed while connected to a temperature-controlled heater plate (37°C) with 5% CO_2. All data were filtered using 0.1-Hz (high pass) and 5-kHz (low pass) Butterworth filters. Action potential thresholds were set manually for each electrode (typically > 6 standard deviations from the mean signal). Sorting of distinct waveforms corresponding to multiple units on one electrode channel were completed in Offline Sorter (v. 4.0, Plexon). Further analysis of firing rate was performed in NeuroExplorer (v. 5.0, Plexon). Mean firing frequency was calculated spikes/second and $\log_{10}$ transformed.

Thioflavin T aggregation assay

The effect of NRN1 on amyloid beta 1-42 ($A\beta_{42}$) aggregation was measured by *in vitro* thioflavin T (ThT) fluorescence assay essentially as previously described (188). Recombinant human $A\beta_{42}$ (20 µg/mL equivalent to 5 µM) from rPeptide (# A-1170-1) was incubated in 1x Tris-buffered Saline (TBS; 150 mM NaCl, 50 mM Tris-HCl, pH 7.6), and 20 µM ThT in the presence or absence of purified recombinant NRN1 (5 µg/mL or 263 nM; Abcam, ab69755) protein. The assay was conducted in 100 µL reaction volumes in quadruplicates using chilled 96 well black clear bottom plates (Corning, #3904). Fluorescence was captured at 420 Ex, 480 Em for 20 hours at 15 min intervals at 37ºC using Synergy H1 (Biotek) microplate reader. ThT alone was measured and subtracted as background fluorescence. Fluorescence intensities were graphed using GraphPad prism.

SDS-PAGE and immunoblot analyses

For human brain homogenates, 10 µg of protein from each sample was mixed with Laemmli sample buffer (Bio-rad) and β-mercaptoethanol, boiled at ~95° C for 10 minutes, spun briefly to collect the volume and loaded into Bolt 4-12% Bis-Tris gels (Invitrogen) and electrophoresed at 160 V for ~30 minutes. Gels were then stained with Coomassie Blue for protein banding visualization.

For products of the ThT aggregation assay, $A\beta_{42}$ fibrils were precipitated by centrifugation at 10,000 x g. The pellet was resuspended in 50 µL 8M urea buffer (8 M urea, 100 mm NaHPO4, pH 8.5) and boiled in Laemmli sample buffer (BioRad, 161-0737) at 98°C for 5 min. Proteins were resolved on Bolt 4-12% Bis-Tris gels (Thermo Fisher Scientific, NW04120BOX) followed by transfer to nitrocellulose membrane using iBlot 2 dry blotting system (ThermoFisher Scientific, IB21001). Membranes were incubated with StartingBlock buffer (ThermoFisher, 37543) for 30 min followed by overnight incubation at 4º in primary antibodies, Aβ (Novus, NBP11-97929) and NRN1 (Abcam, ab64186). Membranes were washed with 1×Tris-buffered saline containing 0.1% Tween 20 (TBS-T) and incubated with fluorophore-conjugated secondary antibodies (AlexaFluor-

680 or AlexaFluor-800) for 1 h at room temperature. Membranes were subsequently washed three times with TBS-Tween and images were captured using an Odyssey Infrared Imaging System (LI-COR Biosciences).

Silver staining

$A\beta_{42}$ fibrils prepared in the ThT assay above were precipitated by centrifugation at 10,000 x g. The pellet was resuspended in 50 µL 8M urea buffer (8 M urea, 100 mm NaHPO4, pH 8.5) and 10 µL of fibrils were boiled in Laemmli sample buffer (BioRad, 161-0737) at 98°C for 5 min. Fibrils were run on Bolt 4-12% Bis-Tris gels (Thermo Fisher Scientific, NW04120BOX) and stained using a silver staining kit (Pierce, 24612) following manufacturers protocols. Briefly, the was rinsed twice in ultrapure water for 5 minutes followed by fixation in 30% ethanol, 10% acetic acid in water. The gel was washed in 10% Ethanol and water. The gel was then incubated in silver stain and developer solutions. Staining was quenched using 5% acetic acid and images were captured using a scanner.

Cortical rat neuronal culture, lysis and proteolytic digestion

Primary rat cortical neurons were generated from E18 Sprague-Dawley rat embryos with minor modifications (Swanger, Mattheyses et al. 2015, Henderson, Greathouse et al. 2019). Neurons were cultured at a density of $4x10^5$ cells per well in 12-well culture plates (Fisher Scientific, catalog no. 353043). Neurons were cultured in Neurobasal medium (Fisher Scientific, catalog no. 21103-049) supplemented with B27 (Fisher Scientific, catalog no.17504-044). Culture maintenance included a half media change every 2-3 days. At DIV 14, neurons were either treated with 150 ng/mL recombinant NRN1 protein (Abcam, ab69755) or vehicle treated with diH_2O for 6 hours. NRN1 concentration was chosen based on published data that identified a plateau in exogenous NRN1 induced effects on transient potassium currents at 150 ng/mL (189). After 6 hours neurons were washed 2x with 1 mL 1X phosphate-buffered saline (PBS). To harvest cells, 1 mL 1X PBS + protease inhibitor (Fisher Scientific, catalog no. 78426) was added and cells were centrifuged

for 2300rpm for 5 minutes at 4°C. Cell pellets were lysed in 200uL 8M urea buffer and HALT protease and phosphatase inhibitor cocktail (1x final concentration). Lysates were sonicated with a probe sonicator 3 times for 10 s with 10 s intervals at 30% amplitude and cleared of cellular debris by centrifugation in a tabletop centrifuge at 18,000 rcf for 3 minutes at 4° C. Protein concentration was determined by BCA assay and one-dimensional SDS-PAGE gels were run followed by Coomassie blue staining as quality control for protein integrity and equal loading before proceeding to protein digestion. Protein homogenates (50 µg) were diluted with 50 mM NH4HCO3 to a final concentration of less than 2 M urea and then treated with 1 mM dithiothreitol (DTT) at 25°C for 30 minutes, followed by 5 mM iodoacetimide (IAA) at 25°C for 30 minutes in the dark. Protein was digested with 1:100 (w/w) lysyl endopeptidase (Wako) at 25°C for 2 hours and further digested overnight with 1:50 (w/w) trypsin (Pierce) at 25°C. Resulting peptides were desalted with a Sep-Pak C18 column (Waters) and dried under vacuum.

TMT labeling for the rat neuronal proteome

Peptides from each individual cell line in the study and a global pooled reference internal standard (GIS) were labeled using the TMTpro 16-plex kit (ThermoFisher Cat#A44520 Lot#VH311511). Labeling was performed essentially as previously described (157, 190). Briefly, each sample (containing 100 µg of peptides) was re-suspended in 100 mM TEAB buffer (100 µL). The TMT labeling reagents were equilibrated to room temperature, and anhydrous ACN (256 µL) was added to each reagent channel. Each channel was gently vortexed for 5 min, and then 41 µL from each TMT channel was transferred to the peptide solutions and allowed to incubate for 1 h at room temperature. The reaction was quenched with 5% (vol/vol) hydroxylamine (8 µl) (Pierce). All 16 channels were then combined and dried by SpeedVac (LabConco) to approximately 150 µL and diluted with 1 mL of 0.1% (vol/vol) TFA, then acidified to a final concentration of 1% (vol/vol) FA and 0.1% (vol/vol) TFA. Peptides were desalted with a 200 mg C18 Sep-Pak column (Waters). Each Sep-Pak column was activated with 3 mL of methanol, washed with 3 mL of 50% (vol/vol)

ACN, and equilibrated with 2×3 mL of 0.1% TFA. The samples were then loaded, washed with 2×3 mL 0.1% (vol/vol) TFA and 2 mL of 1% (vol/vol) FA. Elution was performed with 2 volumes of 1.5 mL 50% (vol/vol) ACN. The eluates were then dried to completeness. High pH fractionation was performed next as described for human samples.

LC-MS/MS for the rat neuronal proteome

All samples were analyzed with a Dionex Ultimate 3000 RSLCnano in capillary flow mode. The analytical column was a 300 µm x 150 mm ID Waters CSH with 1.7 µm beads. Mass spectrometry was performed with a high-field asymmetric waveform ion mobility spectrometry (FAIMS) Pro equipped Orbitrap Eclipse (Thermo) in positive ion mode using data-dependent acquisition with 1.5 second top speed cycles for each FAIMS compensation voltage (CV). Each cycle consisted of one full MS scan followed by as many MS/MS events that could fit within the given 1.5 second cycle time limit. MS scans were collected at a resolution of 120,000 (410-1600 m/z range, $4x10^5$ AGC, 50 ms maximum ion injection time, FAIMS CV of -45 and -65). All higher energy collision-induced dissociation (HCD) MS/MS spectra were acquired at a resolution of 30,000 (0.7 m/z isolation width, 35% collision energy, $1.25×10^5$ AGC target, 54 ms maximum ion time, TurboTMT on). Dynamic exclusion was set to exclude previously sequenced peaks for 20 seconds within a 10-ppm isolation window. All raw files are loaded onto synapse folder https://www.synapse.org/ADresilienceRat.

Data search and protein quantification for the rat neuronal proteome

All raw files (n=96) were analyzed using the Proteome Discoverer Suite (version 2.4) Thermo Scientific). MS/MS spectra were searched against the UniProtKB rat proteome database (downloaded April 2015 with 29370 total sequences). The Sequest HT search engine was used with the following parameters: fully tryptic specificity; maximum of two missed cleavages; minimum peptide length of 6; fixed modifications for TMT tags on lysine residues and peptide N-termini (+304.207 Da) and carbamidomethylation of cysteine residues (+57.02146 Da); variable

modifications for oxidation of methionine residues (+15.99492 Da), deamidation of asparagine and glutamine (+0.984 Da) and phosphorylation of serine, threonine and tyrosine (+79.966); precursor mass tolerance of 10 ppm; and fragment mass tolerance of 0.05 Da. The Percolator node was used to filter peptide spectral matches (PSMs) to a false discovery rate (FDR) of less than 1%. Following spectral assignment, peptides were assembled into proteins and were further filtered based on the combined probabilities of their constituent peptides to a final FDR of 1%. A Multi-consensus was performed to group proteins identified across the individual batches. In cases of redundancy, shared peptides were assigned to the protein sequence in adherence with the principles of parsimony. A total of 125869 peptides mapping to 9799 protein groups. Reporter ions were quantified from MS2 scans using an integration tolerance of 20 ppm with the most confident centroid setting. Only unique and razor (i.e., parsimonious) peptides were considered for quantification. TMT channels 129C, 130N and 130C correspond to NRN1 treated samples and channels 132C, 133N, 133C and 134N correspond to vehicle treated samples which were used for the presented results (**Supplemental Table 13;** https://www.synapse.org/ADresilienceRat).

Rat neuronal proteome overlap with human consensus modules

Human consensus module (39 modules) protein members were converted to rat symbols using the biomaRt package and overlap of rat neuronal proteins was determined for each module. A one-tailed Fisher exact test looking for significant overrepresentation or overlap was employed, and *P* values were corrected for multiple testing using the Benjamini–Hochberg method. R functions fisher.test() and p.adjust() were used to obtain the above statistics (**Supplemental Table 15).**

Additional statistical analyses

All proteomic statistical analyses were performed in R (version 4.0.3). Box plots represent the median and 25th and 75th percentile extremes; thus the hinges of a box represent the interquartile range of the two middle quartiles of data within a group. Error bars extents are defined by the

farthest data points up to 1.5 times the interquartile range away from the box hinges. Correlations were performed using biweight midcorrelation function from the WGCNA package. Differential expression between NRN1 and vehicle treated neurons was determined by student's t-test and corrected for multiple hypothesis testing by ROTS (191) FDR correction (v1.18.0; **Supplemental Table 15).** The ROTS() function was run with parameters B= 100, K==900 and seed set to 1. Differential expression displayed as volcano plots were generated using the ggplot2 package. Go annotation for rat neuron proteins was performed as described for human samples. P values were adjusted for multiple comparisons by FDR correction where indicated.

All analyses from dendritic spine morphometric and MEA results were conducted with Prism 9.0 (GraphPad Software, La Jolla, CA). Data are presented as mean ± SEM, and all graph error bars represent SEM. All statistical tests were two tailed with threshold for statistical significance set at 0.05. Statistical comparisons on spine densities and morphologies are one-way ANOVA with Tukey's comparison's test. Statistical comparisons on mean firing rate are unpaired Student's *t* test.

3.4 Discussion

Understanding how protein targets and pathways influence cognitive resilience to AD represents a promising complimentary approach to traditional translational research efforts. NRN1 has been identified through work from our group and others as a potential mediator of resilience. The work presented in this chapter explores the neuroprotective mechanisms of NRN1 against Aβ insult in a cellular model of AD. Exogenous treatment of NRN1 prevented dendritic spine loss and hyperexcitability induced by exposure to Aβ oligomers. Proteomic evaluation of NRN1 targets link NRN1 exposure with synaptic biology that overlap with human brain resilience modules. The present work contributes to foundational roles of NRN1 in AD neuroprotection and the biological relevance of NRN1 target engagement with human resilience phenotypes.

Dendritic spines are small actin-rich protrusions off dendrites that serve as the postsynaptic sites of the majority of excitatory synapses in the brain. Spines exhibit remarkable variability in size, shape, and density along the length of dendritic branches (192-194). Spine structure is inseparably linked to spine function and spines are classified on the basis of their three-dimensional morphology as stubby, mushroom, thin or filopodia (83, 85). Cognitive decline associated with aging is hypothesized to be driven by subtle alterations in dendritic spine density and morphology in mammals. Thin spine loss occurs with age in the dorsolateral prefrontal cortex and correlates with worsening cognitive performance (101, 102, 181, 195). In parallel, patients with AD can exhibit high rates of epileptic seizure activity which is associated with accelerated cognitive decline (183, 184, 196). In APP transgenic mice, epileptiform activity is an indicator of network hyperexcitability which is driven by degeneration of hippocampal pyramidal neurons' dendrites and dendritic spines (109). Loss of dendrites and spines reduces the total surface area of the cell and renders the neuron more electrically compact. In a compact neuron, synapse currents are translated more frequently which leads to increased action potential output, consequently inducing neuronal hyperexcitability and aberrant circuit synchronization (197).

Similar to APP transgenic mice, exogenously applied $A\beta_{42}$ oligomers can induce dendritic spine degeneration which subsequently causes hyperexcitability in cultured rodent hippocampal neurons (112). Using highly optimized three-dimensional modeling of spines in combination with MEA analyses, we show that exogenously delivered NRN1 protects against $A\beta_{42}$-induced spine degeneration and hyperexcitability. Moreover, our results indicate that in cultures treated with NRN1 alone, alterations in spine density or morphology were not observed. However, NRN1 alone increased mean action potential firing rates. The mechanisms by which NRN1 increases action potential frequency are not due to alterations in spine density or structure, unlike the effects of $A\beta_{42}$. We posit that the elevation in mean firing rates are due to NRN1-mediated modification of the synaptic proteome, which are highlighted by increases in protein abundance from human brain modules M4, M5, and M22 (**Fig. 7).** Yet, it remains to be determined whether the downstream pathways of NRN1-protection against $A\beta_{42}$ are similar to or different from how NRN1 affects the proteome in the absence of $A\beta_{42}$. Notably, Choi et al. showed that over-expression of NRN1 in cultured hippocampal neurons increased mini excitatory postsynaptic current frequency, which mirrors our findings that NRN1 alone increased action potential firing rate (143). Furthermore, electrophysiology studies by An et al. demonstrated that brain infusion of recombinant NRN1 (similar to the reagents used in this study) into Tg2576 APP transgenic mice rescued deficits in hippocampal long-term potentiation in the Schaffer collateral pathway (145). Collectively, these findings support the promise of NRN1 as a therapeutic target to support synaptic mechanisms of resiliency in preclinical stages of AD.

A potential limitation of the current study is that NRN1 neuroprotection was only assessed for Aβ insult and not tau. Quantitative neuropathological studies indicate that asymptomatic cases typically have lower levels of tau pathology but comparable levels of amyloid burden in the brain at autopsy compared to symptomatic AD cases (78). Thus, understanding the impact of NRN1 on Aβ insult is highly relevant to the pathological context observed in resilient brains. Future work

investigating the interaction or effects of NRN1 on tau neuropathology may provide additional insights into NRN1 neuroprotection relevant to at-risk populations.

3.5 Figures

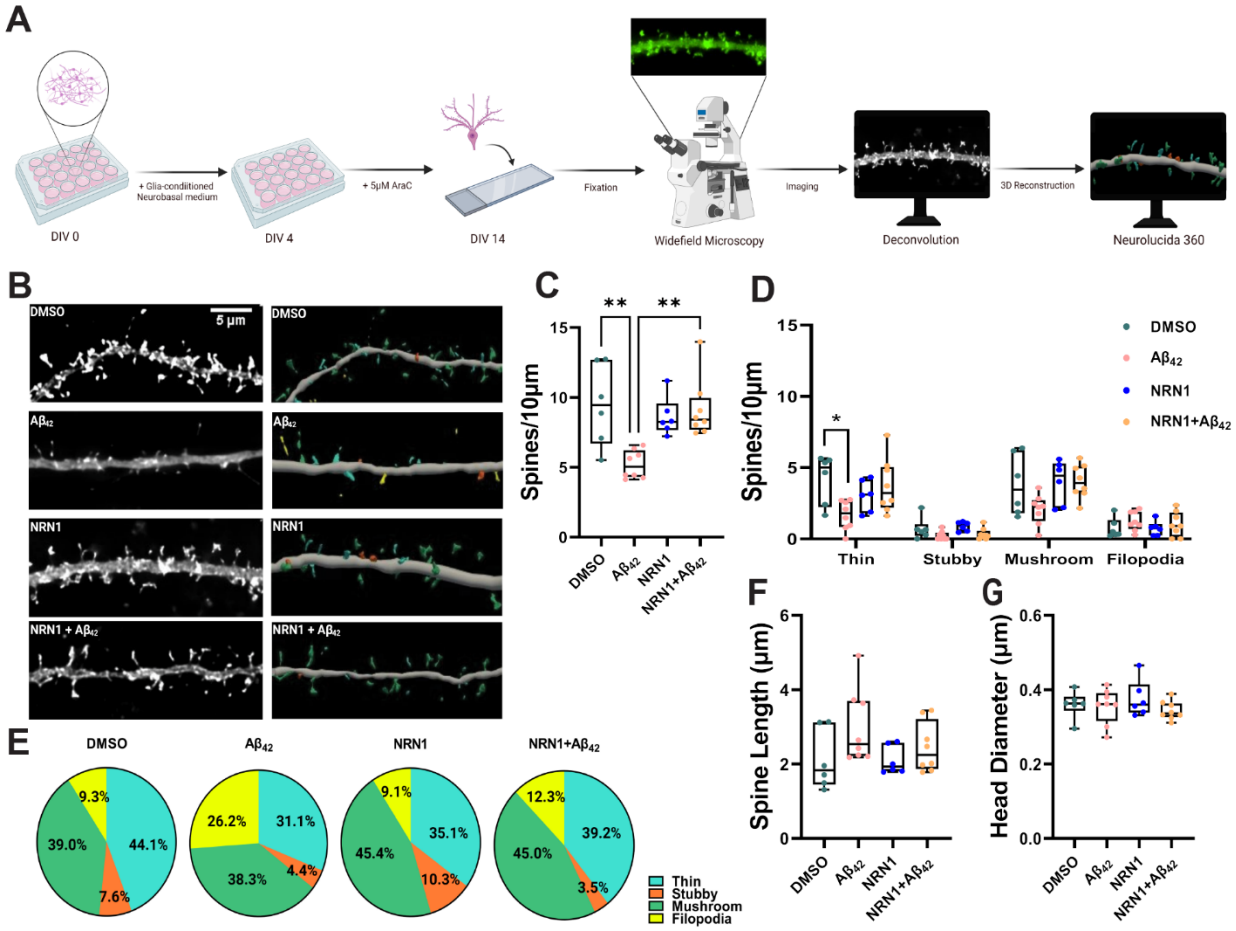
A
DIV 0
+ Glia-conditioned Neurobasal medium
DIV 4
+ 5μM AraC
DIV 14
Fixation
Widefield Microscopy
Imaging
Deconvolution
3D Reconstruction
Neurolucida 360
B
DMSO
5 μm
Aβ42
NRN1
NRN1 + Aβ42
C
Spines/10μm
DMSO
Aβ42
NRN1
NRN1+Aβ42
D
Spines/10μm
Thin
Stubby
Mushroom
Filopodia
E
DMSO
Aβ42
NRN1
NRN1+Aβ42
9.3%
44.1%
39.0%
7.6%
26.2%
31.1%
38.3%
4.4%
9.1%
35.1%
45.4%
10.3%
12.3%
39.2%
45.0%
3.5%
Thin
Stubby
Mushroom
Filopodia
F
Spine Length (μm)
G
Head Diameter (μm)

Figure 3.1: $A\beta_{42}$-induced dendritic spine degeneration is blocked by NRN1. (**A**) Schematic representation of primary rat hippocampal neuron treatment and dendritic spine morphometric analysis. (**B**) Representative maximum-intensity wide-field fluorescent images of hippocampal neurons after deconvolution (left). Corresponding three-dimensional reconstructions of dendrites generated in Neurolucida 360 (right), with dendritic spines color-coded by spine type (blue = thin, orange = stubby, green = mushroom, yellow = filopodia). Scale bar, 5 μm. N = 6 to 8 neurons (one dendrite per neuron) were analyzed per experimental condition. (**C**) Dendritic spine density in hippocampal neurons exposed to DMSO, 500nM $A\beta_{42}$, 150 ng/mL NRN1, or 150 ng/mL NRN1 and 500nM $A\beta_{42}$. **P < 0.01 (DMSO vs. $A\beta_{42}$, actual P = 0.0025) ($A\beta_{42}$ vs NRN1+$A\beta_{42}$, actual P = 0.0026) by one-way ANOVA with Tukey's test. *P < 0.05 ($A\beta_{42}$ vs NRN1, actual P = 0.0177) by one-way ANOVA with Tukey's test. (**D**) Dendritic spine density of thin, stubby, or mushroom spines per 10 μm. *P < 0.05 (DMSO vs. Aβ42, actual P = 0.0218) by one-way ANOVA with Tukey's test. (Thin, $A\beta_{42}$ vs NRN1+$A\beta_{42}$, actual P = 0.0501) (Mushroom, DMSO versus $A\beta_{42}$, actual P = 0.1514) (Mushroom, $A\beta_{42}$ versus NRN1+$A\beta_{42}$, actual P = 0.0598) by one-way ANOVA with Tukey's test. (**E**) Dendritic spine type frequency in hippocampal neurons exposed to DMSO, 500nM $A\beta_{42}$, 150 ng/mL NRN1, or 150 ng/mL NRN1 and 500nM $A\beta_{42}$. (**F**) Overall dendritic spine length and (**G**) head diameter. Related data are shown in **Fig. S7**. Box plots represent median, 25th and 75th percentiles. Box hinges represent the interquartile range of the two middle quartiles with a group. Error bars are based on data points 1.5 times the interquartile range from the box hinge.

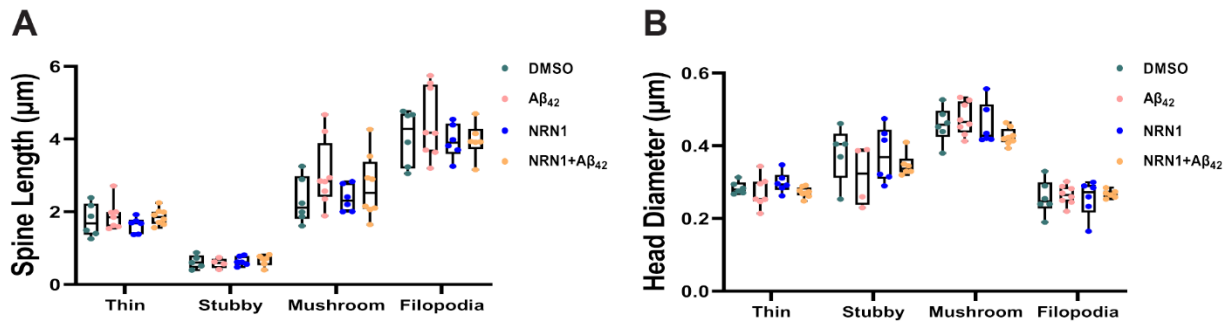
A
Spine Length (µm)
6
4
2
0
Thin
Stubby
Mushroom
Filopodia
DMSO
Aβ42
NRN1
NRN1+Aβ42
B
Head Diameter (µm)
0.6
0.4
0.2
0.0
Thin
Stubby
Mushroom
Filopodia
DMSO
Aβ42
NRN1
NRN1+Aβ42

Figure 3.2: Analysis of dendritic spine length and head diameter among thin, stubby, mushroom spines and filopodia. (A) Dendritic spine length of thin, stubby, or mushroom spines, and filopodia. (B) Dendritic spine head diameter of thin, stubby, or mushroom spines, and filopodia. Box plots represent median, 25th and 75th percentiles. Box hinges represent the interquartile range of the two middle quartiles with a group. Error bars are based on data points 1.5 times the interquartile range from the box hinge.

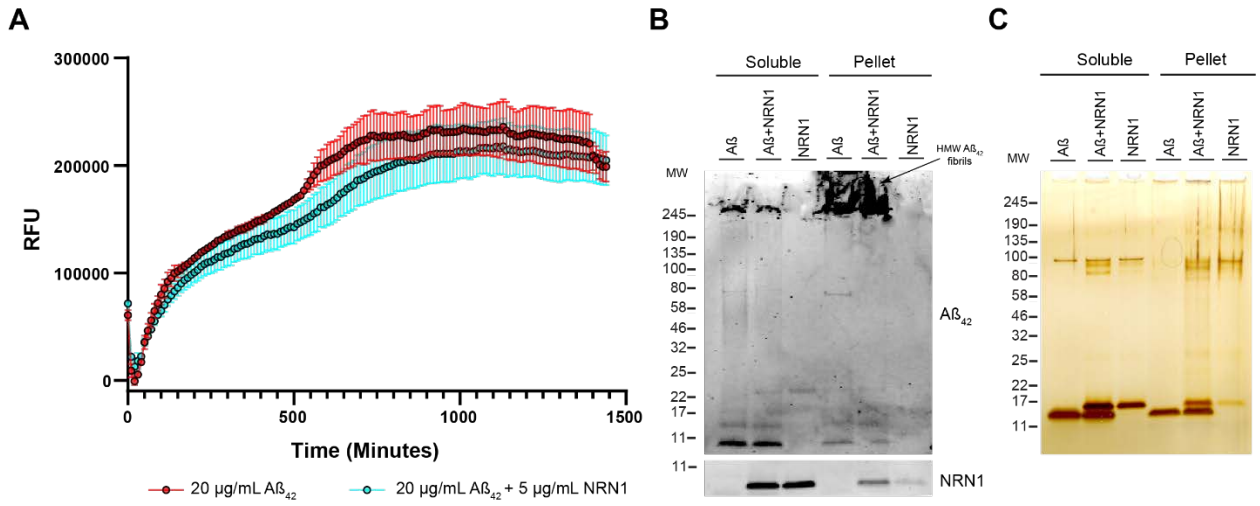
A
300000
200000
100000
0
RFU
0
500
1000
1500
Time (Minutes)
20 µg/mL Aß42
20 µg/mL Aß42 + 5 µg/mL NRN1
B
Soluble
Pellet
Aß
Aß+NRN1
NRN1
HMW Aß42 fibrils
MW
245
190
135
100
80
58
46
32
25
22
17
11
Aß42
NRN1
C

Figure 3.3: Aggregation of Aβ in the presence or absence of NRN1. (**A**) Fibrillation curves of 20 µg/mL $A\beta_{42}$ alone and 20 µg/mL $A\beta_{42}$ + 5 µg/mL NRN1, thioflavin T (ThT) alone was recorded and subtracted as background. Relative fluorescent units (RFU) were recorded every 15 minutes for 20 hours. Points are quadruplicate means ± SEM. (B) Western blot of soluble and pelleted fractions of assay products probed for $A\beta_{42}$ and NRN1. High molecular weight (HMW) fibrils are observed at the top of the gel. (C) Silver stain of soluble and pelleted fractions of assay products.

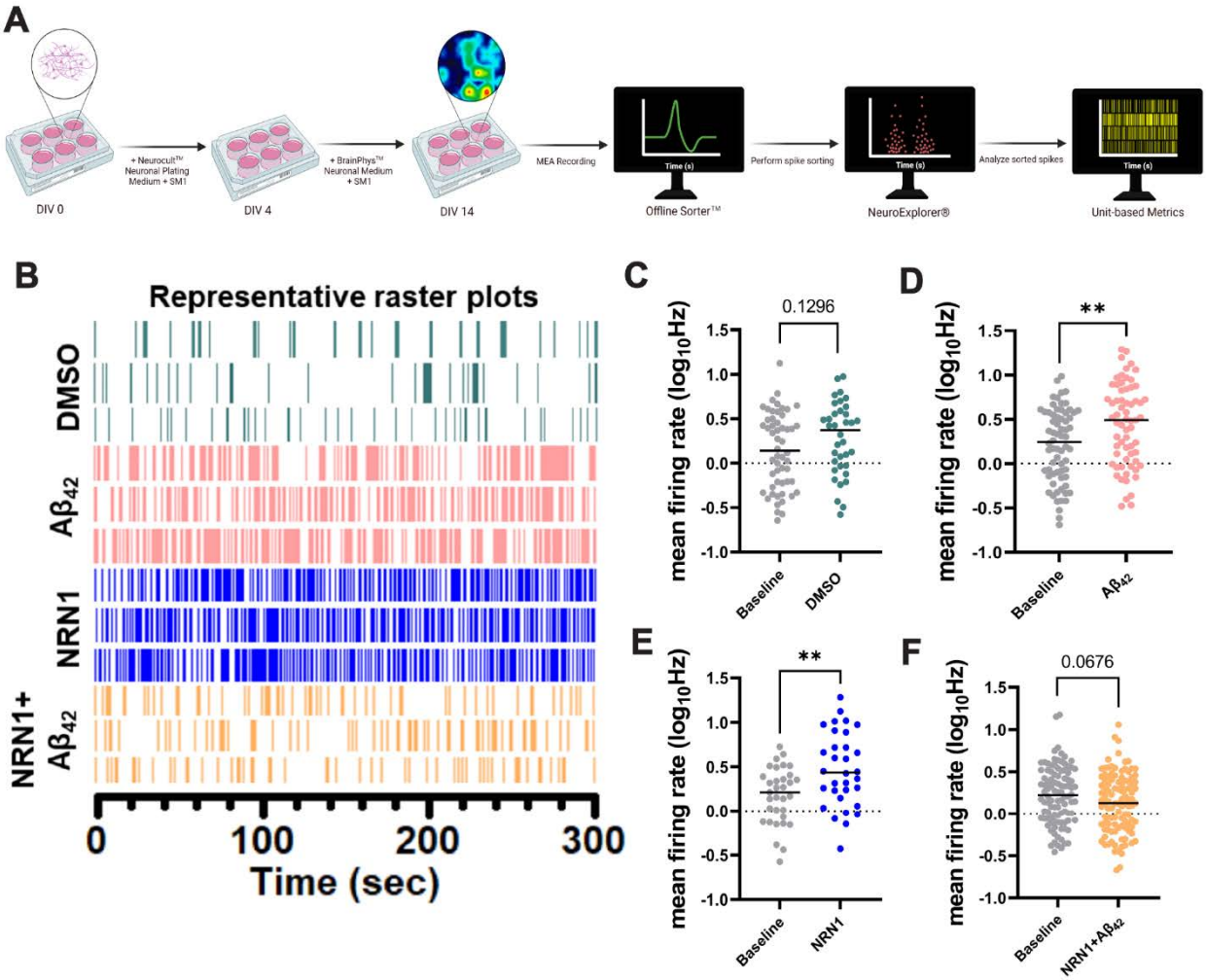
A
DIV 0
+ Neurocult™ Neuronal Plating Medium + SM1
DIV 4
+ BrainPhys™ Neuronal Medium + SM1
DIV 14
MEA Recording
Offline Sorter™
Perform spike sorting
NeuroExplorer®
Analyze sorted spikes
Unit-based Metrics
B
Representative raster plots
DMSO
Aβ42
NRN1
NRN1+ Aβ42
0
100
200
300
Time (sec)
C
0.1296
mean firing rate (log10Hz)
Baseline
DMSO
D
**
Baseline
Aβ42
E
**
Baseline
NRN1
F
0.0676
Baseline
NRN1+Aβ42

Figure 3.4: NRN1 protects against $A\beta_{42}$-induced neuronal hyperexcitability. (**A**) Schematic representation of primary rat hippocampal neuron treatment and single neuron electrophysiology analysis. (**B**) Representative raster plots from three units after exposure to DMSO, 500nM $A\beta_{42}$, 150 ng/mL NRN1, or 150 ng/mL NRN1 and 500nM $A\beta_{42}$. (**C**) Mean firing rate at DIV14 in hippocampal neurons treated with DMSO, compared to baseline (n = 36-54 neurons, unpaired Student's t test; p = 0.1296). (**D**) Mean firing rate at DIV14 in hippocampal neurons treated with 500nM $A\beta_{42}$, compared to baseline (n = 65-68 neurons, unpaired Student's t test; p = 0.0022)**.** (**E**) Mean firing rate at DIV14 in hippocampal neurons treated with 150 ng/mL NRN1, compared to baseline (n = 32-33 neurons, unpaired Student's t test; p = 0.0023)**.** (**F**) Mean firing rate at DIV14 in hippocampal neurons treated with 150 ng/mL NRN1 and 500nM $A\beta_{42}$, compared to baseline (n = 100-107 neurons, unpaired Student's t test; p = 0.0676).

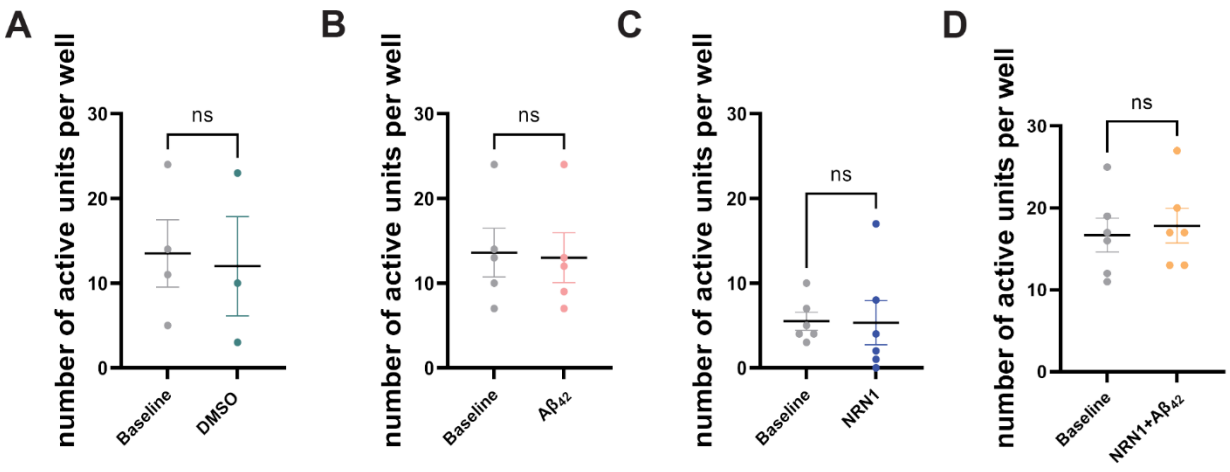
A
number of active units per well
30
20
10
0
ns
Baseline
DMSO
B
number of active units per well
30
20
10
0
ns
Baseline
Aβ42
C
number of active units per well
30
20
10
0
ns
Baseline
NRN1
D
number of active units per well
30
20
10
0
ns
Baseline
NRN1+Aβ42

Figure 3.5: Total number of active neurons per microelectrode array. (**A**) The total number of active neurons per well at DIV 14 in hippocampal neurons treated with DMSO, compared to baseline (n = 3-4 wells with 64 electrodes/well, unpaired Student's t test; p = 0.8339). Data are means + SEM. (**B**) The total number of active neurons per well at DIV 14 in hippocampal neurons treated with 500nM $A\beta_{42}$, compared to baseline (n = 5 wells with 64 electrodes/well, unpaired Student's t test; p = 0.8878). Data are means + SEM. (**C**) The total number of active neurons per well at DIV 14 in hippocampal neurons treated with 150 ng/mL NRN1, compared to baseline (n = 6 wells with 64 electrodes/well, unpaired Student's t test; p = 0.9539). Data are means + SEM. (**D**) The total number of active neurons per well at DIV 14 in hippocampal neurons treated with 150 ng/mL NRN1 and 500nM $A\beta_{42}$, compared to baseline (n = 6 wells with 64 electrodes/well, unpaired Student's t test; p = 0.7035). Data are means + SEM.

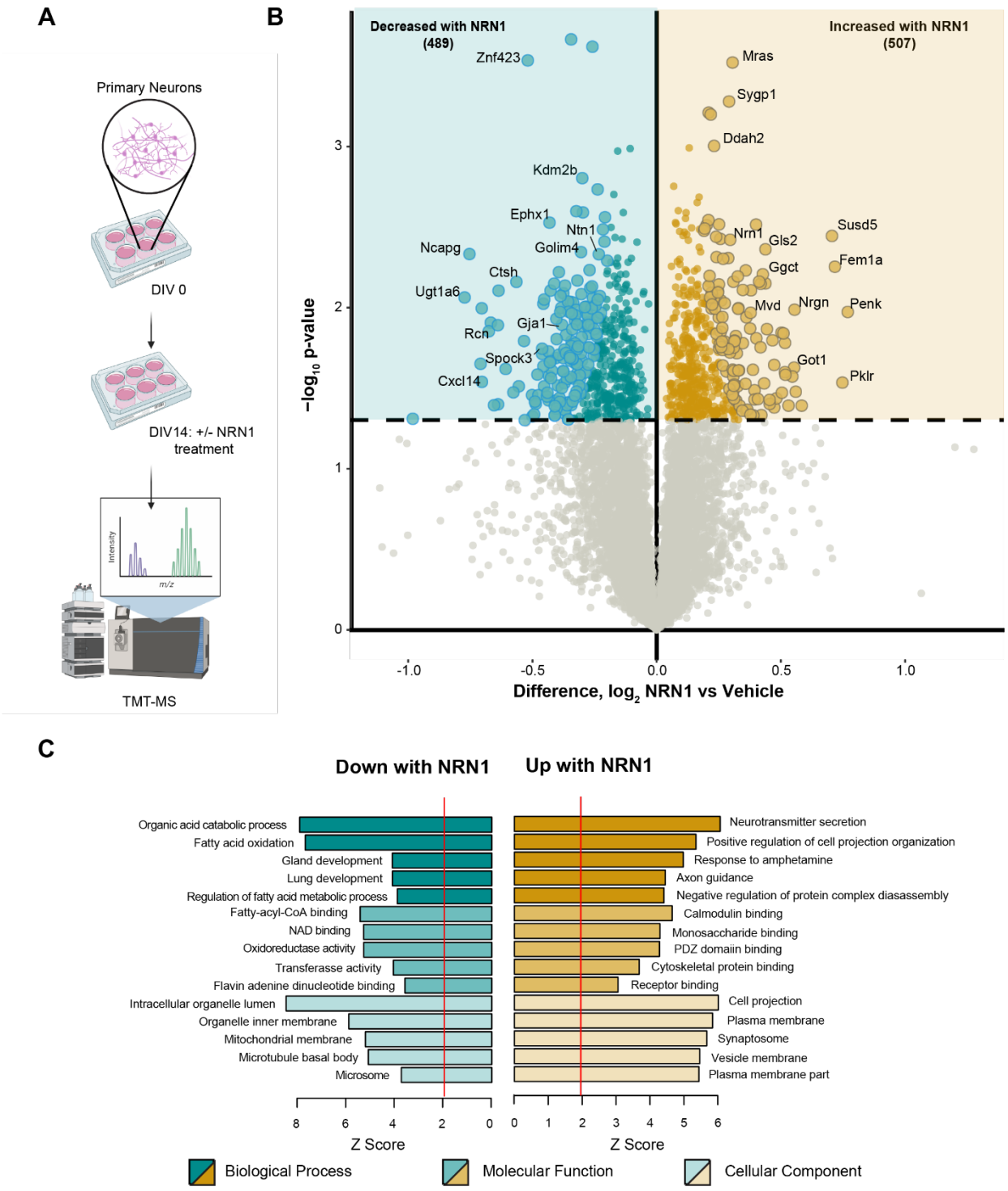
A
Primary Neurons
DIV 0
DIV14: +/- NRN1 treatment
Intensity
m/z
TMT-MS
B
Decreased with NRN1 (489)
Increased with NRN1 (507)
Znf423
Mras
Sygp1
Ddah2
Kdm2b
Ephx1
Ntn1
Golim4
Ncapg
Ctsh
Ugt1a6
Gja1
Rcn
Spock3
Cxcl14
Nrn1
Gls2
Susd5
Fem1a
Ggct
Mvd
Nrgn
Penk
Got1
Pklr
−log10 p-value
Difference, log2 NRN1 vs Vehicle
C
Down with NRN1
Up with NRN1
Organic acid catabolic process
Fatty acid oxidation
Gland development
Lung development
Regulation of fatty acid metabolic process
Fatty-acyl-CoA binding
NAD binding
Oxidoreductase activity
Transferasse activity
Flavin adenine dinucleotide binding
Intracellular organelle lumen
Organelle inner membrane
Mitochondrial membrane
Microtubule basal body
Microsome
Neurotransmitter secretion
Positive regulation of cell projection organization
Response to amphetamine
Axon guidance
Negative regulation of protein complex diasassembly
Calmodulin binding
Monosaccharide binding
PDZ domaiin binding
Cytoskeletal protein binding
Receptor binding
Cell projection
Plasma membrane
Synaptosome
Vesicle membrane
Plasma membrane part
Z Score
Z Score
Biological Process
Molecular Function
Cellular Component

Figure 3.6. NRN1 treatment induces changes in the neuronal proteome related to broad synaptic functions. (**A**) Schematic representation of rat primary cortical neuronal culture workflow in which neurons were maintained in neurobasal medium for 14 days, treated with 150ng/mL of NRN1 and analyzed via TMT-MS. (**B**) Differential protein expression between NRN1 treated and vehicle treated neurons (n=8,238 proteins). Proteins above the dashed line (p=0.05) are considered significantly differentially expressed. Student's t-test was used to calculate pvalues. Large spots are based on reproducibility-optimized test statistic (ROTS) correction of differentially expressed proteins with 10% or less false discovery rate (FDR). (**C**) Gene ontology of significantly differentially expressed proteins in NRN1 treated neurons. A Z-score above 1.96 was considered significant ($p<0.05$).

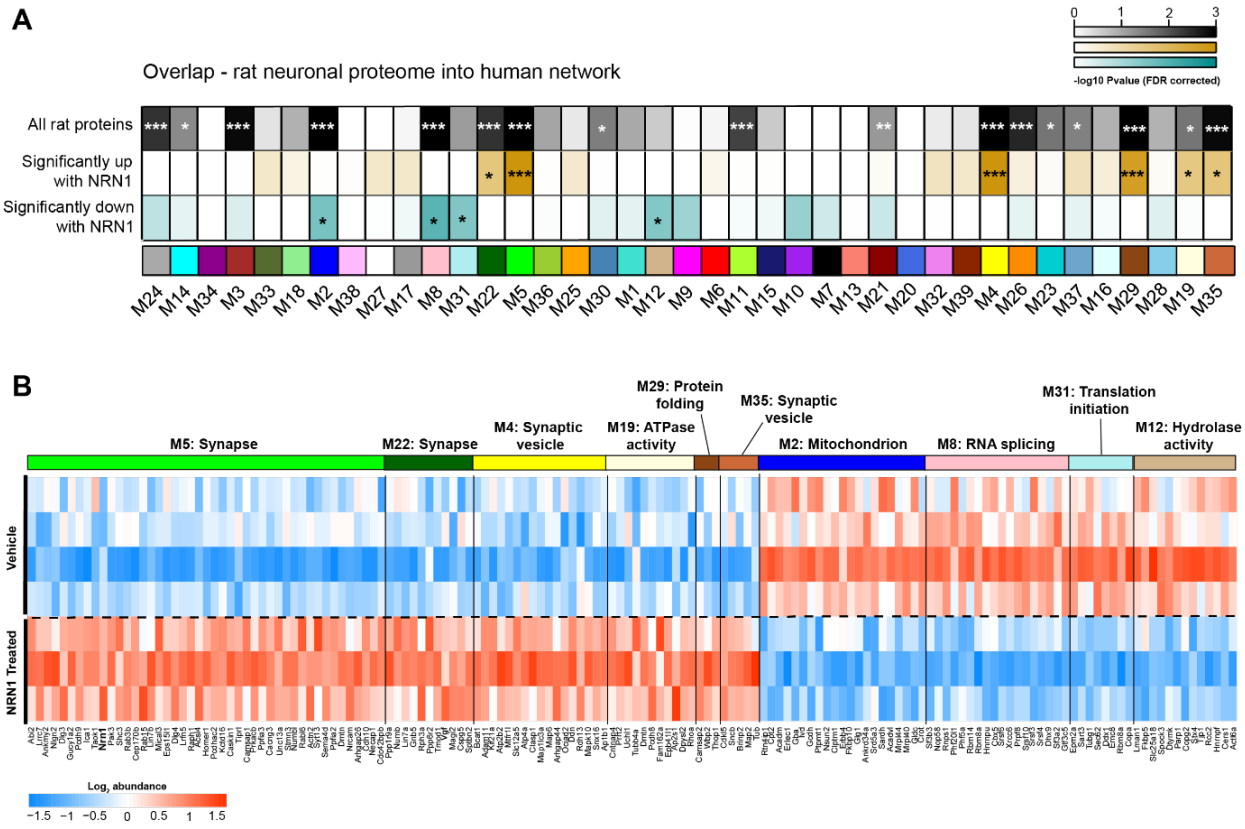
A
Overlap - rat neuronal proteome into human network
0 1 2 3
-log10 Pvalue (FDR corrected)
All rat proteins
Significantly up with NRN1
Significantly down with NRN1
M24 M14 M34 M3 M33 M18 M2 M38 M27 M17 M8 M31 M22 M5 M36 M25 M30 M1 M12 M9 M6 M11 M15 M10 M7 M13 M21 M20 M32 M39 M4 M26 M23 M37 M16 M29 M28 M19 M35
B
M5: Synapse
M22: Synapse
M4: Synaptic vesicle
M19: ATPase activity
M29: Protein folding
M35: Synaptic vesicle
M2: Mitochondrion
M8: RNA splicing
M31: Translation initiation
M12: Hydrolase activity
Vehicle
NRN1 Treated
Log2 abundance
−1.5 −1 −0.5 0 0.5 1 1.5

Figure 3.7: NRN1 engages proteins within modules linked to cognitive resilience in human brain. (**A**) To directly compare NRN1-induced changes in the context of human biology, a Fisher's exact test was used to calculate significant enrichment of proteins from the entire rat proteome (top row), significantly increased with NRN1 (middle row) and significantly decreased with NRN1 (bottom row) treatment across the 39 human consensus modules ($0.05 > p > 0.01$ = *, $0.01 > p > 0.005$ =**, $p < 0.005$ = ***). (**B**) Proteins significantly impacted by NRN1 treatment that overlap with human modules were visualized as a heatmap. Rat protein abundance was compared using Bicor across NRN1 treated and vehicle treated groups.

4.0 Discussion and Future Directions

4.1 Summary and contributions

The concept of cognitive resilience seeks to define the phenomenon in which certain individuals live into advanced age with intact cognitive function despite significant Alzheimer's disease pathology in their brains. This ability to demonstrate physiological and cognitive resilience against toxic pathological accumulation represents a fascinating and information rich area of research that may benefit the development of therapeutic strategies for individuals at risk for dementia. The work presented in this dissertation provides foundational contributions to the characterization and advancement of the molecular basis of cognitive resilience in human neurodegeneration. We used an integrative pipeline that pairs systems-level nomination in multiple human brain regions with experimental mechanistic validation in a primary cell model. Our efforts validate and extend work from our group and others in evaluating key resilience-associated proteins and pathways. This approach enables both unbiased profiling and bidirectional integration of molecular and clinical data. Following the current framework, TMT-MS based proteomic data from two independent studies and a total of three brain regions were incorporated to characterize communities of proteins from an in-depth proteomic dataset strongly related to cognitive resilience. NRN1, a neurotrophic factor previously reported for its association to resilience and synaptic function, was identified as a hub protein in the human consensus network and functionally validated for synaptic resilience against Aβ. To define overlapping neurobiology between NRN1's effects on primary neurons and humans, TMT-MS proteomic data from the model system was fed back into the human brain proteome to identify convergent pathways relevant for resilience.

Within the human brain correlation network, we identified several protein modules positively associated with cognitive resilience and incorporated an enrichment analysis from an independent proteomic dataset to unbiasedly nominate modules relating to cognitive resilience. Among the significant modules, synaptic modules (M22 and M5) were the most strongly enriched

and positively correlated with multiple antemortem cognitive metrics, including cognitive slope. Differential expression analysis of module members from M22 and M5 comparing AsymAD and AD cases identified proteins significantly increased in AsymAD that overlapped with previous PWAS results. NRN1, a neurotrophic factor linked to increased resilience, was among the most significantly increased in AsymAD cases and positively correlated with cognitive scores. Prioritizing NRN1 for mechanistic validation, a cellular model of AD was employed to evaluate the potential neuroprotective functions of NRN1 against Aβ insult, specifically at the level of the synapse. We demonstrated that primary neurons co-treated with NRN1 and Aβ oligomers rescued dendritic spine loss induced by Aβ. NRN1 also prevented Aβ-induced hyperexcitability in primary cells. Proteomic analysis of NRN1 treated neurons identified significant engagement of synaptic biology after incubation and these increased markers largely overlapped with human resilience module members from the consensus brain proteome network (synaptic modules M22 and M5, among others). This work contributes to multiple levels of investigation of cognitive resilience in a cyclic, integrative workflow. A depth of information generated from discovery proteomics highlighted key group-wise differences in molecular signatures and further supported the nomination of NRN1 as a resilience promoting target. Experimental validation of NRN1 synaptic protection extends the role for NRN1 as a physiological mediator of resilience with biological relevance to the human phenotype (**Fig. 4.1**).

4.2 Future directions

4.2.1 *Additional consensus network modules.* The consensus network strategy used in the analysis of our multi-region brain proteome defined 39 co-expression modules. Based on the questions of this specific research project and the previously identified significance of synaptic retention in resilient cases, we prioritized specific modules for more in-depth evaluation. That said, a dataset of this size likely holds information yet to be gleaned. Further, the heterogenous and multifactorial nature of AD suggests more than one mechanism or marker is likely to contribute to

achieving resilience. There were several modules significantly associated with AsymAD cases and cognitive scores in the network that may inform additional pathways uniquely altered in resilience, including those related to immune processes, cellular energetics and metabolism. Likewise, this assertion indicates additional individual protein candidates that could be validated and explored in the context of neuroprotection could be nominated from the current results. Among potentially interesting modules outside the scope of the current project, modules M7 ‘Immune Process’ and M13 ‘Acute Inflammatory Response’ were lower in AsymAD compared to AD. This is consistent with previous findings that resilient cases exhibit altered patterns of immune markers in their brains, with lower levels of pro-inflammatory chemokines and higher levels of anti-inflammatory cytokines reported (81). Future work investigating the role of neuroimmune processes in AsymAD and resiliency is warranted.

4.2.3 *Extensions of the current framework.* Implementation of the current framework for additional levels of analysis will further elaborate unique molecular features in resilient cases. Ongoing work related to this project includes the processing of samples enriched for synaptosomes from human brain tissue as well as incorporation of dendritic spine morphometry data from the same human cases into the network analysis. Moreover, phosphoproteomic evaluation could be informative in both human brain tissue samples as well as mechanistic underpinnings relating to NRN1 induced synaptic changes. Phosphorylation is a post-translational modification (PTMs) critical in regulating several signaling pathways in normal brain function, synaptic regulation and AD. Work from our group has demonstrated methodological proficiency in enriching the phosphoproteome, a stoichiometrically small proportion of the proteome, and reported significant differences between disease states (165). Differences in PTMs in AsymAD could provide a more holistic picture of unique brain changes enabling resilience. Similarly, understanding how NRN1 influences the phosphoproteome within the larger context of synaptic and cognitive resilience is of potential value. Incubation of cerebellar granule cells with NRN1

leads to phosphorylation of ERK1/2, Akt and mTOR for varied lengths of time, critical factors in the MEK-ERK pathway which influences synaptic plasticity and cognitive function (179). Also, provided NRN1 can significantly influence neuronal firing rates and synaptic protein abundances without significant alterations to spine density or morphometry (as demonstrated in the current work), evaluating changes in phosphorylation induced by NRN1 in cell or animal models may contribute to understanding how NRN1 impacts complex synaptic signaling pathways.

4.2.2 Possible neuroimmune functions of NRN1. In recognition of the underexplored contribution of neuroimmune functions in cognitive resilience, similar questions could also be extended to individual resilience candidate proteins. Notably, NRN1 has also been associated with immune modulation in recent years. NRN1 is produced by follicular regulatory T cells and directly influences B cell differentiation, which has been associated with modulation of allergy and autoimmune processes (198). In addition, NRN1 overexpression in the hippocampus in a type 2 diabetes rat model improved related cognitive impairment, brain atrophy, neuronal survival and reduced astrogliosis (199). This work also showed NRN1 exogenous treatment in an astrocyte cell line suppressed astrogliosis following lipopolysaccharide induction through the JAK2/STAT3 pathway. Collectively, this work provides preliminary findings that could be used to extrapolate yet unexplored functions of NRN1 in the CNS and in the context of AD. The role of neuroimmune functions in exacerbating and significantly modifying the course of AD progression is well recognized and anti-inflammatory therapeutics are a developing area of research (200). This evidence of NRN1 exogenous application in ameliorating astrocyte reactivity further supports our hypothesis that NRN1 may exert protective effects as a dual-action (or multi-action) molecular effector capable of increasing proteins and pathways vulnerable in AD such as synaptic biology while decreasing those aberrantly increased in AD (relating to metabolism and cellular energetics as reported here or glial activation as reported elsewhere (199)). Future work will need to increase

understanding of the mechanisms of action enabling NRN1 effects (explored in more detail in the next section).

4.2.4 NRN1 biology. Another consideration for future work includes the exploration of the NRN1 interactome and possible limitations as a therapeutic target. Evidence suggests NRN1 is primarily found in the soluble form in the adult CNS and functions as a ligand (126, 174). However, the receptors involved in exerting NRN1's effects in neurons and at the synapse remain largely unknown. The insulin receptor (IR) is proposed as one potential binding site that would explain the ability of NRN1 to increase Kv4.2 expression and outward K+ currents (189). While blocking IRs prevents this effect of NRN1, there is no current data that directly confirms NRN1 as an IR ligand. Future work on the effects of NRN1 in resilience or otherwise will need to establish the mechanisms enabling its action, including receptors and binding partners.

One potential avenue would be to couple co-immunoprecipitation with quantitative MS to identify protein-protein interactions from either tissue or cultured neurons (complimenting the methods employed here). Unfortunately, much troubleshooting within our group and collaborators has had limited success achieving consistent results with current commercially available antibodies for NRN1. Recently, efforts to produce a robust monoclonal antibody recognizing NRN1 have been reported in the literature, suggesting better reagents may become available and enable these experiments in the near future (201).

Use of spatial proteomics strategies may also represent a viable option in exploring the NRN1 interactome, which could include generation of NRN1-fused TurboID constructs. TurboID is a proximity labeling technique accomplished by a mutated biotin ligase to promiscuously biotinylate nearby interactors (202, 203). Collaborative work among group members has demonstrated optimized methods for implementation of TurboID in vivo and in vitro, adapted for sub-compartment and cell-type specific labeling (204). Development of this method for the NRN1

interactome would require careful troubleshooting and verification to address technical concerns: 1) regarding the comparative size difference of NRN1 (~9-12 kDa) and TurboID (~37kDa ligase alone), potentially obstructing native binding kinetics or affinities, and 2) processing to produce the mature form of NRN1 in which both the signal segment (positions 1-27) and the propeptide segment (positions 117-142) are both removed.

Finally, the temporal effects of NRN1 exposure on neurons requires further investigation. The current work evaluated neuronal changes after incubation with NRN1 for 6 hours, this was based on established protocols from our lab and others (110, 112). As an extension to the current results, samples from an immortalized neuronal cell line (Neuro-2a) treated exogenously with recombinant NRN1 at varied timepoints and concentrations for future biochemical analysis have been collected and could provide more comprehensive downstream molecular insights of NRN1.

4.2.5 Model systems for studying cognitive resilience. Model systems are often selected based on suitability for answering current research questions. Future work from this group will also include replication of current results in additional models. Presently, primary neuronal cultures generated from embryonic rats were used to assess NRN1 neurobiology in the context of AD insult. There are many advantages to this model, however, future work may seek to validate and extend these findings in additional model systems. Preliminary work from this group has repeated NRN1 vs vehicle treatment in human induced pluripotent stem cells (hIPSCs) derived from AD and control cases. Cell cultures of hIPSCs represent an indefinite source of humanized, patient specific cells that may more closely mimic complex human neuronal physiology than rodent derived cells. Samples collected have been processed via TMT-MS and future analysis of this work will assuredly provide additional context for NRN1 induced effects.

Similarly, investigating the neuroprotective effects of NRN1 in vivo is an obvious next step. Rodent models represent a cornerstone in AD research. As such, future work in this context could

consider the timing of NRN1 delivery vs progression of pathology in an attempt to understand potential limitations of NRN1's neuroprotective effects. Parallel to this work, improving the face validity of murine models has received increased attention lately as a path toward understanding novel genetic and proteomic pathways involved in increased or decreased resilience phenotypes. The complex relationship between genetic composition and phenotypic variability observed in human populations, of which is lacking within genetically homogenous inbred mouse strains, has led to the hypothesis that incorporating genetic variability in AD mouse models could improve translatability. In support of this hypothesis, an AD transgenic mouse reference panel (AD-BXD) was recently developed to explore the impact of genetic complexity on phenotypic segregation and translation with human disease features (205). The reference panel was generated by crossing 5XFAD mice on a B6 background with the BXD recombinant inbred strain series derived from B6 and DBA/2J (D2) crosses. Results from this study identified improved AD phenotypes relating to varied age of onset and rate of memory impairment across the resulting strains. Importantly, mice in this panel that exhibited higher resilience phenotypes also had increased levels of NRN1 expression, demonstrating additional support for NRN1 in resilience at multiple levels of analysis. In addition to NRN1, there are likely additional novel genes, proteins or pathways mediating resilience yet to be characterized from this model schema. Towards the goal of increasing knowledge of uniquely adapted systems in resilience, a mutli-region label-free proteomic analysis of genetically complex transgenic mouse brains has recently been conducted (manuscript inc preparation). This work identified several pathways significantly associated with genetic background and contributes to ongoing work to improve Ad model systems capable of recapitulating complex human phenotypes, including resilience.

4.3 Additional considerations

4.3.1 Asymptomatic vs preclinical. There continues to be some debate in the field on how best to define and distinguish true resilience from preclinical AD. Since typical AD cases that

eventually convert to dementia also experience a protracted asymptomatic phase, understanding what distinguishes those that do convert and those that do not will additionally serve to improve diagnostic and treatment strategies in clinical settings. It is important to note, that while we cannot say definitively if apparently resilient cases would have eventually converted to symptomatic disease had they lived longer lives, estimates on the proportions of resilience in AD were calculated in people in their lower to mid 80s (77). Additionally, it is also feasible that among cohorts identified as resilient some may be true resilient while others may be true preclinical. Therein lies just one benefit of comprehensive characterization studies such as the work presented here in improving case stratification and nomination of resilience promoting factors.

4.3.2 NRN1 as a potential biomarker. An important consideration in identifying markers of resilience and differentiating individuals presenting with increased or decreased resilience extends to the application of these findings to clinical usefulness. Biomarkers have been instrumental in diagnosis and monitoring of disease progression. The direct interaction of cerebrospinal fluid (CSF) with the brain represents a rich source to examine pathological protein changes occurring in real time in a living subject (158, 206, 207). Recent work from our group has demonstrated methodological proficiency in deep profiling of the CSF proteome for improving potential biomarkers in diverse groups (208). Notably, NRN1 was measured in this study and found to be significantly decreased in AD cases compared to controls. This supports the feasibility of quantifying changes in NRN1 in human CSF and suggests a potential value for NRN1 as a biomarker of cognitive change in the context of disease pathology. Development of a targeted proteomic assay, such as selected reaction monitoring (SRM), could be implemented to explore not only NRN1 but additional potential resilience candidates including module members from the current censuses network synaptic modules (M5 and M22). The benefits, therefore, of exploring resilience markers in a targeted format could include improved predictive capacity of cognitive

decline in living humans. This in-turn would enable early intervention to improve outcomes and extend quality of life.

4.3.2 An integrative, non-linear workflow. Conventional benchtop-to-bedside strategies for identifying therapeutic targets have generated an abundance of data in clinical trial settings, but unfortunately often fail. Reverse translation, or bedside-to-benchtop, begins with human observational studies and works backwards to pinpoint potential mechanisms and therapeutic targets for investigation. This paradigm allows information from clinical and laboratory settings to follow a cyclical process instead of a linear one, and thereby is tunable and more likely to lead to successful clinical interventions (209). In the current study, we use human postmortem brain proteomic data with incorporated antemortem clinical phenotypic data (e.g., cognitive trajectory in life) to characterize protein modules important for resilience to AD. NRN1 was targeted in this analysis and validated for neuroprotective efficacy in a neuronal model system. Finally, findings from our experimental models were re-integrated back into our human data to generate a distinct collection of proteins and associated biology linked to cognitive resilience in humans with high confidence. Overall, this study followed an integrative, non-linear pipeline for rigorous validation and extension of resilience-associated proteins similarly to the reverse translation paradigm. The current work provides a valuable framework for investigating molecular and physiological underpinnings of resilience directed from patient samples and cognitive changes in life.

4.4 Figures:

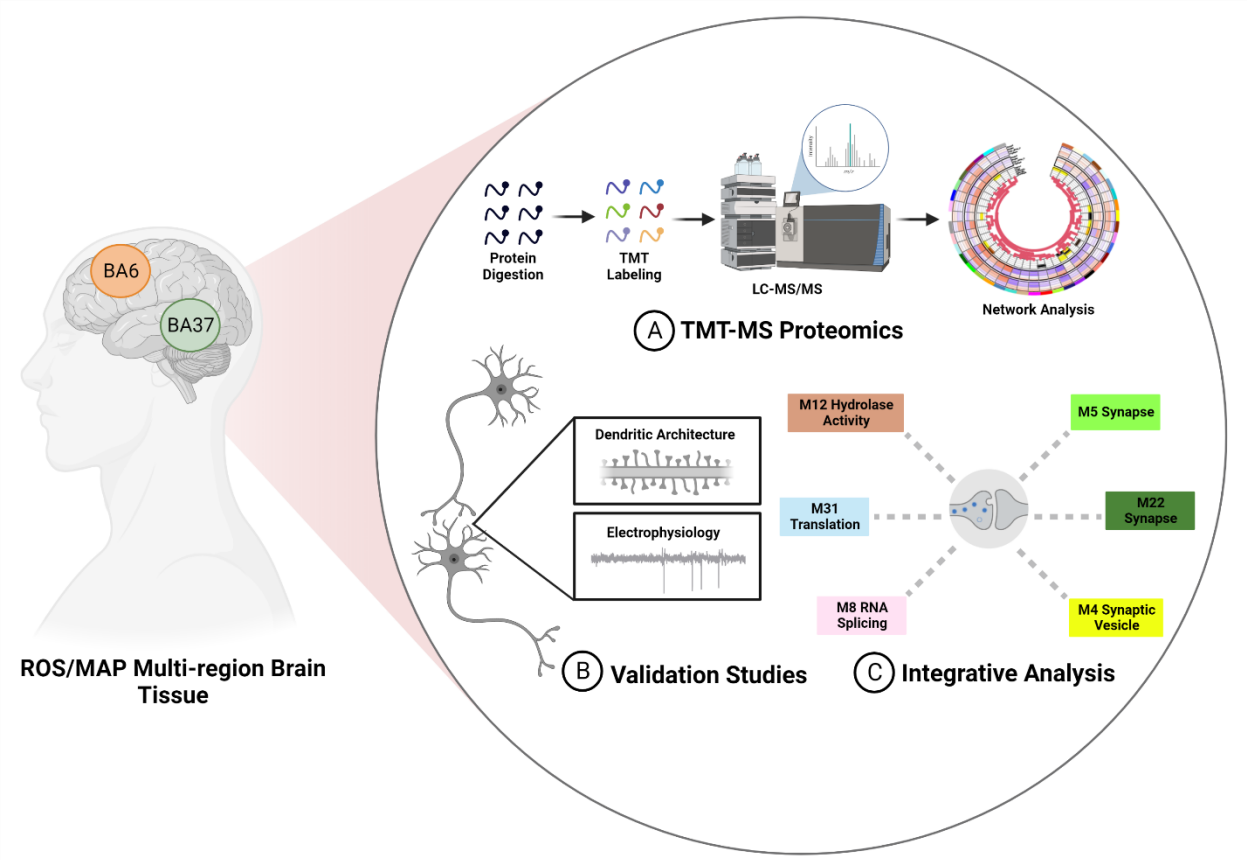

Figure 4.1: Schematic representation of dissertation summary of contributions.

References

1. 2021 Alzheimer's disease facts and figures. Alzheimers Dement. 2021;17(3):327-406. Epub 2021/03/24. doi: 10.1002/alz.12328. PubMed PMID: 33756057.
2. Thal DR, Rub U, Orantes M, Braak H. Phases of A beta-deposition in the human brain and its relevance for the development of AD. Neurology. 2002;58(12):1791-800. Epub 2002/06/27. doi: 10.1212/wnl.58.12.1791. PubMed PMID: 12084879.
3. Braak H, Braak E. Neuropathological stageing of Alzheimer-related changes. Acta Neuropathol. 1991;82(4):239-59. Epub 1991/01/01. doi: 10.1007/BF00308809. PubMed PMID: 1759558.
4. Long JM, Holtzman DM. Alzheimer Disease: An Update on Pathobiology and Treatment Strategies. Cell. 2019;179(2):312-39. Epub 2019/10/01. doi: 10.1016/j.cell.2019.09.001. PubMed PMID: 31564456; PMCID: PMC6778042.
5. Knopman DS, Amieva H, Petersen RC, Chetelat G, Holtzman DM, Hyman BT, Nixon RA, Jones DT. Alzheimer disease. Nat Rev Dis Primers. 2021;7(1):33. Epub 2021/05/15. doi: 10.1038/s41572-021-00269-y. PubMed PMID: 33986301; PMCID: PMC8574196.
6. Ballard C, Gauthier S, Corbett A, Brayne C, Aarsland D, Jones E. Alzheimer's disease. Lancet. 2011;377(9770):1019-31. Epub 2011/03/05. doi: 10.1016/S0140-6736(10)61349-9. PubMed PMID: 21371747.
7. De Strooper B, Karran E. The Cellular Phase of Alzheimer's Disease. Cell. 2016;164(4):603-15. Epub 2016/02/13. doi: 10.1016/j.cell.2015.12.056. PubMed PMID: 26871627.
8. Gouilly D, Rafiq M, Nogueira L, Salabert AS, Payoux P, Peran P, Pariente J. Beyond the amyloid cascade: An update of Alzheimer's disease pathophysiology. Rev Neurol (Paris). 2023. Epub 2023/03/12. doi: 10.1016/j.neurol.2022.12.006. PubMed PMID: 36906457.
9. Mirra SS, Heyman A, McKeel D, Sumi SM, Crain BJ, Brownlee LM, Vogel FS, Hughes JP, van Belle G, Berg L. The Consortium to Establish a Registry for Alzheimer's Disease (CERAD). Part II. Standardization of the neuropathologic assessment of Alzheimer's disease. Neurology. 1991;41(4):479-86. Epub 1991/04/01. doi: 10.1212/wnl.41.4.479. PubMed PMID: 2011243.
10. Bekris LM, Yu CE, Bird TD, Tsuang DW. Genetics of Alzheimer disease. J Geriatr Psychiatry Neurol. 2010;23(4):213-27. Epub 2010/11/04. doi: 10.1177/0891988710383571. PubMed PMID: 21045163; PMCID: PMC3044597.
11. Gatz M, Reynolds CA, Fratiglioni L, Johansson B, Mortimer JA, Berg S, Fiske A, Pedersen NL. Role of genes and environments for explaining Alzheimer disease. Arch Gen Psychiatry. 2006;63(2):168-74. Epub 2006/02/08. doi: 10.1001/archpsyc.63.2.168. PubMed PMID: 16461860.
12. Graff-Radford J, Yong KXX, Apostolova LG, Bouwman FH, Carrillo M, Dickerson BC, Rabinovici GD, Schott JM, Jones DT, Murray ME. New insights into atypical Alzheimer's disease in the era of biomarkers. Lancet Neurol. 2021;20(3):222-34. Epub 2021/02/21. doi: 10.1016/S1474-4422(20)30440-3. PubMed PMID: 33609479; PMCID: PMC8056394.
13. Villain N, Dubois B. Alzheimer's Disease Including Focal Presentations. Semin Neurol. 2019;39(2):213-26. Epub 2019/03/30. doi: 10.1055/s-0039-1681041. PubMed PMID: 30925614.
14. Strittmatter WJ, Saunders AM, Schmechel D, Pericak-Vance M, Enghild J, Salvesen GS, Roses AD. Apolipoprotein E: high-avidity binding to beta-amyloid and increased frequency of type 4 allele in late-onset familial Alzheimer disease. Proc Natl Acad Sci U S A. 1993;90(5):1977-81. Epub 1993/03/01. doi: 10.1073/pnas.90.5.1977. PubMed PMID: 8446617; PMCID: PMC46003.
15. Corder EH, Saunders AM, Strittmatter WJ, Schmechel DE, Gaskell PC, Small GW, Roses AD, Haines JL, Pericak-Vance MA. Gene dose of apolipoprotein E type 4 allele and the risk of Alzheimer's disease in

late onset families. Science. 1993;261(5123):921-3. Epub 1993/08/13. doi: 10.1126/science.8346443. PubMed PMID: 8346443.
16. Kunkle BW, Grenier-Boley B, Sims R, Bis JC, Damotte V, Naj AC, Boland A, Vronskaya M, van der Lee SJ, Amlie-Wolf A, Bellenguez C, Frizatti A, Chouraki V, Martin ER, Sleegers K, Badarinarayan N, Jakobsdottir J, Hamilton-Nelson KL, Moreno-Grau S, Olaso R, Raybould R, Chen Y, Kuzma AB, Hiltunen M, Morgan T, Ahmad S, Vardarajan BN, Epelbaum J, Hoffmann P, Boada M, Beecham GW, Garnier JG, Harold D, Fitzpatrick AL, Valladares O, Moutet ML, Gerrish A, Smith AV, Qu L, Bacq D, Denning N, Jian X, Zhao Y, Del Zompo M, Fox NC, Choi SH, Mateo I, Hughes JT, Adams HH, Malamon J, Sanchez-Garcia F, Patel Y, Brody JA, Dombroski BA, Naranjo MCD, Daniilidou M, Eiriksdottir G, Mukherjee S, Wallon D, Uphill J, Aspelund T, Cantwell LB, Garzia F, Galimberti D, Hofer E, Butkiewicz M, Fin B, Scarpini E, Sarnowski C, Bush WS, Meslage S, Kornhuber J, White CC, Song Y, Barber RC, Engelborghs S, Sordon S, Voijnovic D, Adams PM, Vandenberghe R, Mayhaus M, Cupples LA, Albert MS, De Deyn PP, Gu W, Himali JJ, Beekly D, Squassina A, Hartmann AM, Orellana A, Blacker D, Rodriguez-Rodriguez E, Lovestone S, Garcia ME, Doody RS, Munoz-Fernadez C, Sussams R, Lin H, Fairchild TJ, Benito YA, Holmes C, Karamujic-Comic H, Frosch MP, Thonberg H, Maier W, Roshchupkin G, Ghetti B, Giedraitis V, Kawalia A, Li S, Huebinger RM, Kilander L, Moebus S, Hernandez I, Kamboh MI, Brundin R, Turton J, Yang Q, Katz MJ, Concari L, Lord J, Beiser AS, Keene CD, Helisalmi S, Kloszewska I, Kukull WA, Koivisto AM, Lynch A, Tarraga L, Larson EB, Haapasalo A, Lawlor B, Mosley TH, Lipton RB, Solfrizzi V, Gill M, Longstreth WT, Jr., Montine TJ, Frisardi V, Diez-Fairen M, Rivadeneira F, Petersen RC, Deramecourt V, Alvarez I, Salani F, Ciaramella A, Boerwinkle E, Reiman EM, Fievet N, Rotter JI, Reisch JS, Hanon O, Cupidi C, Andre Uitterlinden AG, Royall DR, Dufouil C, Maletta RG, de Rojas I, Sano M, Brice A, Cecchetti R, George-Hyslop PS, Ritchie K, Tsolaki M, Tsuang DW, Dubois B, Craig D, Wu CK, Soininen H, Avramidou D, Albin RL, Fratiglioni L, Germanou A, Apostolova LG, Keller L, Koutroumani M, Arnold SE, Panza F, Gkatzima O, Asthana S, Hannequin D, Whitehead P, Atwood CS, Caffarra P, Hampel H, Quintela I, Carracedo A, Lannfelt L, Rubinsztein DC, Barnes LL, Pasquier F, Frolich L, Barral S, McGuinness B, Beach TG, Johnston JA, Becker JT, Passmore P, Bigio EH, Schott JM, Bird TD, Warren JD, Boeve BF, Lupton MK, Bowen JD, Proitsi P, Boxer A, Powell JF, Burke JR, Kauwe JSK, Burns JM, Mancuso M, Buxbaum JD, Bonuccelli U, Cairns NJ, McQuillin A, Cao C, Livingston G, Carlson CS, Bass NJ, Carlsson CM, Hardy J, Carney RM, Bras J, Carrasquillo MM, Guerreiro R, Allen M, Chui HC, Fisher E, Masullo C, Crocco EA, DeCarli C, Bisceglio G, Dick M, Ma L, Duara R, Graff-Radford NR, Evans DA, Hodges A, Faber KM, Scherer M, Fallon KB, Riemenschneider M, Fardo DW, Heun R, Farlow MR, Kolsch H, Ferris S, Leber M, Foroud TM, Heuser I, Galasko DR, Giegling I, Gearing M, Hull M, Geschwind DH, Gilbert JR, Morris J, Green RC, Mayo K, Growdon JH, Feulner T, Hamilton RL, Harrell LE, Drichel D, Honig LS, Cushion TD, Huentelman MJ, Hollingworth P, Hulette CM, Hyman BT, Marshall R, Jarvik GP, Meggy A, Abner E, Menzies GE, Jin LW, Leonenko G, Real LM, Jun GR, Baldwin CT, Grozeva D, Karydas A, Russo G, Kaye JA, Kim R, Jessen F, Kowall NW, Vellas B, Kramer JH, Vardy E, LaFerla FM, Jockel KH, Lah JJ, Dichgans M, Leverenz JB, Mann D, Levey AI, Pickering-Brown S, Lieberman AP, Klopp N, Lunetta KL, Wichmann HE, Lyketsos CG, Morgan K, Marson DC, Brown K, Martiniuk F, Medway C, Mash DC, Nothen MM, Masliah E, Hooper NM, McCormick WC, Daniele A, McCurry SM, Bayer A, McDavid AN, Gallacher J, McKee AC, van den Bussche H, Mesulam M, Brayne C, Miller BL, Riedel-Heller S, Miller CA, Miller JW, Al-Chalabi A, Morris JC, Shaw CE, Myers AJ, Wiltfang J, O'Bryant S, Olichney JM, Alvarez V, Parisi JE, Singleton AB, Paulson HL, Collinge J, Perry WR, Mead S, Peskind E, Cribbs DH, Rossor M, Pierce A, Ryan NS, Poon WW, Nacmias B, Potter H, Sorbi S, Quinn JF, Sacchinelli E, Raj A, Spalletta G, Raskind M, Caltagirone C, Bossu P, Orfei MD, Reisberg B, Clarke R, Reitz C, Smith AD, Ringman JM, Warden D, Roberson ED, Wilcock G, Rogaeva E, Bruni AC, Rosen HJ, Gallo M, Rosenberg RN, Ben-Shlomo Y, Sager MA, Mecocci P, Saykin AJ, Pastor P, Cuccaro ML, Vance JM, Schneider JA, Schneider LS, Slifer S, Seeley WW, Smith AG, Sonnen JA, Spina S, Stern RA, Swerdlow RH, Tang M, Tanzi RE, Trojanowski JQ, Troncoso JC, Van Deerlin VM, Van Eldik LJ, Vinters HV, Vonsattel JP, Weintraub S, Welsh-Bohmer KA, Wilhelmsen KC, Williamson J, Wingo TS, Woltjer RL, Wright

CB, Yu CE, Yu L, Saba Y, Pilotto A, Bullido MJ, Peters O, Crane PK, Bennett D, Bosco P, Coto E, Boccardi V, De Jager PL, Lleo A, Warner N, Lopez OL, Ingelsson M, Deloukas P, Cruchaga C, Graff C, Gwilliam R, Fornage M, Goate AM, Sanchez-Juan P, Kehoe PG, Amin N, Ertekin-Taner N, Berr C, Debette S, Love S, Launer LJ, Younkin SG, Dartigues JF, Corcoran C, Ikram MA, Dickson DW, Nicolas G, Campion D, Tschanz J, Schmidt H, Hakonarson H, Clarimon J, Munger R, Schmidt R, Farrer LA, Van Broeckhoven C, M COD, DeStefano AL, Jones L, Haines JL, Deleuze JF, Owen MJ, Gudnason V, Mayeux R, Escott-Price V, Psaty BM, Ramirez A, Wang LS, Ruiz A, van Duijn CM, Holmans PA, Seshadri S, Williams J, Amouyel P, Schellenberg GD, Lambert JC, Pericak-Vance MA, Alzheimer Disease Genetics C, European Alzheimer's Disease I, Cohorts for H, Aging Research in Genomic Epidemiology C, Genetic, Environmental Risk in Ad/Defining Genetic P, Environmental Risk for Alzheimer's Disease C. Genetic meta-analysis of diagnosed Alzheimer's disease identifies new risk loci and implicates Abeta, tau, immunity and lipid processing. Nat Genet. 2019;51(3):414-30. Epub 2019/03/02. doi: 10.1038/s41588-019-0358-2. PubMed PMID: 30820047; PMCID: PMC6463297.

17. Roses AD. Apolipoprotein E alleles as risk factors in Alzheimer's disease. Annu Rev Med. 1996;47:387-400. Epub 1996/01/01. doi: 10.1146/annurev.med.47.1.387. PubMed PMID: 8712790.

18. Heneka MT, Carson MJ, El Khoury J, Landreth GE, Brosseron F, Feinstein DL, Jacobs AH, Wyss-Coray T, Vitorica J, Ransohoff RM, Herrup K, Frautschy SA, Finsen B, Brown GC, Verkhratsky A, Yamanaka K, Koistinaho J, Latz E, Halle A, Petzold GC, Town T, Morgan D, Shinohara ML, Perry VH, Holmes C, Bazan NG, Brooks DJ, Hunot S, Joseph B, Deigendesch N, Garaschuk O, Boddeke E, Dinarello CA, Breitner JC, Cole GM, Golenbock DT, Kummer MP. Neuroinflammation in Alzheimer's disease. Lancet Neurol. 2015;14(4):388-405. Epub 2015/03/21. doi: 10.1016/S1474-4422(15)70016-5. PubMed PMID: 25792098; PMCID: PMC5909703.

19. Guerreiro R, Wojtas A, Bras J, Carrasquillo M, Rogaeva E, Majounie E, Cruchaga C, Sassi C, Kauwe JS, Younkin S, Hazrati L, Collinge J, Pocock J, Lashley T, Williams J, Lambert JC, Amouyel P, Goate A, Rademakers R, Morgan K, Powell J, St George-Hyslop P, Singleton A, Hardy J, Alzheimer Genetic Analysis G. TREM2 variants in Alzheimer's disease. N Engl J Med. 2013;368(2):117-27. Epub 2012/11/16. doi: 10.1056/NEJMoa1211851. PubMed PMID: 23150934; PMCID: PMC3631573.

20. Griciuc A, Serrano-Pozo A, Parrado AR, Lesinski AN, Asselin CN, Mullin K, Hooli B, Choi SH, Hyman BT, Tanzi RE. Alzheimer's disease risk gene CD33 inhibits microglial uptake of amyloid beta. Neuron. 2013;78(4):631-43. Epub 2013/04/30. doi: 10.1016/j.neuron.2013.04.014. PubMed PMID: 23623698; PMCID: PMC3706457.

21. Yaghmoor F, Noorsaeed A, Alsaggaf S, Aljohani W, Scholtzova H, Boutajangout A, Wisniewski T. The Role of TREM2 in Alzheimer's Disease and Other Neurological Disorders. J Alzheimers Dis Parkinsonism. 2014;4(5). Epub 2015/02/11. doi: 10.4172/2161-0460.1000160. PubMed PMID: 25664220; PMCID: PMC4317331.

22. Kulkarni B, Kumar D, Cruz-Martins N, Sellamuthu S. Role of TREM2 in Alzheimer's Disease: A Long Road Ahead. Mol Neurobiol. 2021;58(10):5239-52. Epub 2021/07/19. doi: 10.1007/s12035-021-02477-9. PubMed PMID: 34275100.

23. Colonna M, Butovsky O. Microglia Function in the Central Nervous System During Health and Neurodegeneration. Annu Rev Immunol. 2017;35:441-68. Epub 2017/02/23. doi: 10.1146/annurev-immunol-051116-052358. PubMed PMID: 28226226; PMCID: PMC8167938.

24. Ji K, Akgul G, Wollmuth LP, Tsirka SE. Microglia actively regulate the number of functional synapses. PLoS One. 2013;8(2):e56293. Epub 2013/02/09. doi: 10.1371/journal.pone.0056293. PubMed PMID: 23393609; PMCID: PMC3564799.

25. Rodriguez-Arellano JJ, Parpura V, Zorec R, Verkhratsky A. Astrocytes in physiological aging and Alzheimer's disease. Neuroscience. 2016;323:170-82. Epub 2015/01/18. doi: 10.1016/j.neuroscience.2015.01.007. PubMed PMID: 25595973.

26. Kimelberg HK, Nedergaard M. Functions of astrocytes and their potential as therapeutic targets. Neurotherapeutics. 2010;7(4):338-53. Epub 2010/10/01. doi: 10.1016/j.nurt.2010.07.006. PubMed PMID: 20880499; PMCID: PMC2982258.
27. Sofroniew MV, Vinters HV. Astrocytes: biology and pathology. Acta Neuropathol. 2010;119(1):7-35. Epub 2009/12/17. doi: 10.1007/s00401-009-0619-8. PubMed PMID: 20012068; PMCID: PMC2799634.
28. Sofroniew MV. Molecular dissection of reactive astrogliosis and glial scar formation. Trends Neurosci. 2009;32(12):638-47. Epub 2009/09/29. doi: 10.1016/j.tins.2009.08.002. PubMed PMID: 19782411; PMCID: PMC2787735.
29. Hickman SE, Allison EK, El Khoury J. Microglial dysfunction and defective beta-amyloid clearance pathways in aging Alzheimer's disease mice. J Neurosci. 2008;28(33):8354-60. Epub 2008/08/15. doi: 10.1523/JNEUROSCI.0616-08.2008. PubMed PMID: 18701698; PMCID: PMC2597474.
30. Medeiros R, LaFerla FM. Astrocytes: conductors of the Alzheimer disease neuroinflammatory symphony. Exp Neurol. 2013;239:133-8. Epub 2012/10/16. doi: 10.1016/j.expneurol.2012.10.007. PubMed PMID: 23063604.
31. Pihlaja R, Koistinaho J, Kauppinen R, Sandholm J, Tanila H, Koistinaho M. Multiple cellular and molecular mechanisms are involved in human Abeta clearance by transplanted adult astrocytes. Glia. 2011;59(11):1643-57. Epub 2011/08/10. doi: 10.1002/glia.21212. PubMed PMID: 21826742.
32. Saido T, Leissring MA. Proteolytic degradation of amyloid beta-protein. Cold Spring Harb Perspect Med. 2012;2(6):a006379. Epub 2012/06/08. doi: 10.1101/cshperspect.a006379. PubMed PMID: 22675659; PMCID: PMC3367539.
33. Heneka MT, Golenbock DT, Latz E. Innate immunity in Alzheimer's disease. Nat Immunol. 2015;16(3):229-36. Epub 2015/02/18. doi: 10.1038/ni.3102. PubMed PMID: 25689443.
34. Heppner FL, Ransohoff RM, Becher B. Immune attack: the role of inflammation in Alzheimer disease. Nat Rev Neurosci. 2015;16(6):358-72. Epub 2015/05/21. doi: 10.1038/nrn3880. PubMed PMID: 25991443.
35. Hardy JA, Higgins GA. Alzheimer's disease: the amyloid cascade hypothesis. Science. 1992;256(5054):184-5. Epub 1992/04/10. doi: 10.1126/science.1566067. PubMed PMID: 1566067.
36. Goedert M, Spillantini MG. Tau mutations in frontotemporal dementia FTDP-17 and their relevance for Alzheimer's disease. Biochim Biophys Acta. 2000;1502(1):110-21. Epub 2000/07/19. doi: 10.1016/s0925-4439(00)00037-5. PubMed PMID: 10899436.
37. Martiskainen H, Herukka SK, Stancakova A, Paananen J, Soininen H, Kuusisto J, Laakso M, Hiltunen M. Decreased plasma beta-amyloid in the Alzheimer's disease APP A673T variant carriers. Ann Neurol. 2017;82(1):128-32. Epub 2017/05/31. doi: 10.1002/ana.24969. PubMed PMID: 28556232.
38. Jonsson T, Atwal JK, Steinberg S, Snaedal J, Jonsson PV, Bjornsson S, Stefansson H, Sulem P, Gudbjartsson D, Maloney J, Hoyte K, Gustafson A, Liu Y, Lu Y, Bhangale T, Graham RR, Huttenlocher J, Bjornsdottir G, Andreassen OA, Jonsson EG, Palotie A, Behrens TW, Magnusson OT, Kong A, Thorsteinsdottir U, Watts RJ, Stefansson K. A mutation in APP protects against Alzheimer's disease and age-related cognitive decline. Nature. 2012;488(7409):96-9. Epub 2012/07/18. doi: 10.1038/nature11283. PubMed PMID: 22801501.
39. Nelson PT, Alafuzoff I, Bigio EH, Bouras C, Braak H, Cairns NJ, Castellani RJ, Crain BJ, Davies P, Del Tredici K, Duyckaerts C, Frosch MP, Haroutunian V, Hof PR, Hulette CM, Hyman BT, Iwatsubo T, Jellinger KA, Jicha GA, Kovari E, Kukull WA, Leverenz JB, Love S, Mackenzie IR, Mann DM, Masliah E, McKee AC, Montine TJ, Morris JC, Schneider JA, Sonnen JA, Thal DR, Trojanowski JQ, Troncoso JC, Wisniewski T, Woltjer RL, Beach TG. Correlation of Alzheimer disease neuropathologic changes with cognitive status: a review of the literature. J Neuropathol Exp Neurol. 2012;71(5):362-81. Epub 2012/04/11. doi: 10.1097/NEN.0b013e31825018f7. PubMed PMID: 22487856; PMCID: PMC3560290.

40. Jagust W. Imaging the evolution and pathophysiology of Alzheimer disease. Nat Rev Neurosci. 2018;19(11):687-700. Epub 2018/09/30. doi: 10.1038/s41583-018-0067-3. PubMed PMID: 30266970; PMCID: PMC7032048.
41. Selkoe DJ, Hardy J. The amyloid hypothesis of Alzheimer's disease at 25 years. EMBO Mol Med. 2016;8(6):595-608. Epub 2016/03/31. doi: 10.15252/emmm.201606210. PubMed PMID: 27025652; PMCID: PMC4888851.
42. Hardy J, Selkoe DJ. The amyloid hypothesis of Alzheimer's disease: progress and problems on the road to therapeutics. Science. 2002;297(5580):353-6. Epub 2002/07/20. doi: 10.1126/science.1072994. PubMed PMID: 12130773.
43. Reiman EM, Quiroz YT, Fleisher AS, Chen K, Velez-Pardo C, Jimenez-Del-Rio M, Fagan AM, Shah AR, Alvarez S, Arbelaez A, Giraldo M, Acosta-Baena N, Sperling RA, Dickerson B, Stern CE, Tirado V, Munoz C, Reiman RA, Huentelman MJ, Alexander GE, Langbaum JB, Kosik KS, Tariot PN, Lopera F. Brain imaging and fluid biomarker analysis in young adults at genetic risk for autosomal dominant Alzheimer's disease in the presenilin 1 E280A kindred: a case-control study. Lancet Neurol. 2012;11(12):1048-56. Epub 2012/11/10. doi: 10.1016/S1474-4422(12)70228-4. PubMed PMID: 23137948; PMCID: PMC4181671.
44. Morris JC. Early-stage and preclinical Alzheimer disease. Alzheimer Dis Assoc Disord. 2005;19(3):163-5. Epub 2005/08/25. doi: 10.1097/01.wad.0000184005.22611.cc. PubMed PMID: 16118535.
45. Boyle PA, Wang T, Yu L, Wilson RS, Dawe R, Arfanakis K, Schneider JA, Bennett DA. To what degree is late life cognitive decline driven by age-related neuropathologies? Brain. 2021;144(7):2166-75. Epub 2021/03/21. doi: 10.1093/brain/awab092. PubMed PMID: 33742668; PMCID: PMC8370442.
46. Frisoni GB, Altomare D, Thal DR, Ribaldi F, van der Kant R, Ossenkoppele R, Blennow K, Cummings J, van Duijn C, Nilsson PM, Dietrich PY, Scheltens P, Dubois B. The probabilistic model of Alzheimer disease: the amyloid hypothesis revised. Nat Rev Neurosci. 2022;23(1):53-66. Epub 2021/11/25. doi: 10.1038/s41583-021-00533-w. PubMed PMID: 34815562; PMCID: PMC8840505.
47. Rajan KB, Weuve J, Barnes LL, McAninch EA, Wilson RS, Evans DA. Population estimate of people with clinical Alzheimer's disease and mild cognitive impairment in the United States (2020-2060). Alzheimers Dement. 2021;17(12):1966-75. Epub 2021/05/28. doi: 10.1002/alz.12362. PubMed PMID: 34043283; PMCID: PMC9013315.
48. Dubal DB. Chapter 16 - Sex difference in Alzheimer's disease: An updated, balanced and emerging perspective on differing vulnerabilities. In: Lanzenberger R, Kranz GS, Savic I, editors. Handbook of Clinical Neurology: Elsevier; 2020. p. 261-73.
49. Mayeux R, Stern Y. Epidemiology of Alzheimer disease. Cold Spring Harb Perspect Med. 2012;2(8). Epub 2012/08/22. doi: 10.1101/cshperspect.a006239. PubMed PMID: 22908189; PMCID: PMC3405821.
50. Byers AL, Yaffe K. Depression and risk of developing dementia. Nat Rev Neurol. 2011;7(6):323-31. Epub 2011/05/04. doi: 10.1038/nrneurol.2011.60. PubMed PMID: 21537355; PMCID: PMC3327554.
51. Vilalta-Franch J, Lopez-Pousa S, Llinas-Regla J, Calvo-Perxas L, Merino-Aguado J, Garre-Olmo J. Depression subtypes and 5-year risk of dementia and Alzheimer disease in patients aged 70 years. Int J Geriatr Psychiatry. 2013;28(4):341-50. Epub 2012/05/17. doi: 10.1002/gps.3826. PubMed PMID: 22588687.
52. Zverova M, Fisar Z, Jirak R, Kitzlerova E, Hroudova J, Raboch J. Plasma cortisol in Alzheimer's disease with or without depressive symptoms. Med Sci Monit. 2013;19:681-9. Epub 2013/08/21. doi: 10.12659/MSM.889110. PubMed PMID: 23955525; PMCID: PMC3751335.
53. Ennis GE, An Y, Resnick SM, Ferrucci L, O'Brien RJ, Moffat SD. Long-term cortisol measures predict Alzheimer disease risk. Neurology. 2017;88(4):371-8. Epub 2016/12/18. doi: 10.1212/WNL.0000000000003537. PubMed PMID: 27986873; PMCID: PMC5272965.

54. Shi L, Chen SJ, Ma MY, Bao YP, Han Y, Wang YM, Shi J, Vitiello MV, Lu L. Sleep disturbances increase the risk of dementia: A systematic review and meta-analysis. Sleep Med Rev. 2018;40:4-16. Epub 2017/09/12. doi: 10.1016/j.smrv.2017.06.010. PubMed PMID: 28890168.
55. Livingston G, Huntley J, Sommerlad A, Ames D, Ballard C, Banerjee S, Brayne C, Burns A, Cohen-Mansfield J, Cooper C, Costafreda SG, Dias A, Fox N, Gitlin LN, Howard R, Kales HC, Kivimaki M, Larson EB, Ogunniyi A, Orgeta V, Ritchie K, Rockwood K, Sampson EL, Samus Q, Schneider LS, Selbaek G, Teri L, Mukadam N. Dementia prevention, intervention, and care: 2020 report of the Lancet Commission. Lancet. 2020;396(10248):413-46. Epub 2020/08/03. doi: 10.1016/S0140-6736(20)30367-6. PubMed PMID: 32738937; PMCID: PMC7392084.
56. Kivipelto M, Mangialasche F, Ngandu T. Lifestyle interventions to prevent cognitive impairment, dementia and Alzheimer disease. Nat Rev Neurol. 2018;14(11):653-66. Epub 2018/10/07. doi: 10.1038/s41582-018-0070-3. PubMed PMID: 30291317.
57. Klee M, Leist AK, Veldsman M, Ranson JM, Llewellyn DJ. Socioeconomic Deprivation, Genetics and Risk of Dementia2022;18(S11):e066803. doi: https://doi.org/10.1002/alz.066803.
58. Raina P, Santaguida P, Ismaila A, Patterson C, Cowan D, Levine M, Booker L, Oremus M. Effectiveness of cholinesterase inhibitors and memantine for treating dementia: evidence review for a clinical practice guideline. Ann Intern Med. 2008;148(5):379-97. Epub 2008/03/05. doi: 10.7326/0003-4819-148-5-200803040-00009. PubMed PMID: 18316756.
59. Whitehouse PJ, Price DL, Clark AW, Coyle JT, DeLong MR. Alzheimer disease: evidence for selective loss of cholinergic neurons in the nucleus basalis. Ann Neurol. 1981;10(2):122-6. Epub 1981/08/01. doi: 10.1002/ana.410100203. PubMed PMID: 7283399.
60. Fonte C, Smania N, Pedrinolla A, Munari D, Gandolfi M, Picelli A, Varalta V, Benetti MV, Brugnera A, Federico A, Muti E, Tamburin S, Schena F, Venturelli M. Comparison between physical and cognitive treatment in patients with MCI and Alzheimer's disease. Aging (Albany NY). 2019;11(10):3138-55. Epub 2019/05/28. doi: 10.18632/aging.101970. PubMed PMID: 31127076; PMCID: PMC6555450.
61. Xiang C, Zhang Y. Comparison of Cognitive Intervention Strategies for Individuals With Alzheimer's Disease: A Systematic Review and Network Meta-analysis. Neuropsychol Rev. 2023. Epub 2023/03/18. doi: 10.1007/s11065-023-09584-5. PubMed PMID: 36929474.
62. Haddad HW, Malone GW, Comardelle NJ, Degueure AE, Kaye AM, Kaye AD. Aducanumab, a Novel Anti-Amyloid Monoclonal Antibody, for the Treatment of Alzheimer's Disease: A Comprehensive Review. Health Psychol Res. 2022;10(1):31925. Epub 2022/08/06. doi: 10.52965/001c.31925. PubMed PMID: 35928986; PMCID: PMC9346954.
63. Fillit H, Green A. Aducanumab and the FDA - where are we now? Nat Rev Neurol. 2021;17(3):129-30. Epub 2021/01/15. doi: 10.1038/s41582-020-00454-9. PubMed PMID: 33442064.
64. Schneider L. A resurrection of aducanumab for Alzheimer's disease. Lancet Neurol. 2020;19(2):111-2. Epub 2020/01/25. doi: 10.1016/S1474-4422(19)30480-6. PubMed PMID: 31978357.
65. van Dyck CH, Swanson CJ, Aisen P, Bateman RJ, Chen C, Gee M, Kanekiyo M, Li D, Reyderman L, Cohen S, Froelich L, Katayama S, Sabbagh M, Vellas B, Watson D, Dhadda S, Irizarry M, Kramer LD, Iwatsubo T. Lecanemab in Early Alzheimer's Disease. N Engl J Med. 2023;388(1):9-21. Epub 2022/12/01. doi: 10.1056/NEJMoa2212948. PubMed PMID: 36449413.
66. Cummings J, Lee G, Nahed P, Kambar M, Zhong K, Fonseca J, Taghva K. Alzheimer's disease drug development pipeline: 2022. Alzheimers Dement (N Y). 2022;8(1):e12295. Epub 2022/05/07. doi: 10.1002/trc2.12295. PubMed PMID: 35516416; PMCID: PMC9066743.
67. Salthouse T. Consequences of age-related cognitive declines. Annu Rev Psychol. 2012;63:201-26. Epub 2011/07/12. doi: 10.1146/annurev-psych-120710-100328. PubMed PMID: 21740223; PMCID: PMC3632788.

68. Harada CN, Natelson Love MC, Triebel KL. Normal cognitive aging. Clin Geriatr Med. 2013;29(4):737-52. Epub 2013/10/08. doi: 10.1016/j.cger.2013.07.002. PubMed PMID: 24094294; PMCID: PMC4015335.
69. Resnick SM, Pham DL, Kraut MA, Zonderman AB, Davatzikos C. Longitudinal magnetic resonance imaging studies of older adults: a shrinking brain. J Neurosci. 2003;23(8):3295-301. Epub 2003/04/30. doi: 10.1523/JNEUROSCI.23-08-03295.2003. PubMed PMID: 12716936; PMCID: PMC6742337.
70. Terry RD, Katzman R. Life span and synapses: will there be a primary senile dementia? Neurobiol Aging. 2001;22(3):347-8; discussion 53-4. Epub 2001/05/30. doi: 10.1016/s0197-4580(00)00250-5. PubMed PMID: 11378236.
71. Meier-Ruge W, Ulrich J, Bruhlmann M, Meier E. Age-related white matter atrophy in the human brain. Ann N Y Acad Sci. 1992;673:260-9. Epub 1992/12/26. doi: 10.1111/j.1749-6632.1992.tb27462.x. PubMed PMID: 1485724.
72. Shea YF, Pan Y, Mak HK, Bao Y, Lee SC, Chiu PK, Chan HF. A systematic review of atypical Alzheimer's disease including behavioural and psychological symptoms. Psychogeriatrics. 2021;21(3):396-406. Epub 2021/02/18. doi: 10.1111/psyg.12665. PubMed PMID: 33594793.
73. Boyle PA, Wilson RS, Yu L, Barr AM, Honer WG, Schneider JA, Bennett DA. Much of late life cognitive decline is not due to common neurodegenerative pathologies. Ann Neurol. 2013;74(3):478-89. Epub 2013/06/27. doi: 10.1002/ana.23964. PubMed PMID: 23798485; PMCID: PMC3845973.
74. Dickson DW, Crystal HA, Mattiace LA, Masur DM, Blau AD, Davies P, Yen SH, Aronson MK. Identification of normal and pathological aging in prospectively studied nondemented elderly humans. Neurobiol Aging. 1992;13(1):179-89. Epub 1992/01/01. doi: 10.1016/0197-4580(92)90027-u. PubMed PMID: 1311804.
75. Aizenstein HJ, Nebes RD, Saxton JA, Price JC, Mathis CA, Tsopelas ND, Ziolko SK, James JA, Snitz BE, Houck PR, Bi W, Cohen AD, Lopresti BJ, DeKosky ST, Halligan EM, Klunk WE. Frequent amyloid deposition without significant cognitive impairment among the elderly. Arch Neurol. 2008;65(11):1509-17. Epub 2008/11/13. doi: 10.1001/archneur.65.11.1509. PubMed PMID: 19001171; PMCID: PMC2636844.
76. Rahimi J, Kovacs GG. Prevalence of mixed pathologies in the aging brain. Alzheimers Res Ther. 2014;6(9):82. Epub 2014/11/25. doi: 10.1186/s13195-014-0082-1. PubMed PMID: 25419243; PMCID: PMC4239398.
77. D.A Bennett MJAS, MD; Z. Arvanitakis, MD; J.F. Kelly, MD; N.T Aggarwal, MD; R.C Shah, MD; and R.S Wilson, PhD. Neuropathology of older persons without cognitive impairment from two community-based studies2006.
78. Perez-Nievas BG, Stein TD, Tai HC, Dols-Icardo O, Scotton TC, Barroeta-Espar I, Fernandez-Carballo L, de Munain EL, Perez J, Marquie M, Serrano-Pozo A, Frosch MP, Lowe V, Parisi JE, Petersen RC, Ikonomovic MD, Lopez OL, Klunk W, Hyman BT, Gomez-Isla T. Dissecting phenotypic traits linked to human resilience to Alzheimer's pathology. Brain. 2013;136(Pt 8):2510-26. Epub 2013/07/05. doi: 10.1093/brain/awt171. PubMed PMID: 23824488; PMCID: PMC3722351.
79. Boros BD, Greathouse KM, Gentry EG, Curtis KA, Birchall EL, Gearing M, Herskowitz JH. Dendritic spines provide cognitive resilience against Alzheimer's disease. Ann Neurol. 2017;82(4):602-14. Epub 2017/09/19. doi: 10.1002/ana.25049. PubMed PMID: 28921611; PMCID: PMC5744899.
80. Latimer CS, Burke BT, Liachko NF, Currey HN, Kilgore MD, Gibbons LE, Henriksen J, Darvas M, Domoto-Reilly K, Jayadev S, Grabowski TJ, Crane PK, Larson EB, Kraemer BC, Bird TD, Keene CD. Resistance and resilience to Alzheimer's disease pathology are associated with reduced cortical pTau and absence of limbic-predominant age-related TDP-43 encephalopathy in a community-based cohort. Acta Neuropathol Commun. 2019;7(1):91. Epub 2019/06/09. doi: 10.1186/s40478-019-0743-1. PubMed PMID: 31174609; PMCID: PMC6556006.

81. Barroeta-Espar I, Weinstock LD, Perez-Nievas BG, Meltzer AC, Siao Tick Chong M, Amaral AC, Murray ME, Moulder KL, Morris JC, Cairns NJ, Parisi JE, Lowe VJ, Petersen RC, Kofler J, Ikonomovic MD, Lopez O, Klunk WE, Mayeux RP, Frosch MP, Wood LB, Gomez-Isla T. Distinct cytokine profiles in human brains resilient to Alzheimer's pathology. Neurobiol Dis. 2019;121:327-37. Epub 2018/10/20. doi: 10.1016/j.nbd.2018.10.009. PubMed PMID: 30336198; PMCID: PMC6437670.
82. Stern Y, Barnes CA, Grady C, Jones RN, Raz N. Brain reserve, cognitive reserve, compensation, and maintenance: operationalization, validity, and mechanisms of cognitive resilience. Neurobiol Aging. 2019;83:124-9. Epub 2019/11/17. doi: 10.1016/j.neurobiolaging.2019.03.022. PubMed PMID: 31732015; PMCID: PMC6859943.
83. Hayashi Y, Majewska AK. Dendritic spine geometry: functional implication and regulation. Neuron. 2005;46(4):529-32. Epub 2005/06/10. doi: 10.1016/j.neuron.2005.05.006. PubMed PMID: 15944122.
84. Walker CK, Herskowitz JH. Dendritic Spines: Mediators of Cognitive Resilience in Aging and Alzheimer's Disease. Neuroscientist. 2020:1073858420945964. Epub 2020/08/20. doi: 10.1177/1073858420945964. PubMed PMID: 32812494.
85. Peters A, Kaiserman-Abramof IR. The small pyramidal neuron of the rat cerebral cortex. The synapses upon dendritic spines. Z Zellforsch Mikrosk Anat. 1969;100(4):487-506. Epub 1969/09/22. doi: 10.1007/BF00344370. PubMed PMID: 5351190.
86. Ganeshina O, Berry RW, Petralia RS, Nicholson DA, Geinisman Y. Differences in the expression of AMPA and NMDA receptors between axospinous perforated and nonperforated synapses are related to the configuration and size of postsynaptic densities. J Comp Neurol. 2004;468(1):86-95. Epub 2003/12/04. doi: 10.1002/cne.10950. PubMed PMID: 14648692.
87. Morrison JH, Baxter MG. The ageing cortical synapse: hallmarks and implications for cognitive decline. Nat Rev Neurosci. 2012;13(4):240-50. Epub 2012/03/08. doi: 10.1038/nrn3200. PubMed PMID: 22395804; PMCID: PMC3592200.
88. Bourne J, Harris KM. Do thin spines learn to be mushroom spines that remember? Curr Opin Neurobiol. 2007;17(3):381-6. Epub 2007/05/15. doi: 10.1016/j.conb.2007.04.009. PubMed PMID: 17498943.
89. Kasai H, Hayama T, Ishikawa M, Watanabe S, Yagishita S, Noguchi J. Learning rules and persistence of dendritic spines. Eur J Neurosci. 2010;32(2):241-9. Epub 2010/07/22. doi: 10.1111/j.1460-9568.2010.07344.x. PubMed PMID: 20646057.
90. Kasai H, Matsuzaki M, Noguchi J, Yasumatsu N, Nakahara H. Structure-stability-function relationships of dendritic spines. Trends Neurosci. 2003;26(7):360-8. Epub 2003/07/10. doi: 10.1016/S0166-2236(03)00162-0. PubMed PMID: 12850432.
91. Kasai H, Fukuda M, Watanabe S, Hayashi-Takagi A, Noguchi J. Structural dynamics of dendritic spines in memory and cognition. Trends Neurosci. 2010;33(3):121-9. Epub 2010/02/09. doi: 10.1016/j.tins.2010.01.001. PubMed PMID: 20138375.
92. Helm MS, Dankovich TM, Mandad S, Rammner B, Jahne S, Salimi V, Koerbs C, Leibrandt R, Urlaub H, Schikorski T, Rizzoli SO. A large-scale nanoscopy and biochemistry analysis of postsynaptic dendritic spines. Nat Neurosci. 2021;24(8):1151-62. Epub 2021/06/26. doi: 10.1038/s41593-021-00874-w. PubMed PMID: 34168338.
93. Spacek J, Harris KM. Three-dimensional organization of smooth endoplasmic reticulum in hippocampal CA1 dendrites and dendritic spines of the immature and mature rat. J Neurosci. 1997;17(1):190-203. Epub 1997/01/01. doi: 10.1523/JNEUROSCI.17-01-00190.1997. PubMed PMID: 8987748; PMCID: PMC6793680.
94. Harris KM, Jensen FE, Tsao B. Three-dimensional structure of dendritic spines and synapses in rat hippocampus (CA1) at postnatal day 15 and adult ages: implications for the maturation of synaptic

physiology and long-term potentiation. J Neurosci. 1992;12(7):2685-705. Epub 1992/07/01. PubMed PMID: 1613552; PMCID: PMC6575840.
95. Freire M. Effects of dark rearing on dendritic spines in layer IV of the mouse visual cortex. A quantitative electron microscopical study. J Anat. 1978;126(Pt 1):193-201. Epub 1978/05/01. PubMed PMID: 649498; PMCID: PMC1235723.
96. Sheng M, Kim E. The postsynaptic organization of synapses. Cold Spring Harb Perspect Biol. 2011;3(12). Epub 2011/11/03. doi: 10.1101/cshperspect.a005678. PubMed PMID: 22046028; PMCID: PMC3225953.
97. Majewska A, Tashiro A, Yuste R. Regulation of spine calcium dynamics by rapid spine motility. J Neurosci. 2000;20(22):8262-8. Epub 2000/11/09. doi: 10.1523/JNEUROSCI.20-22-08262.2000. PubMed PMID: 11069932; PMCID: PMC6773195.
98. Burke SN, Barnes CA. Neural plasticity in the ageing brain. Nat Rev Neurosci. 2006;7(1):30-40. Epub 2005/12/24. doi: 10.1038/nrn1809. PubMed PMID: 16371948.
99. Peters A, Morrison JH, Rosene DL, Hyman BT. Feature article: are neurons lost from the primate cerebral cortex during normal aging? Cereb Cortex. 1998;8(4):295-300. Epub 1998/07/03. doi: 10.1093/cercor/8.4.295. PubMed PMID: 9651126.
100. Pakkenberg B, Gundersen HJ. Neocortical neuron number in humans: effect of sex and age. J Comp Neurol. 1997;384(2):312-20. Epub 1997/07/28. PubMed PMID: 9215725.
101. Dumitriu D, Hao J, Hara Y, Kaufmann J, Janssen WG, Lou W, Rapp PR, Morrison JH. Selective changes in thin spine density and morphology in monkey prefrontal cortex correlate with aging-related cognitive impairment. J Neurosci. 2010;30(22):7507-15. doi: 10.1523/jneurosci.6410-09.2010. PubMed PMID: 20519525; PMCID: PMC2892969.
102. Young ME, Ohm DT, Dumitriu D, Rapp PR, Morrison JH. Differential effects of aging on dendritic spines in visual cortex and prefrontal cortex of the rhesus monkey. Neuroscience. 2014;274:33-43. Epub 20140520. doi: 10.1016/j.neuroscience.2014.05.008. PubMed PMID: 24853052; PMCID: PMC4108992.
103. Geinisman Y, deToledo-Morrell L, Morrell F, Persina IS, Rossi M. Age-related loss of axospinous synapses formed by two afferent systems in the rat dentate gyrus as revealed by the unbiased stereological dissector technique. Hippocampus. 1992;2(4):437-44. Epub 1992/10/01. doi: 10.1002/hipo.450020411. PubMed PMID: 1308200.
104. Geinisman Y, de Toledo-Morrell L, Morrell F. Loss of perforated synapses in the dentate gyrus: morphological substrate of memory deficit in aged rats. Proc Natl Acad Sci U S A. 1986;83(9):3027-31. Epub 1986/05/01. doi: 10.1073/pnas.83.9.3027. PubMed PMID: 3458260; PMCID: PMC323440.
105. Robert D. Terry M, " Eliezer Masliah, MD," David P. Salmon, PhD," Nelson Butters, PhD,? Richard DeTeresa, BS," Robert Hill, PhD,* Lawrence A. Hansen, MD," and Robert Katzman, MD" Physical basis of cogntive alternations in alzheimers disease: synapse loss is the major correlate of cogntive impairment. annual neurology. 1991(30):572-80.
106. Steven T. DeKosky MaSWS, PhD. Synapse loss in frontal cortex biopsies in Alzheimer's disease: correlation with cognitive severity. Annual neurology. 1990;27:457-64.
107. Dorostkar MM, Zou C, Blazquez-Llorca L, Herms J. Analyzing dendritic spine pathology in Alzheimer's disease: problems and opportunities. Acta Neuropathol. 2015;130(1):1-19. Epub 2015/06/13. doi: 10.1007/s00401-015-1449-5. PubMed PMID: 26063233; PMCID: PMC4469300.
108. Zempel H, Mandelkow EM. Linking amyloid-beta and tau: amyloid-beta induced synaptic dysfunction via local wreckage of the neuronal cytoskeleton. Neurodegener Dis. 2012;10(1-4):64-72. Epub 2011/12/14. doi: 10.1159/000332816. PubMed PMID: 22156588.
109. Šišková Z, Justus D, Kaneko H, Friedrichs D, Henneberg N, Beutel T, Pitsch J, Schoch S, Becker A, von der Kammer H, Remy S. Dendritic structural degeneration is functionally linked to cellular

hyperexcitability in a mouse model of Alzheimer's disease. Neuron. 2014;84(5):1023-33. Epub 20141113. doi: 10.1016/j.neuron.2014.10.024. PubMed PMID: 25456500.
110. Lacor PN, Buniel MC, Furlow PW, Clemente AS, Velasco PT, Wood M, Viola KL, Klein WL. Abeta oligomer-induced aberrations in synapse composition, shape, and density provide a molecular basis for loss of connectivity in Alzheimer's disease. J Neurosci. 2007;27(4):796-807. Epub 2007/01/26. doi: 10.1523/JNEUROSCI.3501-06.2007. PubMed PMID: 17251419; PMCID: PMC6672917.
111. Spires TL, Meyer-Luehmann M, Stern EA, McLean PJ, Skoch J, Nguyen PT, Bacskai BJ, Hyman BT. Dendritic spine abnormalities in amyloid precursor protein transgenic mice demonstrated by gene transfer and intravital multiphoton microscopy. J Neurosci. 2005;25(31):7278-87. doi: 10.1523/jneurosci.1879-05.2005. PubMed PMID: 16079410; PMCID: PMC1820616.
112. Henderson BW, Greathouse KM, Ramdas R, Walker CK, Rao TC, Bach SV, Curtis KA, Day JJ, Mattheyses AL, Herskowitz JH. Pharmacologic inhibition of LIMK1 provides dendritic spine resilience against beta-amyloid. Sci Signal. 2019;12(587). Epub 2019/06/27. doi: 10.1126/scisignal.aaw9318. PubMed PMID: 31239325.
113. Lashuel HA, Lansbury PT, Jr. Are amyloid diseases caused by protein aggregates that mimic bacterial pore-forming toxins? Q Rev Biophys. 2006;39(2):167-201. Epub 2006/09/19. doi: 10.1017/S0033583506004422. PubMed PMID: 16978447.
114. Palop JJ, Mucke L. Amyloid-beta-induced neuronal dysfunction in Alzheimer's disease: from synapses toward neural networks. Nat Neurosci. 2010;13(7):812-8. Epub 2010/06/29. doi: 10.1038/nn.2583. PubMed PMID: 20581818; PMCID: PMC3072750.
115. Ittner LM, Gotz J. Amyloid-beta and tau--a toxic pas de deux in Alzheimer's disease. Nat Rev Neurosci. 2011;12(2):65-72. Epub 2011/01/05. doi: 10.1038/nrn2967. PubMed PMID: 21193853.
116. Ittner LM, Ke YD, Delerue F, Bi M, Gladbach A, van Eersel J, Wolfing H, Chieng BC, Christie MJ, Napier IA, Eckert A, Staufenbiel M, Hardeman E, Gotz J. Dendritic function of tau mediates amyloid-beta toxicity in Alzheimer's disease mouse models. Cell. 2010;142(3):387-97. Epub 2010/07/27. doi: 10.1016/j.cell.2010.06.036. PubMed PMID: 20655099.
117. Chabrier MA, Cheng D, Castello NA, Green KN, LaFerla FM. Synergistic effects of amyloid-beta and wild-type human tau on dendritic spine loss in a floxed double transgenic model of Alzheimer's disease. Neurobiol Dis. 2014;64:107-17. Epub 2014/01/21. doi: 10.1016/j.nbd.2014.01.007. PubMed PMID: 24440055; PMCID: PMC4072239.
118. Roberson ED, Halabisky B, Yoo JW, Yao J, Chin J, Yan F, Wu T, Hamto P, Devidze N, Yu GQ, Palop JJ, Noebels JL, Mucke L. Amyloid-beta/Fyn-induced synaptic, network, and cognitive impairments depend on tau levels in multiple mouse models of Alzheimer's disease. J Neurosci. 2011;31(2):700-11. Epub 2011/01/14. doi: 10.1523/JNEUROSCI.4152-10.2011. PubMed PMID: 21228179; PMCID: PMC3325794.
119. Roberson ED, Scearce-Levie K, Palop JJ, Yan F, Cheng IH, Wu T, Gerstein H, Yu GQ, Mucke L. Reducing endogenous tau ameliorates amyloid beta-induced deficits in an Alzheimer's disease mouse model. Science. 2007;316(5825):750-4. Epub 2007/05/05. doi: 10.1126/science.1141736. PubMed PMID: 17478722.
120. Ittner A, Ittner LM. Dendritic Tau in Alzheimer's Disease. Neuron. 2018;99(1):13-27. Epub 2018/07/13. doi: 10.1016/j.neuron.2018.06.003. PubMed PMID: 30001506.
121. Arnold SE, Louneva N, Cao K, Wang LS, Han LY, Wolk DA, Negash S, Leurgans SE, Schneider JA, Buchman AS, Wilson RS, Bennett DA. Cellular, synaptic, and biochemical features of resilient cognition in Alzheimer's disease. Neurobiol Aging. 2013;34(1):157-68. Epub 2012/05/05. doi: 10.1016/j.neurobiolaging.2012.03.004. PubMed PMID: 22554416; PMCID: PMC3478410.
122. Wingo AP, Dammer EB, Breen MS, Logsdon BA, Duong DM, Troncosco JC, Thambisetty M, Beach TG, Serrano GE, Reiman EM, Caselli RJ, Lah JJ, Seyfried NT, Levey AI, Wingo TS. Large-scale proteomic analysis of human brain identifies proteins associated with cognitive trajectory in advanced age. Nat

Commun. 2019;10(1):1619. Epub 2019/04/10. doi: 10.1038/s41467-019-09613-z. PubMed PMID: 30962425; PMCID: PMC6453881.
123. Yu L, Tasaki S, Schneider JA, Arfanakis K, Duong DM, Wingo AP, Wingo TS, Kearns N, Thatcher GRJ, Seyfried NT, Levey AI, De Jager PL, Bennett DA. Cortical Proteins Associated With Cognitive Resilience in Community-Dwelling Older Persons. JAMA Psychiatry. 2020. Epub 2020/07/02. doi: 10.1001/jamapsychiatry.2020.1807. PubMed PMID: 32609320; PMCID: PMC7330835.
124. Johnson ECB, Carter EK, Dammer EB, Duong DM, Gerasimov ES, Liu Y, Liu J, Betarbet R, Ping L, Yin L, Serrano GE, Beach TG, Peng J, De Jager PL, Haroutunian V, Zhang B, Gaiteri C, Bennett DA, Gearing M, Wingo TS, Wingo AP, Lah JJ, Levey AI, Seyfried NT. Large-scale deep multi-layer analysis of Alzheimer's disease brain reveals strong proteomic disease-related changes not observed at the RNA level. Nat Neurosci. 2022;25(2):213-25. Epub 2022/02/05. doi: 10.1038/s41593-021-00999-y. PubMed PMID: 35115731; PMCID: PMC8825285.
125. Nedivi E, Hevroni D, Naot D, Israeli D, Citri Y. Numerous candidate plasticity-related genes revealed by differential cDNA cloning. Nature. 1993;363(6431):718-22. Epub 1993/06/24. doi: 10.1038/363718a0. PubMed PMID: 8515813.
126. Fujino T, Wu Z, Lin WC, Phillips MA, Nedivi E. cpg15 and cpg15-2 constitute a family of activity-regulated ligands expressed differentially in the nervous system to promote neurite growth and neuronal survival. J Comp Neurol. 2008;507(5):1831-45. Epub 2008/02/12. doi: 10.1002/cne.21649. PubMed PMID: 18265009; PMCID: PMC2828060.
127. Naeve GS, Ramakrishnan M, Kramer R, Hevroni D, Citri Y, Theill LE. Neuritin: a gene induced by neural activity and neurotrophins that promotes neuritogenesis. Proc Natl Acad Sci U S A. 1997;94(6):2648-53. Epub 1997/03/18. doi: 10.1073/pnas.94.6.2648. PubMed PMID: 9122250; PMCID: PMC20143.
128. Sato H, Fukutani Y, Yamamoto Y, Tatara E, Takemoto M, Shimamura K, Yamamoto N. Thalamus-derived molecules promote survival and dendritic growth of developing cortical neurons. J Neurosci. 2012;32(44):15388-402. Epub 2012/11/02. doi: 10.1523/jneurosci.0293-12.2012. PubMed PMID: 23115177; PMCID: PMC6621586.
129. Putz U, Harwell C, Nedivi E. Soluble CPG15 expressed during early development rescues cortical progenitors from apoptosis. Nat Neurosci. 2005;8(3):322-31. Epub 2005/02/16. doi: 10.1038/nn1407. PubMed PMID: 15711540; PMCID: PMC3075944.
130. Cantallops I, Cline HT. Rapid activity-dependent delivery of the neurotrophic protein CPG15 to the axon surface of neurons in intact Xenopus tadpoles. Dev Neurobiol. 2008;68(6):744-59. Epub 2008/04/03. doi: 10.1002/dneu.20529. PubMed PMID: 18383547.
131. Cantallops I, Haas K, Cline HT. Postsynaptic CPG15 promotes synaptic maturation and presynaptic axon arbor elaboration in vivo. Nat Neurosci. 2000;3(10):1004-11. Epub 2000/10/04. doi: 10.1038/79823. PubMed PMID: 11017173.
132. Fujino T, Leslie JH, Eavri R, Chen JL, Lin WC, Flanders GH, Borok E, Horvath TL, Nedivi E. CPG15 regulates synapse stability in the developing and adult brain. Genes Dev. 2011;25(24):2674-85. Epub 2011/12/23. doi: 10.1101/gad.176172.111. PubMed PMID: 22190461; PMCID: PMC3248687.
133. Zhao QR, Lu JM, Yao JJ, Zhang ZY, Ling C, Mei YA. Neuritin reverses deficits in murine novel object associative recognition memory caused by exposure to extremely low-frequency (50 Hz) electromagnetic fields. Sci Rep. 2015;5:11768. Epub 2015/07/04. doi: 10.1038/srep11768. PubMed PMID: 26138388; PMCID: PMC4650637.
134. Lu JM, Liu DD, Li ZY, Ling C, Mei YA. Neuritin Enhances Synaptic Transmission in Medial Prefrontal Cortex in Mice by Increasing CaV3.3 Surface Expression. Cereb Cortex. 2017;27(7):3842-55. Epub 2017/05/06. doi: 10.1093/cercor/bhx082. PubMed PMID: 28475719.

135. Subramanian J, Michel K, Benoit M, Nedivi E. CPG15/Neuritin Mimics Experience in Selecting Excitatory Synapses for Stabilization by Facilitating PSD95 Recruitment. Cell Rep. 2019;28(6):1584-95.e5. Epub 2019/08/08. doi: 10.1016/j.celrep.2019.07.012. PubMed PMID: 31390571; PMCID: PMC6740334.
136. Alme MN, Wibrand K, Dagestad G, Bramham CR. Chronic fluoxetine treatment induces brain region-specific upregulation of genes associated with BDNF-induced long-term potentiation. Neural Plast. 2007;2007:26496. Epub 2008/02/28. doi: 10.1155/2007/26496. PubMed PMID: 18301726; PMCID: PMC2248427.
137. Dyrvig M, Christiansen SH, Woldbye DP, Lichota J. Temporal gene expression profile after acute electroconvulsive stimulation in the rat. Gene. 2014;539(1):8-14. Epub 2014/02/13. doi: 10.1016/j.gene.2014.01.072. PubMed PMID: 24518690.
138. Son H, Banasr M, Choi M, Chae SY, Licznerski P, Lee B, Voleti B, Li N, Lepack A, Fournier NM, Lee KR, Lee IY, Kim J, Kim JH, Kim YH, Jung SJ, Duman RS. Neuritin produces antidepressant actions and blocks the neuronal and behavioral deficits caused by chronic stress. Proc Natl Acad Sci U S A. 2012;109(28):11378-83. Epub 2012/06/27. doi: 10.1073/pnas.1201191109. PubMed PMID: 22733766; PMCID: PMC3396528.
139. Prats C, Arias B, Ortet G, Ibáñez MI, Moya J, Pomarol-Clotet E, Fañanás L, Fatjó-Vilas M. Neurotrophins role in depressive symptoms and executive function performance: Association analysis of NRN1 gene and its interaction with BDNF gene in a non-clinical sample. J Affect Disord. 2017;211:92-8. Epub 2017/01/21. doi: 10.1016/j.jad.2016.11.017. PubMed PMID: 28107668.
140. Fatjó-Vilas M, Prats C, Pomarol-Clotet E, Lázaro L, Moreno C, González-Ortega I, Lera-Miguel S, Miret S, Muñoz MJ, Ibáñez I, Campanera S, Giralt-López M, Cuesta MJ, Peralta V, Ortet G, Parellada M, González-Pinto A, McKenna PJ, Fañanás L. Involvement of NRN1 gene in schizophrenia-spectrum and bipolar disorders and its impact on age at onset and cognitive functioning. World J Biol Psychiatry. 2016;17(2):129-39. Epub 2015/12/25. doi: 10.3109/15622975.2015.1093658. PubMed PMID: 26700405.
141. Prats C, Arias B, Moya-Higueras J, Pomarol-Clotet E, Parellada M, González-Pinto A, Peralta V, Ibáñez MI, Martín M, Fañanás L, Fatjó-Vilas M. Evidence of an epistatic effect between Dysbindin-1 and Neuritin-1 genes on the risk for schizophrenia spectrum disorders. Eur Psychiatry. 2017;40:60-4. Epub 2016/11/18. doi: 10.1016/j.eurpsy.2016.07.006. PubMed PMID: 27855309.
142. Chandler D, Dragović M, Cooper M, Badcock JC, Mullin BH, Faulkner D, Wilson SG, Hallmayer J, Howell S, Rock D, Palmer LJ, Kalaydjieva L, Jablensky A. Impact of Neuritin 1 (NRN1) polymorphisms on fluid intelligence in schizophrenia. Am J Med Genet B Neuropsychiatr Genet. 2010;153b(2):428-37. Epub 2009/07/02. doi: 10.1002/ajmg.b.30996. PubMed PMID: 19569075.
143. Choi Y, Lee K, Ryu J, Kim HG, Jeong AY, Woo RS, Lee JH, Hyun JW, Hahn S, Kim JH, Kim HS. Neuritin attenuates cognitive function impairments in tg2576 mouse model of Alzheimer's disease. PLoS One. 2014;9(8):e104121. Epub 2014/08/08. doi: 10.1371/journal.pone.0104121. PubMed PMID: 25101829; PMCID: PMC4125179.
144. Hsiao K, Chapman P, Nilsen S, Eckman C, Harigaya Y, Younkin S, Yang F, Cole G. Correlative memory deficits, Abeta elevation, and amyloid plaques in transgenic mice. Science. 1996;274(5284):99-102. Epub 1996/10/04. doi: 10.1126/science.274.5284.99. PubMed PMID: 8810256.
145. An K, Jung JH, Jeong AY, Kim HG, Jung SY, Lee K, Kim HJ, Kim SJ, Jeong TY, Son Y, Kim HS, Kim JH. Neuritin can normalize neural deficits of Alzheimer's disease. Cell Death Dis. 2014;5(11):e1523. Epub 2014/11/14. doi: 10.1038/cddis.2014.478. PubMed PMID: 25393479; PMCID: PMC4260736.
146. Jack CR, Jr., Knopman DS, Jagust WJ, Shaw LM, Aisen PS, Weiner MW, Petersen RC, Trojanowski JQ. Hypothetical model of dynamic biomarkers of the Alzheimer's pathological cascade. Lancet Neurol. 2010;9(1):119-28. Epub 2010/01/20. doi: 10.1016/S1474-4422(09)70299-6. PubMed PMID: 20083042; PMCID: PMC2819840.

147. Scheltens P, De Strooper B, Kivipelto M, Holstege H, Chételat G, Teunissen CE, Cummings J, van der Flier WM. Alzheimer's disease. The Lancet. 2021;397(10284):1577-90. doi: 10.1016/S0140-6736(20)32205-4.
148. Duyckaerts C, Delatour B, Potier MC. Classification and basic pathology of Alzheimer disease. Acta Neuropathol. 2009;118(1):5-36. Epub 2009/04/22. doi: 10.1007/s00401-009-0532-1. PubMed PMID: 19381658.
149. Sperling RA, Aisen PS, Beckett LA, Bennett DA, Craft S, Fagan AM, Iwatsubo T, Jack CR, Jr., Kaye J, Montine TJ, Park DC, Reiman EM, Rowe CC, Siemers E, Stern Y, Yaffe K, Carrillo MC, Thies B, Morrison-Bogorad M, Wagster MV, Phelps CH. Toward defining the preclinical stages of Alzheimer's disease: recommendations from the National Institute on Aging-Alzheimer's Association workgroups on diagnostic guidelines for Alzheimer's disease. Alzheimer's & dementia : the journal of the Alzheimer's Association. 2011;7(3):280-92. Epub 2011/04/21. doi: 10.1016/j.jalz.2011.03.003. PubMed PMID: 21514248.
150. Neuner SM, Telpoukhovskaia M, Menon V, O'Connell KMS, Hohman TJ, Kaczorowski CC. Translational approaches to understanding resilience to Alzheimer's disease. Trends Neurosci. 2022;45(5):369-83. Epub 2022/03/22. doi: 10.1016/j.tins.2022.02.005. PubMed PMID: 35307206; PMCID: PMC9035083.
151. Stern Y, Arenaza-Urquijo EM, Bartres-Faz D, Belleville S, Cantilon M, Chetelat G, Ewers M, Franzmeier N, Kempermann G, Kremen WS, Okonkwo O, Scarmeas N, Soldan A, Udeh-Momoh C, Valenzuela M, Vemuri P, Vuoksimaa E, the Reserve R, Protective Factors PIAED, Conceptual Frameworks W. Whitepaper: Defining and investigating cognitive reserve, brain reserve, and brain maintenance. Alzheimers Dement. 2020;16(9):1305-11. Epub 2018/09/18. doi: 10.1016/j.jalz.2018.07.219. PubMed PMID: 30222945; PMCID: PMC6417987.
152. Yao T, Sweeney E, Nagorski J, Shulman JM, Allen GI. Quantifying cognitive resilience in Alzheimer's Disease: The Alzheimer's Disease Cognitive Resilience Score. PLoS One. 2020;15(11):e0241707. Epub 2020/11/06. doi: 10.1371/journal.pone.0241707. PubMed PMID: 33152028; PMCID: PMC7643963.
153. Honer WG, Barr AM, Sawada K, Thornton AE, Morris MC, Leurgans SE, Schneider JA, Bennett DA. Cognitive reserve, presynaptic proteins and dementia in the elderly. Transl Psychiatry. 2012;2:e114. Epub 2012/07/27. doi: 10.1038/tp.2012.38. PubMed PMID: 22832958; PMCID: PMC3365257.
154. Bennett DA, Buchman AS, Boyle PA, Barnes LL, Wilson RS, Schneider JA. Religious Orders Study and Rush Memory and Aging Project. J Alzheimers Dis. 2018;64(s1):S161-S89. Epub 2018/06/06. doi: 10.3233/JAD-179939. PubMed PMID: 29865057; PMCID: PMC6380522.
155. Tanaka S, Honda M, Sadato N. Modality-specific cognitive function of medial and lateral human Brodmann area 6. J Neurosci. 2005;25(2):496-501. Epub 2005/01/14. doi: 10.1523/JNEUROSCI.4324-04.2005. PubMed PMID: 15647494; PMCID: PMC6725497.
156. Thangavel R, Sahu SK, Van Hoesen GW, Zaheer A. Modular and laminar pathology of Brodmann's area 37 in Alzheimer's disease. Neuroscience. 2008;152(1):50-5. Epub 2008/01/29. doi: 10.1016/j.neuroscience.2007.12.025. PubMed PMID: 18222045; PMCID: PMC2350243.
157. Johnson ECB, Dammer EB, Duong DM, Ping L, Zhou M, Yin L, Higginbotham LA, Guajardo A, White B, Troncoso JC, Thambisetty M, Montine TJ, Lee EB, Trojanowski JQ, Beach TG, Reiman EM, Haroutunian V, Wang M, Schadt E, Zhang B, Dickson DW, Ertekin-Taner N, Golde TE, Petyuk VA, De Jager PL, Bennett DA, Wingo TS, Rangaraju S, Hajjar I, Shulman JM, Lah JJ, Levey AI, Seyfried NT. Large-scale proteomic analysis of Alzheimer's disease brain and cerebrospinal fluid reveals early changes in energy metabolism associated with microglia and astrocyte activation. Nat Med. 2020;26(5):769-80. Epub 2020/04/15. doi: 10.1038/s41591-020-0815-6. PubMed PMID: 32284590; PMCID: PMC7405761.
158. Jack CR, Jr., Bennett DA, Blennow K, Carrillo MC, Dunn B, Haeberlein SB, Holtzman DM, Jagust W, Jessen F, Karlawish J, Liu E, Molinuevo JL, Montine T, Phelps C, Rankin KP, Rowe CC, Scheltens P, Siemers E, Snyder HM, Sperling R, Contributors. NIA-AA Research Framework: Toward a biological definition of

Alzheimer's disease. Alzheimers Dement. 2018;14(4):535-62. Epub 2018/04/15. doi: 10.1016/j.jalz.2018.02.018. PubMed PMID: 29653606; PMCID: PMC5958625.
159. Seyfried NT, Dammer EB, Swarup V, Nandakumar D, Duong DM, Yin L, Deng Q, Nguyen T, Hales CM, Wingo T, Glass J, Gearing M, Thambisetty M, Troncoso JC, Geschwind DH, Lah JJ, Levey AI. A Multi-network Approach Identifies Protein-Specific Co-expression in Asymptomatic and Symptomatic Alzheimer's Disease. Cell Syst. 2017;4(1):60-72 e4. Epub 2016/12/19. doi: 10.1016/j.cels.2016.11.006. PubMed PMID: 27989508; PMCID: PMC5269514.
160. Langfelder P, Horvath S. WGCNA: an R package for weighted correlation network analysis. BMC Bioinformatics. 2008;9:559. Epub 2008/12/31. doi: 10.1186/1471-2105-9-559. PubMed PMID: 19114008; PMCID: PMC2631488.
161. Chai K, Zhang X, Tang H, Gu H, Ye W, Wang G, Chen S, Wan F, Liang J, Shen D. The Application of Consensus Weighted Gene Co-expression Network Analysis to Comparative Transcriptome Meta-Datasets of Multiple Sclerosis in Gray and White Matter. Front Neurol. 2022;13:807349. Epub 2022/03/15. doi: 10.3389/fneur.2022.807349. PubMed PMID: 35280300; PMCID: PMC8907380.
162. Wilson RS, Arnold SE, Schneider JA, Tang Y, Bennett DA. The relationship between cerebral Alzheimer's disease pathology and odour identification in old age. J Neurol Neurosurg Psychiatry. 2007;78(1):30-5. Epub 2006/10/03. doi: 10.1136/jnnp.2006.099721. PubMed PMID: 17012338; PMCID: PMC2117790.
163. Balsis S, Benge JF, Lowe DA, Geraci L, Doody RS. How Do Scores on the ADAS-Cog, MMSE, and CDR-SOB Correspond? Clin Neuropsychol. 2015;29(7):1002-9. Epub 2015/12/01. doi: 10.1080/13854046.2015.1119312. PubMed PMID: 26617181.
164. Ping L, Duong DM, Yin L, Gearing M, Lah JJ, Levey AI, Seyfried NT. Global quantitative analysis of the human brain proteome in Alzheimer's and Parkinson's Disease. Sci Data. 2018;5:180036. Epub 2018/03/14. doi: 10.1038/sdata.2018.36. PubMed PMID: 29533394; PMCID: PMC5848788.
165. Ping L, Kundinger SR, Duong DM, Yin L, Gearing M, Lah JJ, Levey AI, Seyfried NT. Global quantitative analysis of the human brain proteome and phosphoproteome in Alzheimer's disease. Sci Data. 2020;7(1):315. Epub 2020/09/29. doi: 10.1038/s41597-020-00650-8. PubMed PMID: 32985496; PMCID: PMC7522715.
166. Johnson ECB, Dammer EB, Duong DM, Yin L, Thambisetty M, Troncoso JC, Lah JJ, Levey AI, Seyfried NT. Deep proteomic network analysis of Alzheimer's disease brain reveals alterations in RNA binding proteins and RNA splicing associated with disease. Mol Neurodegener. 2018;13(1):52. Epub 2018/10/06. doi: 10.1186/s13024-018-0282-4. PubMed PMID: 30286791; PMCID: PMC6172707.
167. Mertins P, Tang LC, Krug K, Clark DJ, Gritsenko MA, Chen L, Clauser KR, Clauss TR, Shah P, Gillette MA, Petyuk VA, Thomas SN, Mani DR, Mundt F, Moore RJ, Hu Y, Zhao R, Schnaubelt M, Keshishian H, Monroe ME, Zhang Z, Udeshi ND, Mani D, Davies SR, Townsend RR, Chan DW, Smith RD, Zhang H, Liu T, Carr SA. Reproducible workflow for multiplexed deep-scale proteome and phosphoproteome analysis of tumor tissues by liquid chromatography-mass spectrometry. Nat Protoc. 2018;13(7):1632-61. Epub 2018/07/11. doi: 10.1038/s41596-018-0006-9. PubMed PMID: 29988108; PMCID: PMC6211289.
168. Wingo TS, Duong DM, Zhou M, Dammer EB, Wu H, Cutler DJ, Lah JJ, Levey AI, Seyfried NT. Integrating Next-Generation Genomic Sequencing and Mass Spectrometry To Estimate Allele-Specific Protein Abundance in Human Brain. J Proteome Res. 2017;16(9):3336-47. Epub 2017/07/12. doi: 10.1021/acs.jproteome.7b00324. PubMed PMID: 28691493; PMCID: PMC5698003.
169. McKenzie AT, Moyon S, Wang M, Katsyv I, Song WM, Zhou X, Dammer EB, Duong DM, Aaker J, Zhao Y, Beckmann N, Wang P, Zhu J, Lah JJ, Seyfried NT, Levey AI, Katsel P, Haroutunian V, Schadt EE, Popko B, Casaccia P, Zhang B. Multiscale network modeling of oligodendrocytes reveals molecular components of myelin dysregulation in Alzheimer's disease. Mol Neurodegener. 2017;12(1):82. Epub 2017/11/08. doi: 10.1186/s13024-017-0219-3. PubMed PMID: 29110684; PMCID: PMC5674813.

170. Sharma K, Schmitt S, Bergner CG, Tyanova S, Kannaiyan N, Manrique-Hoyos N, Kongi K, Cantuti L, Hanisch UK, Philips MA, Rossner MJ, Mann M, Simons M. Cell type- and brain region-resolved mouse brain proteome. Nat Neurosci. 2015;18(12):1819-31. Epub 2015/11/03. doi: 10.1038/nn.4160. PubMed PMID: 26523646; PMCID: PMC7116867.
171. Zhang Y, Chen K, Sloan SA, Bennett ML, Scholze AR, O'Keeffe S, Phatnani HP, Guarnieri P, Caneda C, Ruderisch N, Deng S, Liddelow SA, Zhang C, Daneman R, Maniatis T, Barres BA, Wu JQ. An RNA-sequencing transcriptome and splicing database of glia, neurons, and vascular cells of the cerebral cortex. J Neurosci. 2014;34(36):11929-47. Epub 2014/09/05. doi: 10.1523/JNEUROSCI.1860-14.2014. PubMed PMID: 25186741; PMCID: PMC4152602.
172. Yu L, Tasaki S, Schneider JA, Arfanakis K, Duong DM, Wingo AP, Wingo TS, Kearns N, Thatcher GRJ, Seyfried NT, Levey AI, De Jager PL, Bennett DA. Cortical Proteins Associated With Cognitive Resilience in Community-Dwelling Older Persons. JAMA Psychiatry. 2020;77(11):1172-80. Epub 2020/07/02. doi: 10.1001/jamapsychiatry.2020.1807. PubMed PMID: 32609320; PMCID: PMC7330835.
173. Mostafavi S, Gaiteri C, Sullivan SE, White CC, Tasaki S, Xu J, Taga M, Klein HU, Patrick E, Komashko V, McCabe C, Smith R, Bradshaw EM, Root DE, Regev A, Yu L, Chibnik LB, Schneider JA, Young-Pearse TL, Bennett DA, De Jager PL. A molecular network of the aging human brain provides insights into the pathology and cognitive decline of Alzheimer's disease. Nat Neurosci. 2018;21(6):811-9. Epub 2018/05/29. doi: 10.1038/s41593-018-0154-9. PubMed PMID: 29802388; PMCID: PMC6599633.
174. Nedivi E, Wu GY, Cline HT. Promotion of dendritic growth by CPG15, an activity-induced signaling molecule. Science. 1998;281(5384):1863-6. Epub 1998/09/22. doi: 10.1126/science.281.5384.1863. PubMed PMID: 9743502; PMCID: PMC3088013.
175. Javaherian A, Cline HT. Coordinated motor neuron axon growth and neuromuscular synaptogenesis are promoted by CPG15 in vivo. Neuron. 2005;45(4):505-12. Epub 2005/02/22. doi: 10.1016/j.neuron.2004.12.051. PubMed PMID: 15721237.
176. Picard N, Leslie JH, Trowbridge SK, Subramanian J, Nedivi E, Fagiolini M. Aberrant development and plasticity of excitatory visual cortical networks in the absence of cpg15. J Neurosci. 2014;34(10):3517-22. Epub 2014/03/07. doi: 10.1523/jneurosci.2955-13.2014. PubMed PMID: 24599452; PMCID: PMC3942571.
177. Altelaar AF, Frese CK, Preisinger C, Hennrich ML, Schram AW, Timmers HT, Heck AJ, Mohammed S. Benchmarking stable isotope labeling based quantitative proteomics. J Proteomics. 2013;88:14-26. Epub 2012/10/23. doi: 10.1016/j.jprot.2012.10.009. PubMed PMID: 23085607.
178. Sandberg A, Branca RM, Lehtio J, Forshed J. Quantitative accuracy in mass spectrometry based proteomics of complex samples: the impact of labeling and precursor interference. J Proteomics. 2014;96:133-44. Epub 2013/11/12. doi: 10.1016/j.jprot.2013.10.035. PubMed PMID: 24211767.
179. Yao JJ, Zhao QR, Lu JM, Mei YA. Functions and the related signaling pathways of the neurotrophic factor neuritin. Acta Pharmacol Sin. 2018;39(9):1414-20. Epub 2018/03/30. doi: 10.1038/aps.2017.197. PubMed PMID: 29595190; PMCID: PMC6289377.
180. Hurst C, Pugh DA, Abreha MH, Duong DM, Dammer EB, Bennett DA, Herskowitz JH, Seyfried NT. Integrated Proteomics to Understand the Role of Neuritin (NRN1) as a Mediator of Cognitive Resilience to Alzheimer's Disease. Mol Cell Proteomics. 2023:100542. Epub 2023/04/07. doi: 10.1016/j.mcpro.2023.100542. PubMed PMID: 37024090.
181. Boros BD, Greathouse KM, Gearing M, Herskowitz JH. Dendritic spine remodeling accompanies Alzheimer's disease pathology and genetic susceptibility in cognitively normal aging. Neurobiol Aging. 2019;73:92-103. Epub 20180921. doi: 10.1016/j.neurobiolaging.2018.09.003. PubMed PMID: 30339964; PMCID: PMC6251733.
182. Henderson BW, Greathouse KM, Ramdas R, Walker CK, Rao TC, Bach SV, Curtis KA, Day JJ, Mattheyses AL, Herskowitz JH. Pharmacologic inhibition of LIMK1 provides dendritic spine resilience

against β-amyloid. Sci Signal. 2019;12(587). Epub 20190625. doi: 10.1126/scisignal.aaw9318. PubMed PMID: 31239325; PMCID: PMC7088434.
183. Sanchez PE, Zhu L, Verret L, Vossel KA, Orr AG, Cirrito JR, Devidze N, Ho K, Yu GQ, Palop JJ, Mucke L. Levetiracetam suppresses neuronal network dysfunction and reverses synaptic and cognitive deficits in an Alzheimer's disease model. Proc Natl Acad Sci U S A. 2012;109(42):E2895-903. Epub 20120806. doi: 10.1073/pnas.1121081109. PubMed PMID: 22869752; PMCID: PMC3479491.
184. Vossel KA, Ranasinghe KG, Beagle AJ, Mizuiri D, Honma SM, Dowling AF, Darwish SM, Van Berlo V, Barnes DE, Mantle M, Karydas AM, Coppola G, Roberson ED, Miller BL, Garcia PA, Kirsch HE, Mucke L, Nagarajan SS. Incidence and impact of subclinical epileptiform activity in Alzheimer's disease. Ann Neurol. 2016;80(6):858-70. Epub 20161107. doi: 10.1002/ana.24794. PubMed PMID: 27696483; PMCID: PMC5177487.
185. Riedl J, Crevenna AH, Kessenbrock K, Yu JH, Neukirchen D, Bista M, Bradke F, Jenne D, Holak TA, Werb Z, Sixt M, Wedlich-Soldner R. Lifeact: a versatile marker to visualize F-actin. Nat Methods. 2008;5(7):605-7. Epub 2008/06/10. doi: 10.1038/nmeth.1220. PubMed PMID: 18536722; PMCID: PMC2814344.
186. Riedl J, Flynn KC, Raducanu A, Gartner F, Beck G, Bosl M, Bradke F, Massberg S, Aszodi A, Sixt M, Wedlich-Soldner R. Lifeact mice for studying F-actin dynamics. Nat Methods. 2010;7(3):168-9. Epub 2010/03/03. doi: 10.1038/nmeth0310-168. PubMed PMID: 20195247.
187. Greathouse KM, Boros BD, Deslauriers JF, Henderson BW, Curtis KA, Gentry EG, Herskowitz JH. Distinct and complementary functions of rho kinase isoforms ROCK1 and ROCK2 in prefrontal cortex structural plasticity. Brain Struct Funct. 2018;223(9):4227-41. Epub 20180908. doi: 10.1007/s00429-018-1748-4. PubMed PMID: 30196430; PMCID: PMC6252131.
188. Naiki H, Higuchi K, Hosokawa M, Takeda T. Fluorometric determination of amyloid fibrils in vitro using the fluorescent dye, thioflavine T. Analytical biochemistry. 1989;177(2):244-9.
189. Yao JJ, Gao XF, Chow CW, Zhan XQ, Hu CL, Mei YA. Neuritin activates insulin receptor pathway to up-regulate Kv4.2-mediated transient outward K+ current in rat cerebellar granule neurons. J Biol Chem. 2012;287(49):41534-45. Epub 2012/10/16. doi: 10.1074/jbc.M112.390260. PubMed PMID: 23066017; PMCID: PMC3510849.
190. Ping L, Duong DM, Yin L, Gearing M, Lah JJ, Levey AI, Seyfried NT. Global quantitative analysis of the human brain proteome in Alzheimer's and Parkinson's Disease. Scientific Data. 2018;5(1):180036. doi: 10.1038/sdata.2018.36.
191. Suomi T, Seyednasrollah F, Jaakkola MK, Faux T, Elo LL. ROTS: An R package for reproducibility-optimized statistical testing. PLoS Comput Biol. 2017;13(5):e1005562. Epub 2017/05/26. doi: 10.1371/journal.pcbi.1005562. PubMed PMID: 28542205; PMCID: PMC5470739.
192. Elston GN, DeFelipe J. Spine distribution in cortical pyramidal cells: a common organizational principle across species. Prog Brain Res. 2002;136:109-33. doi: 10.1016/s0079-6123(02)36012-6. PubMed PMID: 12143375.
193. Jacobs B, Driscoll L, Schall M. Life-span dendritic and spine changes in areas 10 and 18 of human cortex: a quantitative Golgi study. J Comp Neurol. 1997;386(4):661-80. PubMed PMID: 9378859.
194. Jacobs B, Schall M, Prather M, Kapler E, Driscoll L, Baca S, Jacobs J, Ford K, Wainwright M, Treml M. Regional dendritic and spine variation in human cerebral cortex: a quantitative golgi study. Cereb Cortex. 2001;11(6):558-71. doi: 10.1093/cercor/11.6.558. PubMed PMID: 11375917.
195. Dickstein DL, Kabaso D, Rocher AB, Luebke JI, Wearne SL, Hof PR. Changes in the structural complexity of the aged brain. Aging Cell. 2007;6(3):275-84. Epub 20070426. doi: 10.1111/j.1474-9726.2007.00289.x. PubMed PMID: 17465981; PMCID: PMC2441530.
196. Palop JJ, Chin J, Roberson ED, Wang J, Thwin MT, Bien-Ly N, Yoo J, Ho KO, Yu GQ, Kreitzer A, Finkbeiner S, Noebels JL, Mucke L. Aberrant excitatory neuronal activity and compensatory remodeling of

inhibitory hippocampal circuits in mouse models of Alzheimer's disease. Neuron. 2007;55(5):697-711. doi: 10.1016/j.neuron.2007.07.025. PubMed PMID: 17785178; PMCID: PMC8055171.
197. Johnston D, Magee JC, Colbert CM, Cristie BR. Active properties of neuronal dendrites. Annu Rev Neurosci. 1996;19:165-86. doi: 10.1146/annurev.ne.19.030196.001121. PubMed PMID: 8833440.
198. Gonzalez-Figueroa P, Roco JA, Papa I, Nunez Villacis L, Stanley M, Linterman MA, Dent A, Canete PF, Vinuesa CG. Follicular regulatory T cells produce neuritin to regulate B cells. Cell. 2021;184(7):1775-89 e19. Epub 2021/03/13. doi: 10.1016/j.cell.2021.02.027. PubMed PMID: 33711260.
199. Zhang Z, Zhou H, Zhou J. Neuritin inhibits astrogliosis to ameliorate diabetic cognitive dysfunction. J Mol Endocrinol. 2021;66(4):259-72. Epub 2021/03/18. doi: 10.1530/JME-20-0321. PubMed PMID: 33729996; PMCID: PMC8111324.
200. Budni J, Garcez ML, de Medeiros J, Cassaro E, Bellettini-Santos T, Mina F, Quevedo J. The Anti-Inflammatory Role of Minocycline in Alzheimer s Disease. Curr Alzheimer Res. 2016;13(12):1319-29. Epub 2016/08/20. doi: 10.2174/1567205013666160819124206. PubMed PMID: 27539598.
201. Papadogianni G, Ravens I, Hassan A, Flatley A, Feederle R, Bernhardt G, Georgiev H. Establishment and Functional Characterization of Murine Monoclonal Antibodies Recognizing Neuritin. Antibodies (Basel). 2023;12(2). Epub 2023/04/24. doi: 10.3390/antib12020028. PubMed PMID: 37092449; PMCID: PMC10123642.
202. Cho KF, Branon TC, Udeshi ND, Myers SA, Carr SA, Ting AY. Proximity labeling in mammalian cells with TurboID and split-TurboID. Nat Protoc. 2020;15(12):3971-99. Epub 2020/11/04. doi: 10.1038/s41596-020-0399-0. PubMed PMID: 33139955.
203. Branon TC, Bosch JA, Sanchez AD, Udeshi ND, Svinkina T, Carr SA, Feldman JL, Perrimon N, Ting AY. Efficient proximity labeling in living cells and organisms with TurboID. Nat Biotechnol. 2018;36(9):880-7. Epub 2018/08/21. doi: 10.1038/nbt.4201. PubMed PMID: 30125270; PMCID: PMC6126969.
204. Sunna S, Bowen C, Zeng H, Rayaprolu S, Kumar P, Bagchi P, Dammer EB, Guo Q, Duong DM, Bitarafan S, Natu A, Wood L, Seyfried NT, Rangaraju S. Cellular proteomic profiling using proximity labelling by TurboID-NES in microglial and neuronal cell lines. Mol Cell Proteomics. 2023:100546. Epub 2023/04/16. doi: 10.1016/j.mcpro.2023.100546. PubMed PMID: 37061046.
205. Neuner SM, Heuer SE, Huentelman MJ, O'Connell KMS, Kaczorowski CC. Harnessing Genetic Complexity to Enhance Translatability of Alzheimer's Disease Mouse Models: A Path toward Precision Medicine. Neuron. 2019;101(3):399-411 e5. Epub 2019/01/01. doi: 10.1016/j.neuron.2018.11.040. PubMed PMID: 30595332; PMCID: PMC6886697.
206. Olsson B, Lautner R, Andreasson U, Ohrfelt A, Portelius E, Bjerke M, Holtta M, Rosen C, Olsson C, Strobel G, Wu E, Dakin K, Petzold M, Blennow K, Zetterberg H. CSF and blood biomarkers for the diagnosis of Alzheimer's disease: a systematic review and meta-analysis. Lancet Neurol. 2016;15(7):673-84. Epub 2016/04/14. doi: 10.1016/S1474-4422(16)00070-3. PubMed PMID: 27068280.
207. Sperling RA, Aisen PS, Beckett LA, Bennett DA, Craft S, Fagan AM, Iwatsubo T, Jack CR, Jr., Kaye J, Montine TJ, Park DC, Reiman EM, Rowe CC, Siemers E, Stern Y, Yaffe K, Carrillo MC, Thies B, Morrison-Bogorad M, Wagster MV, Phelps CH. Toward defining the preclinical stages of Alzheimer's disease: recommendations from the National Institute on Aging-Alzheimer's Association workgroups on diagnostic guidelines for Alzheimer's disease. Alzheimers Dement. 2011;7(3):280-92. Epub 2011/04/26. doi: 10.1016/j.jalz.2011.03.003. PubMed PMID: 21514248; PMCID: PMC3220946.
208. Modeste E, Ping L, Watson CM, Duong DM, Dammer EB, Johnson ECB, Roberts BR, Lah JJ, Levey AI, Seyfried NT. Quantitative proteomics of cerebrospinal fluid from African Americans and Caucasians reveals shared and divergent changes in Alzheimer’s disease2022:2022.12.07.519393. doi: 10.1101/2022.12.07.519393 %J bioRxiv.

209. Shakhnovich V. It's Time to Reverse our Thinking: The Reverse Translation Research Paradigm. Clin Transl Sci. 2018;11(2):98-9. Epub 2018/02/10. doi: 10.1111/cts.12538. PubMed PMID: 29423973; PMCID: PMC5866972.